MIGUEL HERNÁNDEZ UNIVERSITY OF ELCHE

Doctoral Program in Industrial and Telecommunication Technologies

UPPER-LIMB KINEMATIC ANALYSIS AND ARTIFICIAL INTELLIGENT TECHNIQUES FOR NEUROREHABILITATION AND ASSISTIVE ENVIRONMENTS

ARTURO BERTOMEU MOTOS

Supervisor: NICOLÁS MANUEL GARCÍA ARACIL
Biomedical Neuroengineering Research Group
Department of Systems Engineering and Automation

Thesis submitted for the degree of Doctor of Philosophy
Elche, September 2019

ORIGINALITY DECLARATION

I hereby declare that this thesis and the research herein presented was originated and composed by myself, except where other work has been appropriately referenced and credited.

Elche, September 2019

Arturo Bertomeu Motos

The presented PhD dissertation is sustained by a compendium of peer-reviewed publications previously published in indexed journals according to the last Journal Citation Reports (JCR). Listed are the publications that form the main work of the thesis:

Bertomeu-Motos, A.; Lledó, L. D.; Díez, J. A.; Catalan, J. M.; Ezquerro, S.; Badesa, F. J. and Garcia-Aracil, N. (2015b), 'Estimation of Human Arm Joints Using Two Wireless Sensors in Robotic Rehabilitation Tasks', *Sensors* **15**(12), pp. 30571–30583, DOI: 10.3390/s151229818

- Journal Title: Sensors (ISSN: 1424-8220)

- JCR-SCI Impact Factor (2015): 2.033.

- Category: Instruments & Instrumentation, Quartile Q1 (12/56).

Bertomeu-Motos, A.; Blanco, A.; Badesa, F. J.; Barios, J. A.; Zollo, L. and Garcia-Aracil, N. (2018), 'Human arm joints reconstruction algorithm in rehabilitation therapies assisted by end-effector robotic devices', *Journal of NeuroEngineering and Rehabilitation* **15**(1), p. 10, DOI: 10.1186/s12984-018-0348-0

- Journal Title: J. NeuroEng. Rehabil. (ISSN: 1743-0003).

- JCR-SCI Impact Factor (2018): 3.582.

- Category: Rehabilitation, Quartile Q1 (4/65).

Bertomeu-Motos, A.; Ezquerro, S.; Barios, J. A.; Lledó, L. D.; Domingo, S.; Nann, M.; Martin, S.; Soekadar, S. R. and Garcia-Aracil, N. (2019), 'User activity recognition system to improve the performance of environmental control interfaces: a pilot study with patients', *Journal of NeuroEngineering and Rehabilitation* **16**(1), p. 10, DOI: 10.1186/s12984-018-0477-5

- Journal Title: J. NeuroEng. Rehabil. (ISSN: 1743-0003).

- JCR-SCI Impact Factor (2018[1]): 3.582.

- Category: Rehabilitation, Quartile Q1 (4/65).

---

1 JCR-SCI Impact Factor of the year of publication is not available.

UNIVERSITAS
Miguel Hernández

AUTHORIZATION FOR SUBMITTING THE DOCTORAL THESIS

Supervisor: Nicolás Manuel García Aracil

Thesis Title: **Upper-limb Kinematic Analysis and Artificial Intelligent Techniques for Neurorehabilitation and Assistive Environments**

Author: Arturo Bertomeu Motos

Department of Systems Engineering and Automation
Miguel Hernández University of Elche

The undersigned thesis supervisor certify that THIS DOCTORAL THESIS HAS BEEN MADE UNDER MY SUPERVISION by Arturo Bertomeu Motos at the Department of Systems Engineering and Automation, Miguel Hernández University of Elche, and I hereby AUTHORIZE ITS SUBMISSION.

Elche, September 2019

Nicolás Manuel García Aracil

DOCTORAL PROGRAM IN INDUSTRIAL AND TELECOMMUNICATION TECHNOLOGIES

Dr. Óscar Reinoso García, Coordinator of the Doctoral Program in Industrial and Telecommunication Technologies at Miguel Hernández University of Elche,

CERTIFIES

That the work carried out by Arturo Bertomeu Motos, entitled **Upper-limb Kinematic Analysis and Artificial Intelligent Techniques for Neurorehabilitation and Assistive Environments**, has been supervised by Dr. Nicolás Manuel García Aracil, and that this work is adequate to be read and defended as a doctoral thesis to the corresponding jury in Miguel Hernández University of Elche.

And for the record and appropriate purposes, this certificate is issued.

Elche, September 2019

Óscar Reinoso García

X

ABSTRACT

Stroke, one of the leading causes of death and disability around the world, usually affects the motor cortex causing weakness or paralysis in the limbs of one side of the body. Research efforts in neurorehabilitation technology have focused on the development of robotic devices to restore motor and cognitive function in impaired individuals, having the potential to deliver high-intensity and motivating therapy.

End-effector-based devices have become an usual tool in the upper-limb neurorehabilitation due to the ease of adapting to patients. However, they are unable to measure the joint movements during the exercise. Thus, the first part of this thesis is focused on the development of a kinematic reconstruction algorithm that can be used in a real rehabilitation environment, without disturbing the normal patient-clinician interaction. On the basis of the algorithm found in the literature that presents some instabilities, a new algorithm is developed. The proposed algorithm is the first one able to online estimate not only the upper-limb joints, but also the trunk compensation using only two non-invasive wearable devices, placed onto the shoulder and upper arm of the patient. This new tool will allow the therapist to perform a comprehensive assessment combining the range of movement with clinical assessment scales.

Knowing that the intensity of the therapy improves the outcomes of neurorehabilitation, a 'self-managed' rehabilitation system can allow the patients to continue the rehabilitation at home. This thesis proposes a system to online measure a set of upper-limb rehabilitation gestures, and intelligently evaluates the quality of the exercise performed by the patients. The assessment is performed through the study of the performed movement as a whole as well as evaluating each joint independently. The first results are promising and suggest that this system can became a a new tool to complement the clinical therapy at home and improve the rehabilitation outcomes.

Finally, severe motor condition can remain after rehabilitation process. Thus, a technology solution for these patients and people with severe motor disabilities is proposed. An intelligent environmental control interface is developed with the ability to adapt its scan control to the residual capabilities of the user. Furthermore, the system estimates the intention of the user from the environmental information

and the behavior of the user, helping in the navigation through the interface, improving its independence at home.

RESUMEN

El accidente cerebrovascular o ictus es una de las causas principales de muerte y discapacidad a nivel mundial. Normalmente afecta a la corteza motora causando debilidad o parálisis en las articulaciones del mismo lado del cuerpo. Los esfuerzos de investigación dentro de la tecnología de neurorehabilitación se han centrado en el desarrollo de dispositivos robóticos para restaurar las funciones motoras y cognitivas en las personas con esta discapacidad, teniendo un gran potencial para ofrecer una terapia de alta intensidad y motivadora.

Los dispositivos basados en efector final se han convertido en una herramienta habitual en la neurorehabilitación de miembro superior ya que es muy sencillo adaptarlo a los pacientes. Sin embargo, éstos no son capaces de medir los movimientos articulares durante la realización del ejercicio. Por tanto, la primera parte de esta tesis se centra en el desarrollo de un algoritmo de reconstrucción cinemática que pueda ser usado en un entorno de rehabilitación real, sin perjudicar a la interacción normal entre el paciente y el clínico. Partiendo de la base que propone el algoritmo encontrado en la literatura, el cual presenta algunas inestabilidades, se ha desarrollado un nuevo algoritmo. El algoritmo propuesto es el primero capaz de estimar en tiempo real no sólo las articulaciones del miembro superior, sino también la compensación del tronco usando solamente dos dispositivos no invasivos y portátiles, colocados sobre el hombro y el brazo del paciente. Esta nueva herramienta permite al terapeuta realizar una valoración más exhaustiva combinando el rango de movimiento con las escalas de valoración clínicas.

Sabiendo que la intensidad de la terapia mejora los resultados de la recuperación del ictus, un sistema de rehabilitación 'auto-gestionado' permite a los pacientes continuar con la rehabilitación en casa. Esta tesis propone un sistema para medir en tiempo real un conjunto de gestos de miembro superior y evaluar de manera inteligente la calidad del ejercicio realizado por el paciente. La valoración se hace a través del estudio del movimiento ejecutado en su conjunto, así como evaluando cada articulación independientemente. Los primeros resultados son prometedores y apuntan a que este sistema puede convertirse en una nueva herramienta para complementar la terapia clínica en casa y mejorar los resultados de la rehabilitación.

Finalmente, después del proceso de rehabilitación pueden quedar secuelas motoras graves. Por este motivo, se propone una solución tecnológica para estas personas y para personas con discapacidades motoras severas. Así, se ha desarrollado una interfaz de control de entorno inteligente capaz de adaptar su control a las capacidades residuales del usuario. Además, el sistema estima la intención del usuario a partir de la información del entorno y el comportamiento del usuario, ayudando en la navegación a través de la interfaz, mejorando su independencia en el hogar.

A mi abuelo José.
A mis padres.
A mi familia.

ACKNOWLEDGMENTS

Esta tesis ha sido el resultado de un trabajo duro y constante en el que ha habido tiempo para todo, disfrutar investigando, aprender en cada congreso, días interminable en el laboratorio, risas, estancias, experimentaciones y un largo etcétera. Muchas gracias a todas las personas que me han acompañado durante este intenso viaje.

Primero quería agradecer a mi director de tesis por la oportunidad que me ha dado de formar parte de su equipo y de la confianza depositada durante todos estos años. También a Ricardo por iniciarme en el mundo de la investigación, transmitiéndome la cultura del esfuerzo, teniendo siempre en cuenta hasta el más mínimo detalle. A Santi y a Juan por ofrecerme siempre el punto de vista clínico y enseñarme que los pacientes son siempre lo primero, aunque a veces se me siga olvidando, soy ingeniero. Como no podía faltar, gracias a Álvaro, Ariadna y María Dolores, esta aventura empezó junto a vosotros y, aunque hayamos compartido poco tiempo en los laboratorios, hemos pasado grandes momentos tanto dentro como fuera de ellos. Y también al resto de compañeros de laboratorio con los que he tenido el placer de trabajar, ofreciéndome su particular punto de vista.

Gracias a mis amigos, todos vosotros habéis aportado algo de una manera u otra a esta tesis, porque siempre estáis ahí cuando se os necesita y cuando no también.

Finalmente, gracias a mis padres y a mi familia por confiar siempre en mí, apoyándome en los buenos y malos momentos, sin vosotros esto no habría sido posible. Tío Pedro, esto es un poquito tuyo, me has demostrado que el trabajo duro tiene sus resultados y que el detalle es importante, aunque no se aprecie en el resultado final. Y que decirte a ti Andrea, gracias por estar siempre a mi lado, por confiar en mí en todo momento, por tener paciencia y por acompañarme hasta el fin del mundo si hace falta. Esta tesis ha sido un trabajo en equipo desde el primer momento, me has dado siempre la solución que necesitaba y me has animado en todo momento a continuar.

Algoritmos, Robots, bla bla, end.

CONTENTS

LIST OF FIGURES

LIST OF TABLES

ACRONYMS

ABI   Acquired Brain Injury

ADL   Activities of Daily Living

AT   Assistive Technology

BCI   Brain-Computer Interface

CNS   Central Nervous System

CRF   Conditional Random Fields

DH   Denavit-Hartenberg

DTW   Dynamic Time Warping

DoF   Degree of Freedom

DWMT   Daniels and Worthingham's Muscle Testing score

ECI   Environment Control Interface

EEG   Electroencephalography

sEMG   surface Electromyography

EOG   Electrooculography

ERD   Event-Related Desynchronization

HCI   Human-Computer Interaction

IMU   Inertial Measurement Unit

JCR   Journal Citation Reports

MARG Magnetic Angular Rate Gravity

OIESGP Online Infinite Echo-State Gaussian Process

PNF   Proprioceptive Neuromuscular Facilitation

R   Correlation

RMSE Root Mean Square Error

ROM   Range of Movement

SCI   Spinal Cord Injury

SD   Standard Deviation

SMR   Sensorimotor Rhythm

SVM   Support Vector Machine

VR   Virtual Reality

INTRODUCTION

The human brain is a complex network of billions of neurons accompanied by glial cells that not only provide support and protection for neurons, but also are involved in the active control of neuronal activity and synaptic neurotransmission (Araque et al., 1999). Furthermore, lifelong learning makes neural connections constantly formed and reorganized. Moreover, adult hippocampal neurogenesis, the addition of new neurons throughout life, has been recently detected in the human brain by Moreno-Jiménez et al. (2019).

The brain serves as the center of the nervous system and, together with the spinal cord, makes up the Central Nervous System (CNS). However, an Acquired Brain Injury (ABI), i. e. a sudden brain damage caused by events after birth, involves injury in the CNS leading a permanent or temporary change in functioning, depending on the affected area of the brain. ABI results from either traumatic brain injury or non-traumatic injury, such as stroke, brain tumor, hypoxia or ischemia, that can cause cognitive, physical, emotional, or behavioral impairments. Over the past few years, stroke has become the second world cause of death (Donnan et al., 2008); it is caused by a disturbance in the blood supply to the brain either by a blockage, isquemic, or by a rupture of a blood vessel, hemorrhagic. Within this thesis, rehabilitation and assistance are focused on people who suffered from a stroke affecting the motor cortex, usually presenting symptoms of weakness, namely hemiparesis, or complete paralysis, namely hemiplegia, in one entire side of the body.

From the onset of stroke, patients experience different mechanisms of recovery involved with plasticity in the intact brain (Murphy and Corbett, 2009). Furthermore, spontaneous behavioral recovery takes an important role in the early stage of the injury, when the brain is galvanized to initiate repair (Cramer, 2008). Even functional behavior of stroke survivors are unlikely to be identical to pre-stroke patterns, strategies promoting synapse and network level plasticity lead to an important functional recovery (Taub et al., 2002; Kleim and Jones, 2008; Kerr et al., 2011). Indeed, motor and cognitive rehabilitation aims to improve the quality of life of patients through dedicated rehabilitative strategies. These therapies enhance motor impairments, one of the

main disabilities associated with stroke (Schaechter, 2004; Dimyan and Cohen, 2011), through both physical and occupational therapy exercises.

Robot-aided neurorehabilitation therapy, integrated into a multi-disciplinary program, plays a significant role in motor and cognitive recovery at different stages of stroke recovery: acute, subacute and chronic phases (Volpe et al., 2000; Lo et al., 2010; Klamroth-Marganska et al., 2014). These robotic systems have the potential to deliver high-intensity, challenging, motivating and reproducible therapy making the training tasks and exercises meaningful and important for the patient. Robotic devices for upper limb used in neurorehabilitation can be divided in two main groups: exoskeleton-based and end-effector-based. Exoskeleton-based robots allow to accurately control the kinematic configuration of the corresponding joints, while end-effector-based robots apply mechanical forces to the distal part of the limb, as shown in Figure 1.1. The fusion of these kind of therapies with new technologies, such as Virtual Reality (VR), functional electrical stimulation, Brain-Computer Interface (BCI) or brain stimulation, have demonstrated to be a poweful tool to maximize patient recovery (Krebs et al., 1998; Alon et al., 2007; Bohil et al., 2011; Chaudhary et al., 2016). Furthermore, this technology offers multiple objective data that, together with clinical assessment scales, allows the therapist to get a comprehensive assessment about the patient's improvements.
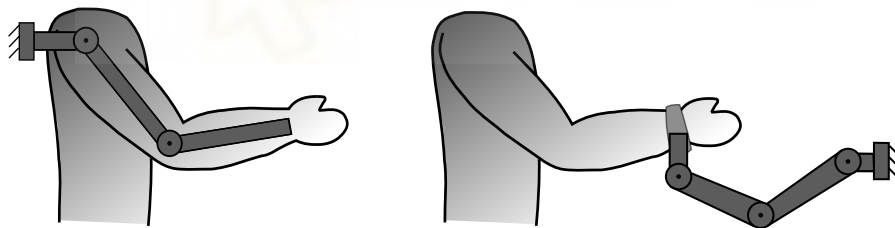
Figure 1.1: Robotic devices for upper limb used in neurorehabilitation can be divided in exoskeleton-based *(left)*, and end-effector-based type *(right)*.

Finally, after rehabilitation process, most stroke survivors still experience significant motor limitations several months or years after the incident (Kwakkel et al., 2003; Meyer et al., 2015). This affects negatively their activities of daily living (ADL) in which they need help with daily tasks or walking, decreasing their participation in social activities. The improvement of smart devices and technology are pushing research in the field of assistance to people with disabilities, including stroke survivors, moving technology from laboratories

and controlled environments to homes, enhancing their independence (Bradley and Poppen, 2003; Matarić et al., 2007).

1.1 MOTIVATION AND OBJECTIVES

About 6.8 million people in the world died in 2016 as a result of neurological disorders, according to World Health Organisation (2018a), and as the global population ages, an increase to 8 million is estimated in 2030, according to World Health Organisation (2018b); this effect results in a global and regional burden of stroke (Feigin et al., 2014). Different studies show that patients who have impairments after stroke and are expected to be able to return home, are likely to benefit from inpatient rehabilitation. These improvements in movement and language skills are possible at any time after stroke (Dobkin, 2005). In addition, European Comission (2010) presented a strategy promoting a barrier-free Europe and empowering people with disabilities, around one in six people in the European Union, so they can enjoy their rights and fully participate in society and economy. Only in Spain, the cost of cerebrovascular disease is estimated in 6.000 millions of euros per year (Mar et al., 2013) and 104.701 new cases of ABI occur every year, according to Federación Española de Daño Cerebral (2016). The Valencian Community is one of the first autonomous communities to implement an strategy for attention to brain damage, in which the robotic and virtual rehabilitation are included (Generalitat Valenciana, 2017).

As previously stated, robotics in the field of neurorehabilitation has proved to be a powerful tool in upper-limb motor recovery for stroke patients (Lum et al., 2002; Cameirão et al., 2012; Duret et al., 2019). Robot-aided therapy enables highly repetitive, intensive, and adaptive training and offers quantifiable physical data to the therapist, complementing the clinical assessment scales, such as Fugl-Meyer (Fugl-Meyer et al., 1975) or Asworth (Bohannon and Smith, 1987), among others (Santisteban et al., 2016). Since the first end-effector-based robot for upper limbs used in neurorehabilitation, the MIT-Mannus (Hogan et al., 1992), these devices have become the most used devices owing to the ease of attachment to the affected limb in patients with different pathologies and their demonstrated positive outcomes (Kwakkel et al., 2007; 2019). However, these devices are unable to measure or control the ROM of the upper limb during the rehabilitation tasks, a very important parameter in monitoring recov-

ery progress during stroke rehabilitation (Hingtgen et al., 2006; Beebe and Lang, 2009).

On the other hand, majority of the studies are focused on how new technology can be used to enhance the rehabilitation process at clinical environments but, nevertheless, just few approaches try to offer a technology solution when stroke survivors have to return home and deal with the residual motor impairments. In this field, intelligent rehabilitation systems for upper limbs in home environments can enhance cognitive and motor recovery during and after the rehabilitation process performed in the clinic. Furthermore, the environmental information and the person behaviors at home enable machine learning techniques to understand daily routines, offering a powerful 'assistance as needed' tool and, therefore, favoring the inclusion of the people with severe motor impairments in daily tasks (Bradley and Poppen, 2003).

This thesis endeavors to develop an objective tool to measure, in real time, the upper-limb joints in neurorehabilitation therapies assisted by end-effector-based robots and validate it in a real rehabilitation scenario. Furthermore, as the intensity of the therapy takes an important part in stroke recovery, this thesis aims to propose an artificial intelligent solution to fill the time interval between clinical sessions and after therapy through a system for 'self-managed' rehabilitation. Finally, to contribute to the assistance at home of people who suffer from severe motor impairments after stroke rehabilitation, caused by a neurodegenerative disease or Spinal Cord Injury (SCI), it is attempted to develop an intelligent environment control interface (ECI) and test it through people with different pathology in order to improve their independence at home. Furthermore, it is intended to adapt the system control to the residual user capabilities.

The focus on the neurorehabilitation is grounded on the firm belief that objective data provided by robots are becoming an important part in the assessment of the patient evaluation during the therapy, on the one hand, and that intelligent solutions for home environments can improve the recovery after stroke, on the other. Furthermore, help in the performance of ADL has the capacity to offer independence for people with severe motor impairments, decreasing their sense of isolation (Bradley and Poppen, 2003).

1.2 CONTRIBUTIONS

The work presented in this thesis provides the following contributions:

- It improves the previous upper-limb kinematic reconstruction algorithm for robot-aided neurorehabilitation therapies, introduced by Papaleo et al. (2015). It is based on the same technique, the estimation of the seven joint variables through the augmented Jacobian (Kreutz-Delgado et al., 1990) for end-effector-based devices, using only one accelerometer. The proposed method for estimating the joint movements is more stable against undesired shoulder movements, without losing precision. This problem is further discuss in Section 3.8, reviling the necessity to measure the trunk compensation during the rehabilitation exercise.

- It develops a novel technique to online measure not only the upper-limb movements, but also the shoulder displacement in robot-aided neurorehabilitation therapies. It uses only two wearable devices, one placed onto the upper arm and the other onto the shoulder. Thus, it modifies the previous proposed method, fixing the flexion-extension and the ulnar-radial deviation movements of the wrist, tight by most end-effector-based robots. The proposed algorithm is successfully tested in clinical environments, offering a new tool to assess the motor recovery of the patients.

- It describes a novel upper-limb gesture assessment method that fuses a machine learning classification model with the measurement of the distance between the expert and patient joint movements. The promising finding is that the applied technique is able to online evaluate the quality of the movement performed by the patient, deciding the next step in the rehabilitation exercise. Thus, this system can become a new tool for 'self-managed' rehabilitation at home.

- It proposes an intelligent ECI that uses the environmental information and the user behaviors to detect the intention of the users easing the navigation through it. Furthermore, it is able to adapt to the residual capabilities of the users favoring its use by people with many different motor or cognitive impairments. Thus, this ECI enhances the independence of people with severe motor impairments at home.

Appendix B lists and describes the publications derived from this thesis.

1.3 THESIS ROADMAP

This thesis is organized over six chapters followed by two appendix:

- **Chapter** 2 provides background that is relevant for the developments reported in the thesis. Specifically, it reports on robot devices for upper limb neurorehabilitation, it provides an overview of motion capture systems for rehabilitation, and it introduces works on intelligent technology solutions for rehabilitation and assistance at home.

- **Chapter** 3 introduces an stable upper-limb kinematic reconstruction algorithm for robot-aided neurorehabilitation therapies, using only the information provided by an accelerometer placed onto the upper arm. Furthermore, the validation of the algorithm is performed in a simulated and real scenarios. Finally, this algorithm is studied in a clinical environment with patients demonstrating the improvements performed over the Papaleo et al. algorithm.

- **Chapter** 4 solves the problem of the fixed shoulder assumption presented in the previous chapter. It introduces a modification of the algorithm in order to estimate not only the upper-limb joint variables but also the shoulder displacements. Thus, this method enables to measure the ROM and trunk compensation without disturbing the patient-clinician interaction in real neurorehabilitation environments.

- **Chapter** 5 presents two applications of artificial intelligent solutions, one for stroke rehabilitation of the upper-limbs at home, the other for enhance the independence of people with severe motor capabilities. The former proposed a system to measure and classify a set of predefined gestures, and intelligently assess the quality of the performed movement guiding the patient through the rehabilitation exercise. The latter uses the information acquired from the environment and the user behaviors to detect the intention of the user and ease the navigation through an intelligent ECI.

- Finally, **Chapter** 6 summarizes this thesis and draws conclusions based on the findings of the work reported here. In addition, the chapter discusses potential directions for future research on topics covered within this thesis.

- **Appendix** A describes the robots, sensors, and components that were used along the different scenarios presented in this thesis.

- **Appendix** B presents the prints of the compendium of peer-reviewed publications, previously published in indexed journals according to the last JCR.

1.4 PUBLICATIONS

This section contains references and short summaries of all peer-reviewed publications made during the course of this PhD that form the main work of the thesis, with the relevant chapters in which they are contained:

Bertomeu-Motos, **A.**; Blanco, A.; Badesa, F. J.; Barios, J. A.; Zollo, L. and Garcia-Aracil, N. (2018), 'Human arm joints reconstruction algorithm in rehabilitation therapies assisted by end-effector robotic devices', *Journal of NeuroEngineering and Rehabilitation* **15**(1), p. 10, DOI: 10.1186/s12984-018-0348-0

  - Validates a novel technique to online estimate the upper-limb kinematic configuration for neurorehabilitation therapies with end-effector-based robotic devices. It solves the instabilities that the previous algorithm had when it was applied in clinical environments.

  - Chapter 3 is based on this article.

Bertomeu-Motos, **A.**; Lledó, L. D.; Díez, J. A.; Catalan, J. M.; Ezquerro, S.; Badesa, F. J. and Garcia-Aracil, N. (2015b), 'Estimation of Human Arm Joints Using Two Wireless Sensors in Robotic Rehabilitation Tasks', *Sensors* **15**(12), pp. 30571–30583, DOI: 10.3390/s151229818

  - Presents and validates a novel algorithm to online estimate not only the upper-limb kinematic configuration but also the shoulder displacements, a very important information to perform a comprehensive assessment, for robot-aided neurorehabilitation therapies.

  - Chapter 4 is based on this article.

Bertomeu-Motos, **A.**; Ezquerro, S.; Barios, J. A.; Lledó, L. D.; Domingo, S.; Nann, M.; Martin, S.; Soekadar, S. R. and Garcia-Aracil, N. (2019), 'User activity recognition system to improve the performance of environmental control interfaces: a pilot study with patients', *Journal of NeuroEngineering and Rehabilitation* **16**(1), p. 10, DOI: `10.1186/ s12984-018-0477-5`

- Proposes a novel intelligent ECI for people with severe motor disabilities able to estimate the user intention and assist in the navigation and control through the interface. It uses a multimodal system in order to exploit the residual motor capabilities of the user, and learn from the user behavior and the relevant environmental information.

- Section 5.2 is based on this article.

BACKGROUND

Two main research fields inspired this thesis, the neurorehabilitation therapies assisted by robots and the intelligent technology solutions for people with motor and cognitive impairments. This chapter aims to review the relevant articles from these fields that are significant to later chapters of the thesis.

The chapter is organized as follows. In Section 2.1, the most common robotic devices used in neurorehabilitation therapies for upper limbs are briefly introduced, with a particular emphasis on works that demonstrate the effectiveness of these devices. Section 2.2 then discusses studies that introduce different strategies to measure the kinematic behavior of the body while the patient performs a rehabilitation exercise. These strategies go from motion analysis to VR feedback in rehabilitation games. Then, Section 2.3 presents a literature review in the field of technology solutions for home environments and how elderly, children, and people with disabilities benefit from it. Finally, Section 2.4 summarizes the chapter.

2.1 ROBOTIC DEVICES FOR UPPER-LIMB NEUROREHABILITATION THERAPIES

After an ABI, neurorehabilitation therapy aims to recover the motor and cognitive functions. It is known that repetitive and intensive training enhance the neuroplasticity of the brain improving the results of the therapy (Krebs et al., 1998). These features can be exploited by robots, reducing the workload of the therapists and offering a new rehabilitation and assessment tool. In the last 30 years, multiple projects and research studies are developing a wide variety of upper--limb robots for rehabilitation that, although they have proven their effectiveness, their availability in clinical setting is limited and only few rehabilitation robots can be found on the market. Comparing the mechanical structure of the robotic devices found in literature, two categories are considered and described in this section: end-effector-based and exoskeleton-based devices (Maciejasz et al., 2014), even though there are many systems fusing both structures. The main

difference between this two devices is how the movement is transferred from the device to the patient's upper extremity. In addition, both groups usually offer task-specific interactive virtual reality games to promote motivation and the possibility of repeating the exercise without the presence of the therapist.

2.1.1   *End-effector-based Devices*

The first upper-limb neurorehabilitation robot was developed by Hogan et al., in 1992. It was an end-effector-based device where the hand of the patient is attached to the end effector of the robot, actuating at the wrist joint and allowing to perform planar movements with the arm. Furthermore, this robot offered different levels of assistance to promote learning.

Table 2.1: End-effector-based devices for upper-limb rehabilitation.

System name	Institution	Supported Movements	Studies
InMotion[1]	Bionik Laboratories[2]	Shoulder and elbow	Krebs et al. (1998), Krebs et al. (2004)
iPAM	University of Leeds	Shoulder, elbow and wrist	Jackson et al. (2007), Culmer et al. (2011)
Gentle/S	University of Reading	Shoulder, elbow and wrist	Loureiro et al. (2003), Amirabdollahian et al. (2007), Kwakkel et al. (2007), Coote et al. (2008)
MIME	Standfor University	Shoulder and elbow	Burgar et al. (2000), Lum et al. (2002), Lum et al. (2006)
PUPArm	Miguel Hernández University	Shoulder and elbow	Llinares et al. (2013), Lledó et al. (2016)

Since then, multiple end-effector-based robots have been developed due to its simple mechanical structure and control algorithm. They also offer an easy set-up, allowing their use by patients with many

---

1 Based on MIT-Manus (Hogan et al., 1992)
2 Resulting from research at the Newman Laboratory for Biomechanics and Human Rehabilitation at the Massachusetts institute of technology

different pathology. However, the control of the limb configuration during the exercise is limited and it is difficult to isolate specific movements of a particular joint. Table 2.1 presents the most relevant end-effector-based rehabilitation robots and their clinical studies that show its effectiveness in neurorehabilitation therapies.

2.1.2 *Exoskeleton-based Devices*

The exoskeleton-based devices aim to apply mechanical force at the limb joints based in a structure that mirrors the skeletal structure of the human limb. Thus, a particular joint of the limb is directly moved through a particular joint of the device, and each segment of the limb is attached to the corresponding segment of the device. This structure allows independent and precise control of movements at the desired joints. Lower limb exoskeleton have been widely used in clinical environments since 1960s, improving the patient's recovery efficacy (Colombo et al., 2000; Veneman et al., 2007; Yan et al., 2015). However, upper-limb exoskeletons have been only recently developed and, in contrast to end-effector based devices, their effects are not strongly demonstrated (Jarrassé et al., 2014). Indeed, at the end of 2011 the first upper-limb exoskeleton was released(Riener et al., 2011).

Table 2.2: Exoskeleton-based devices for upper-limb rehabilitation

SYSTEM NAME	INSTITUTION	SUPPORTED MOVEMENTS	STUDIES
ARMin	ETH Zurich	Shoulder and elbow	Nef et al. (2007), Staubli et al. (2009)
T-WREX	University of California	Shoulder, elbow and wrist	Sanchez et al. (2004), Housman et al. (2007)
L-EXOS	Scuola Superiore Sant'Anna	Shoulder and elbow	Montagner et al. (2007)
RUPERT	Arizona State University	Shoulder, elbow and wrist	He et al. (2005)

Unlike end-effector devices, exoskeletons need an individual adjustment of the length of the device segments according to the patient limb in order to avoid injuries. Therefore, setting-up these devices for a particular patients may take a significant amount of time. Furthermore,

the rotation of the device joints must be aligned with the center of rotation of the human limb and must be able to adapt according to the changes of joint positions during movements, specially in the shoulder joint (Kiguchi et al., 2003). For this reason, the complexity of the mechanical design and the control algorithm are usually higher than of the end-effector-based devices, one of the possible reasons of the slow development of these devices. The most relevant exoskeleton-based devices and their clinical studies are presented in Table 2.2.

2.2   MOTION CAPTURE SYSTEMS FOR REHABILITATION

The motion capture aims to record the movement of a subject in real life and translate it into digital data to perform an extensive biomechanic analysis. This field is widely studied motivated by their multiple application in athletic performance analysis, human-robot interaction or activity monitoring (Aggarwal and Cai, 1999). In rehabilitation, these systems offer an objective measurement tool to assess motor recovery of stroke patients (Repnik et al., 2018). They are being combined with clinical assessment scales, in which the ROM of the limbs are subjectively evaluated (Santisteban et al., 2016). In addition, the information provided by these systems is also used as an input data in the development of VR-based games for rehabilitation therapies, namely serious games. These games offer visual feedback to the patient during the exercise, integrating the patient into the virtual environment and optimizing the motivation and commitment (Burke et al., 2009). Regarding the technology used to measure the body motion, three categories are considered and described in this section: optoelectronic, vision-based and wearable inertial-based device systems (Zhou and Hu, 2008).

2.2.1   *Optoelectronic Systems*

The use of multiple cameras in controlled environments to estimate 3D coordinates of retro-reflective markers from 2D cameras projections has been extensively applied (Abdel-Aziz et al., 2015), firstly used for motion tracking by Johansson (1975). This motion capture systems use a set of markers attached onto the body or onto a specific body segment (Carse et al., 2013; Murphy et al., 2011), and they can be divided in two groups: active and passive systems. Active systems usually use infrared light emitting markers, mostly LEDs, which are then

acquired by the cameras. Passive systems use retro-reflective markers and infrared cameras to detect the incoming radiation provided by the markers.

Optoelectronic systems, even they are usually expensive, are widely used in biomechanical analysis due to the high precision presented (Windolf et al., 2008). They calculate the joint centers and the segment orientations by optimizing skeletal parameters from the markers (Charlton et al., 2004). Thus, these systems are usually used as a 'ground truth' to evaluate the motion measurements performed through a different system(Zhou et al., 2006). However, they must be used in a specific area, whenever the cameras can visualize the markers, and in controlled environments, avoiding marker occlusions (Wu and Boulanger, 2011; Federolf, 2013).

2.2.2 *Vision-based Systems*

This technique exploits cameras to track movement of human body, identifying standard bony landmarks through computer vision algorithms and overcoming the occlusion problem. These methods aim to segment the image into regions and extract the subject information from the acquired image, viewed as a single object or as an articulated motion. In 1999, Aggarwal and Cai reviewed work prior to 1998 concluding that the recognition of human motion was just in its infancy. They used a taxonomy with three categories: body structure analysis, tracking and recognition. Then, Moeslund and Granum introduced the functional structure of motion capture systems as a subsequent processing phases: initialization, tracking, pose estimation, and recognition, however, not all systems needed to include this four processes.

In 2007, Poppe divided the human motion into modeling and estimation phase, based on the new trends of research. Is in the estimation phase, the process to find the most likely human pose with respect to the human body model, where the neurorehabilitation takes advantage. It uses this estimation to monitor the capabilities of the patients, integrating them with VR-based games.

In the last decade, serious games have proven their effectiveness in neurorehabilitation and they are becoming more popular due to the low cost of high speed cameras, facilitating the development of games in real time (Burke et al., 2009). These games also allow to implement low-cost rehabilitation therapies at home and application

in elderly care (Saini et al., 2012; Webster and Celik, 2014). Finally, motion monitoring during rehabilitation exercises is used to correct compensatory postures in real time, as well as cognitive assessment (Taati et al., 2012; González-Ortega et al., 2014). Vision-based systems, as well as optoelectronic systems, must deal with limited environments and the potential obstruction of the cameras.

2.2.3 *Wearable Inertial-based Device Systems*

Unlike the systems previously described, inertial-based devices systems can be unobtrusively attached to the body limbs, monitoring patient movements in both clinic and home contexts due to the development of small sensors in the past decade. One of the first wearable sensor used for detection of human movement was an inertial device, studied by Saunders et al. in 1953. However, the use of inertial sensors was not a popular choice for motion tracking systems until their performance did not improve, being more compact and light. For example, in 1996, Veltink et al. proposed a method to differentiate static and dynamic activities using only an uniaxial accelerometer. Then, in 1998, Bussmann et al. was able to quantify different physical activities through four body-fixed accelerometers.

The following year, Bachmann et al. proposed a fusion of an accelerometer, a gyroscope and a magnetometer, namely magnetic angular rate gravity (MARG), to determine the orientation of a body human segment. Bachmann et al. solved the singularities associated with Euler angles, that make them unsuitable for use in body tracking application, introducing the quaternions as an alternative method of orientation representation. However, MARG devices can suffer from a loss of accuracy due to magnetic disturbances. Thus, in 2002, Mayagoitia et al. proposed a combination of only an accelerometer and a gyroscope, namely inertial measurement unit (IMU), as an alternative to optical motion analysis systems becoming the most common wearable sensor used for human motion capture.

From here, multiple research studies have developed systems capable of measuring the kinematic configuration of the lower-limb joints (Cooper et al., 2009; Seel et al., 2014; Fong and Chan, 2010) and upper-limbs joints (Zhou et al., 2006; 2008; Pérez et al., 2010), as well as systems that are able to classify motor activities (Novak et al., 2014; Valero et al., 2016). These studies are based on the calculation of the orientation associated with these devices using different types of fil-

tration algorithms (Marins et al., 2001; Sabatini, 2006; Madgwick et al., 2011; Mihelj et al., 2018). Finally, in the recent years, many studies are developing algorithms to avoid the magnetic disturbances of the MARG in order to increase its application areas (Šlajpah et al., 2017).

2.3 TECHNOLOGY SOLUTIONS FOR HOME ENVIRONMENTS

Technology, rehabilitation and assistance have a long individual history. However, the first use of a fusion of clinical rehabilitation and technology, in the field of ABI, appeared in 1992, with the first therapeutic arm robot, the MIT-Manus (Hogan et al., 1992). Thenceforth, many research studies have demonstrated that the technology in this field enhances the efficiency of neurorehabilitation therapies and provides objective data to assess the recovery progress (Basteris et al., 2014).

On the other hand, in 1998, the Association of Assistive Technology Act Programs introduced the Technology-Related Assistance for Individuals with Disabilities Act, motivating the scientific community to improve the functional needs of individuals with disabilities through assistive technology (AT). In this passage, AT device was defined as "any item, piece of equipment, or product system, whether acquired commercially, modified, or customized, that is used to increase, maintain, or improve functional capabilities of individual with disabilities". Since then, many studies provide technology solutions to assist people with disabilities in many different areas, such as communication or environmental control.

Thus, this section introduces a literature review of the technology applied to both rehabilitation and assistance fields, that, in the recent years, many technology solutions have left the laboratories caused by the continuous evolution of scientific research.

2.3.1 *Stroke Rehabilitation*

Disability and dependence associated with reduced motor function following stroke impact on the quality of life of patients, carers and family (Nichols-Larsen et al., 2005), and national economies (Truelsen et al., 2005). As said in Section 2.1, intense and repetitive therapy improves the rehabilitation outcomes in which robot-aided rehabilitation plays an important role in motor and cognitive recovery. However, in 2013, Demain et al. reported a discontinuity between therapy in hospital and at home, with long waits before home-based therapy.

Furthermore, people with stroke and their families suggested the use of new systems at home for 'self-managed' rehabilitation, after being taught at hospital, to fill the gap between clinical sessions optimizing functional recovery.

The home-based robotic systems must be safe to be used in home environments, as well as being able to easily configure and use without the therapist support. Furthermore, the therapist must remotely access to the device, collect the data gathered and ensure that appropriate therapy is being performed. Thus, in recent years, home-based systems for upper-limb rehabilitation are emerging owed to the good results demonstrated in clinical environments, such as end-effector based robots (Sivan et al., 2014; Nijenhuis et al., 2015), sensor-based virtual reality (Wittmann et al., 2016), or collaborative tele-rehabilitation (Johnson et al., 2008; Dodakian et al., 2017), offering a set of predefined exercises to be performed at home.

2.3.2 *Assistance in Daily Activities*

In the case of AT for assistance at home in ADL, different studies agree that technology has potential for enhancing the capabilities of people with physical disabilities. This technology aims to translate the user intention into functional interaction for communication or environmental control, among others (Tai et al., 2008). This translation can be divided in access technology, devices and processes that acquire and analyze the residual capabilities of the user and transform them into control signals, and user interface, usually a display screen, that shows the possible actions to be performed on the environment, namely ECI. Thus, the measurement of the effectiveness of the AT must consider the evaluation of this two elements.

There exist multiple access technology since this technology need to be adapted to the residual capacities of each individual users. The systems based on surface electromyography (sEMG) are non-invasive systems that record the electrical activity generated by muscles. One of the first systems was developed by Gryfe et al., in 1996, which enabled users with amyotrophic lateral sclerosis and virtually no movement to communicate and manipulate their environment with sEMG. Since then, many different studies have demonstrated the use of sEMG for Human-Computer Interaction (HCI) in patients with voluntary muscle contraction (Chen et al., 2002; Merletti and Parker, 2004; Ahsan et al., 2009).

In addition, eye movements are widely used for communication systems using oculography in two different ways: eye tracking systems and electrooculography (EOG) systems. Eye tracking systems compute the gaze direction measuring the offset between corneal reflection and pupil center through an infrared camera (Hansen and Ji, 2010). In 1998, Jakob described the first successful use of the eye movements tracking as in input for HCI. After that, eye-based HCI has matured considerably evolving from stationary setting to head-mounted eye tracking (Bulling and Gellersen, 2010). Today, multiple commercial eye tracking systems can be found, such as Tobii [3] or Pupil glasses [4]. On the other hand, the EOG systems measure the electric potential generated by the muscles around the eyes when the user changes gaze direction. In 1996, the first successful study was presented by Gips et al., which enabled people with disabilities to control a computer with an EOG-based system. Then, in 2009, a novel embedded EOG goggles were introduced by Bulling et al., they were able to long-term record data and stream processed EOG signals over Bluetooth with dry electrodes. Nowadays, these systems are widely used in multiple scenarios such as assistance, communication or activity recognition (Barea et al., 2011; Bulling et al., 2011; Soekadar et al., 2016).

The last access technology presented here is the electroencephalography (EEG), usually the only input signal that users with any physical ability can use to communicate with the environment. In 1929, EEG was firstly recorded in human by Berger, who also invented the electroencephalogram. This fact opened a new field of study with great potential in neurological diseases detection or direct environmental communication with the brain, among others. From there, many studies were conducted in which the EEG was analyzed (Gibbs et al., 1937; Blakemore and Cooper, 1970). But it was not until 1977, when Vidal developed a first BCI system, in which a human controlled a cursor in a 2D maze through EEG signals. Then, the interest in the development of BCI systems increased and, in 2000s, several studies achieved communication systems that do not depend on nerves and muscles activity. Thus, EEG became a new output channel for the brain with an adaptive capacity to optimize performance, appearing non-invasive and invasive techniques (Birbaumer et al., 2000; Donchin et al., 2000; Wolpaw et al., 2000; Wolpaw et al., 2002). In recent years, the technology improvements allow to bring non-invasive BCI systems out of the laboratory environments, offering grater independence

---

3 https://www.tobii.com/
4 https://pupil-labs.com/

to people with severe motor disability at home (Sellers et al., 2010; Miralles et al., 2015).

It was not found any research focused only in the development of a multipurpose ECI for assistance. However, the HCI and BCI systems introduced here were developed under different control interfaces. They were used as a single purpose interfaces, such as mouse control, communication, or external devices control, being able to only achieve the desired tasks.

2.4   CONCLUSION

This chapter presented theoretical and empirical works that investigate the use of robotic devices in neurorehabilitation therapies for post-stroke patients. It was demonstrated that both end-effector-based and exoskeleton-based devices improved the rehabilitation outcomes, although end-effector-based robots are most used in clinical environments due to the versatility they have to different pathologies. The chapter also highlighted the importance of objectively measure the motor improvements along neurorehabilitation therapy. Moreover, it was argued that clinical assessment scales should be supported by the information collected through these devices, with a particular emphasis in measuring the ROM of the limbs during the rehabilitation exercises with the robotic devices.

Since one of the aims of this thesis is to develop an algorithm for upper-limb kinematic reconstruction in neurorehabilitation with end-effector-based robots, the discussion moved to works investigating motion capturing systems in the field of rehabilitation. Wearable inertial-based device systems were found as the less intrusive system, i. e. it does not disturb the normal development of a therapy in which the therapist and the patients are continuously interacting. The first upper-limb kinematic reconstruction algorithm was introduced by Mihelj (2006), this method estimated the upper-limb joints with two accelerometers placed onto the upper arm. Subsequently, Papaleo et al. improved the algorithm using only the information provided by one accelerometer, but it was validated in a constrained and artificial environments with patients. The last step was performed by Morales Vidal, he developed an off-line algorithm, based on the same principle as Papaleo et al., introducing an approach to bring the kinematic reconstruction to a clinical environment, however this method was only tested in a simulated scenario. Therefore, this thesis seeks to go

beyond this algorithm and develop an online algorithm, establishing a protocol to be used in a real robot-aided neurorehabilitation therapy.

Technology solutions for home environments background was introduced within the last section, where new technology solutions for rehabilitation and assistance at home are necessary. It was argued that rehabilitation systems for home are increasing but there are still no clinical studies that support them. Finally, AT was proven to have great potential for those who suffer severe motor impairments as the advancements of access technology are taking these systems out of the laboratories.

UPPER-LIMB KINEMATICS RECONSTRUCTION ALGORITHM

This chapter describes the kinematic reconstruction algorithm, introduced by Morales Vidal, with the necessary modifications in order to online estimate the upper-limb joint movements in robot-aided neurorehabilitation therapies with end-effector-based devices. Section 3.1 presents the kinematic model of the upper limb used throughout this thesis and the protocol established to manually measure the upper arm and the forearm lengths. Then, the resolution of the upper-limb inverse kinematics, through the augmented Jacobian introduced by Kreutz-Delgado et al., and the estimation of the elbow pose, i. e. the orientation and the position, are introduced in Section 3.2 and Section 3.3, respectively. The estimation of the initial position of the upper-limb is presented in Section 3.4, it determines the starting point of the numerical integration proposed. Then, Section 3.5 shows the validation results obtained in a simulation environment and Section 3.6 in a real scenario with healthy subjects. In addition, Section 3.7 studies the stability of this algorithm and the Papaleo et al. algorithm in clinical environments with patients. Finally, Section 3.8 summarizes this chapter and discusses the limitations of the proposed algorithm.

Research from this chapter has been previously published in Bertomeu-Motos et al. (2015a) and Bertomeu-Motos et al. (2018).

3.1 KINEMATIC UPPER-LIMB MODEL

The human upper limb is a complex system of three segments: the upper arm, the forearm, and the hand. This extremity can be seen as a kinematic chain with seven rotational degrees of freedom (DoFs). From a mechanical point of view, the mobility of the shoulder, although it can be studied as a complex joint including scapular movements (Bagg and Forrest, 1988; Lenarčič and Umek, 1994; Inman et al., 1996), in this thesis it is modeled as a spherical joint of three DoFs, the abduction-adduction (sAB-AD), the flexion-extension (sF-E), and the internal-external rotation (sRot). The elbow can be modeled as a double-hinge joint with two DoFs, the flexion-extension (eF-E) and the

pronation-supination (wP-S). Even though the wP-S is an anatomical part of the elbow joint, it is considered as a mechanical joint of the wrist and, therefore, the wrist joint is modeled as a spherical joint with three DoFs, the wP-S, the ulnar-radial deviation (wDev) and the flexion-extension (wF-E).

Figure 3.1 shows the kinematic chain of the right upper limb with the corresponding rotational movements, where the length of the upper arm and the forearm are expressed as l_u and l_f, respectively.
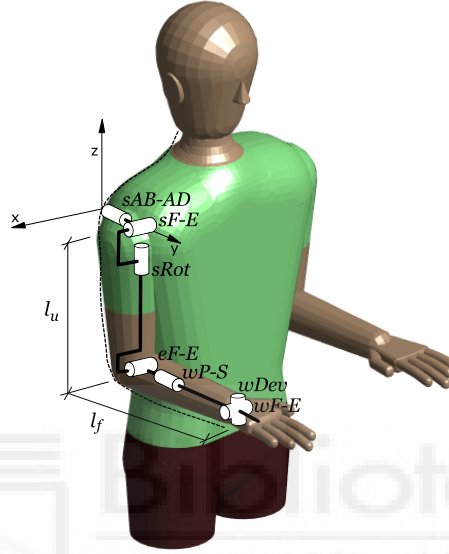
Figure 3.1: Kinematic chain of the right upper limb with each rotational joint movement, l_u and l_f define the length of the upper arm and the forearm, respectively.

Following the Denavit-Hartenberg (DH) convention (Denavit and Hartenberg, 1955), the reference frames of each joint movement have been selected for each limb as shown in Figure 3.2, the first reference frame is placed in the shoulder joint, indicated as $S0$. The corresponding DH parameters, presented in Table 3.1, determined the homogeneous transformation matrix necessary to calculate the forward kinematics from the frame i to the frame $i-1$, expressed as $^{i-1}T_i(q_i)$, with $i \in [1, 7]$.

Thus, the matrices related to the shoulder, elbow and wrist joints remain, respectively, as

$$^{0}T_3(q_1, q_2, q_3) = T_s = {}^{0}T_1(q_1) \cdot {}^{1}T_2(q_2) \cdot {}^{2}T_3(q_3), \qquad (3.1)$$

$$^{3}T_4(q_4) = T_e, \qquad (3.2)$$

$$^{4}T_7(q_5, q_6, q_7) = T_w = {}^{4}T_5(q_5) \cdot {}^{5}T_6(q_6) \cdot {}^{6}T_7(q_7), \qquad (3.3)$$

(a) Right limb.   (b) Left limb.
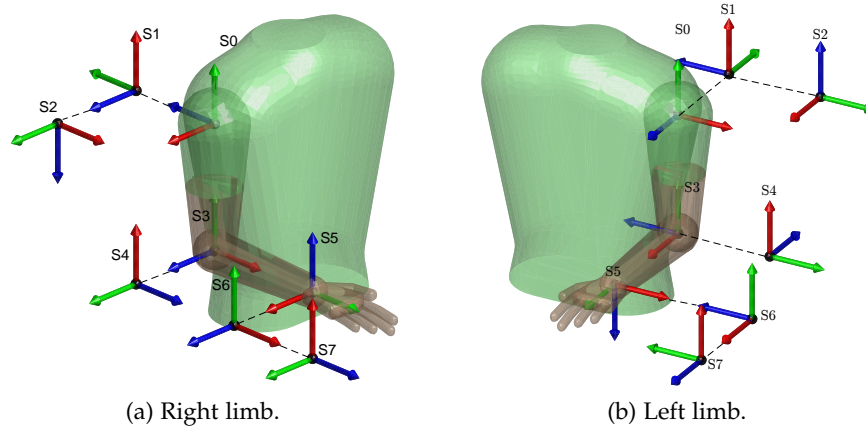
Figure 3.2: Reference systems of each joint variable following the DH convention presented on each upper limb.

and the forward kinematics that relates the hand pose as a function of all joint variables ($\vec{q}$) is obtained as

$$^0T_7\left(\vec{q}\right) = T_s \cdot T_e \cdot T_w. \tag{3.4}$$

Table 3.1: DH parameters of the upper limbs ($i \in [1, 7]$).

JOINT MOVEMENT	RIGHT UPPER LIMB				LEFT UPPER LIMB			
	θ_i	d_i	a_i	α_i	θ_i	d_i	a_i	α_i
sAB-AD	$\pi/2 + q_1$	0	0	$\pi/2$	$\pi/2 + q_1$	0	0	$-\pi/2$
sF-E	$3\pi/2 + q_2$	0	0	$\pi/2$	$3\pi/2 + q_2$	0	0	$-\pi/2$
sRot	q_3	l_u	0	$-\pi/2$	q_3	$-l_u$	0	$\pi/2$
eF-E	$\pi/2 + q_4$	0	0	$\pi/2$	$\pi/2 + q_4$	0	0	$-\pi/2$
wP-S	$\pi/2 + q_5$	l_f	0	$\pi/2$	$\pi/2 + q_5$	$-l_f$	0	$-\pi/2$
wDev	$\pi/2 + q_6$	0	0	$\pi/2$	$\pi/2 + q_6$	0	0	$-\pi/2$
wF-E	$\pi/2 + q_7$	0	0	$\pi/2$	$\pi/2 + q_7$	0	0	$\pi/2$

In addition, this thesis proposes a protocol to manually measure the upper-limb segments following Norton and Olds (1996). The upper arm is measured from the lateral side of the acromion to the proximal radius head, in the elbow, and the length of the forearm is determined from the proximal radius head to the radial styloid, the distal part of the radius.

3.2   INVERSE KINEMATICS ALGORITHM

In 1990, Kreutz-Delgado et al. presented a kinematic analysis for seven DoFs serial link manipulators with revolute joints to uniquely determine the inverse kinematics. The redundancy of these robots was characterized by a scalar variable, defined here as 'swivel angle' (α). Thus, if the upper limb is visualized as a redundant manipulator with seven DoFs, the swivel angle is defined as the angle between the plane shaped by the shoulder, elbow and wrist joints; and a reference plane (SVW), as shown in Figure 3.3.
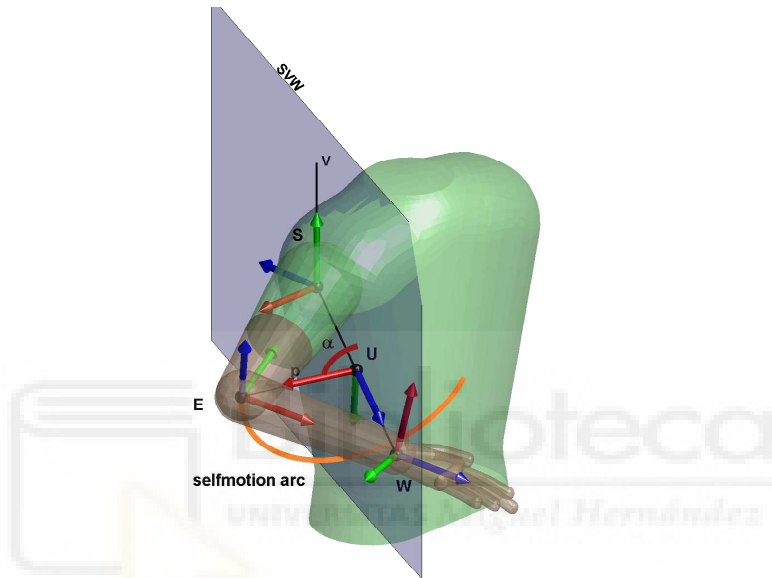
Figure 3.3: Graphic representation of the swivel angle.

Then, the inverse kinematics computation of these redundant manipulators is given by the augmented Jacobian ($J_A(\vec{q})$) (Kreutz-Delgado et al., 1990), which gives end-effector location and α as a function of the joint variables. It is expressed as

$$J_A(\vec{q}) = \begin{bmatrix} J_g(\vec{q}) \\ J_\alpha(\vec{q}) \end{bmatrix},\qquad(3.5)$$

where $J_g(\vec{q})$ is the geometric Jacobian of the upper-limb, i.e. the contribution of the joint speed vectors to the hand velocity, and $J_\alpha(\vec{q})$ is the α Jacobian, i.e. the contribution of the joint velocities with respect

to the rate of change of α. Thus, the inverse kinematics algorithm computed through $J_A(\vec{q})$, remains

$$\dot{\vec{q}} = J_A^{-1}(\vec{q}) \left\{ \begin{bmatrix} \vec{v} \\ \dot{\alpha} \end{bmatrix} + K \cdot \vec{err} \right\}. \tag{3.6}$$

Equation (3.6) expresses the joints velocity vector ($\dot{\vec{q}}$) regarding the inverse of the augmented Jacobian given the hand velocity vector ($\vec{v}$) and the amount of change of α ($\dot{\alpha}$). The term $\vec{err}$ is introduced to correct the error of the numerical integration method proposed, as the end-effector pose corresponding to the computed joint variables differ from the desired one (Siciliano et al., 2010). The gain matrix K is a positive definite matrix that determines the convergence rate to zero of the error.

In order to estimate the joint variables of the upper limb close to the singularities of this redundant manipulator, a damped least-squares inverse of the augmented Jacobian (J_A^*) is replaced to J_A in (3.6), this matrix is defined by Siciliano et al. as

$$J_A^* = J_A^T \left(J_A \cdot J_A^T + k^2 \cdot I \right)^{-1}, \tag{3.7}$$

where k is a damping factor that, chosen properly, permits a joint variable to be close to the singularity area, and I is the 7×7 identity matrix. Finally, the joint variables at time t_k, with $1 \leq k \leq n$ where $n \in \mathbb{N}$, are estimated as

$$\vec{q}(t_k) = \vec{q}(t_{k-1}) + \dot{\vec{q}}(t_k)\Delta t, \tag{3.8}$$

being $\vec{q}(t_{k-1})$ the previous joint variables and Δt the sampling rate. The estimation of the joint variables at time $k = 0$, necessary to initialize the proposed method, is presented in Section 3.4. The proposed numerical integration avoids huge jumps in consecutive joint variables, that can appear caused by jerk movements of the patient, as they can not be anatomically performed.

3.3 ELBOW JOINT POSE ESTIMATION

The kinematic reconstruction algorithm proposed in this thesis is developed to be used in robot-aided rehabilitation therapies with end-effector-based devices. In this context, the position of the wrist joint is provided by the robot since the hand of the patient is attached to

the end effector of the device. Furthermore, the shoulder joint pose is measured before the exercise and it is assumed fixed. Therefore, the estimation of the elbow joint pose is the key point of this algorithm, necessary to estimate the upper-limb joint variables through the augmented Jacobian (Kreutz-Delgado et al., 1990). This joint is estimated through the upper arm acceleration measured with an accelerometer device placed onto this segment. The acceleration data has two components, the static acceleration, related to the gravity, and the dynamic acceleration, related to the upper-limb movement. However, if slow movements are assumed, given the application to stroke rehabilitation, the static component dominates over the dynamic component and, therefore, the dynamic term of the acceleration can be removed. Thus, the proposed algorithm uses only the static acceleration in order to estimate the elbow joint pose. The mathematical description is performed for the right upper limb, the same principle is used to perform the left upper-limb kinematics reconstruction but with the proper DH parameters.

The main goal of this algorithm is to determine the proper orientation of the accelerometer when the patient performs the rehabilitation exercise, and therefore the elbow joint pose. The reference position of the upper limb is here defined as the position where $\vec{q} = \vec{0}$, shown in Figure 3.4. From this reference position, from the DH parameters, and from the initial values, the following matrices are known:

- T_r: homogeneous transformation matrix of $S0$, externally measured before the exercise.

- $^{r}T_w$: homogeneous transformation matrix from $S7$ to $S0$, given by end-effector robot.

- $^{r}R_{acc_0}$: reference rotation matrix from the accelerometer orientation to $S0$.

- $^{acc_0}R_e$: reference rotation matrix from $S4$ to the accelerometer orientation.

We start from the hypothesis that exists a rotation matrix ($^{acc_0}R_{acc}$) that relates the static acceleration at a known reference position ($^{acc_0}V_g$) with the acceleration at a random position of the upper limb ($^{acc}V_g$), defined as

$$^{acc_0}V_g = {}^{acc_0}R_{acc} \cdot {}^{acc}V_g, \tag{3.9}$$

where $^{acc_0}V_g = [\ 0\ 1\ 0\ ]^T$, normalized with respect to the gravity acceleration value.
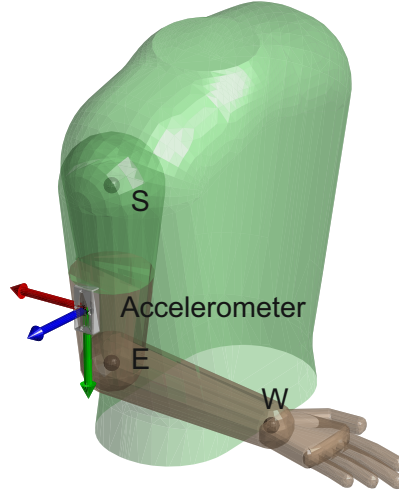
Figure 3.4: Reference position of the right upper limb.

However, it exists infinite rotation matrices that satisfies (3.9), but one possible solution can be obtained as

$$^{acc_0}\tilde{R}_{acc} = I + M + M^2 \frac{1 - \cos{(\theta)}}{\sin^2{(\theta)}}, \tag{3.10}$$

with

$$M = \begin{bmatrix} 0 & -V_z & V_y \\ V_z & 0 & -V_x \\ -V_y & V_x & 0 \end{bmatrix},$$

$$V = {}^{acc_0}V_g \times {}^{acc}V_g,$$

$$sin(\theta) = \|V\|,$$

$$cos(\theta) = {}^{acc_0}V_g \cdot {}^{acc}V_g.$$

Then, as the plane shaped by the X and Y axes of $^{acc_0}\tilde{R}_{acc}$ (Π plane in Figure 3.5) does not include the known wrist joint pose, the real rotation that the accelerometer suffers is computed forcing the Π plane to include the wrist joint. Thus, the Π plane is rotated around the gravity vector (g), placed at the shoulder joint, a specific angle (γ) until it includes the known shoulder (S) and wrist (W) joints, as shown in Figure 3.5, and therefore the proper accelerometer rotation is estimated.

The γ angle is the angle between W and its projection in Π ($\tilde{W}$), where $\tilde{W}$ is defined as

$$\tilde{W} = (g \cdot \hat{W}) g + \cos{(\gamma)} \left(\hat{W} - (g \cdot \hat{W}) g\right) - \sin{(\gamma)} \left(g \times \hat{W}\right), \tag{3.11}$$
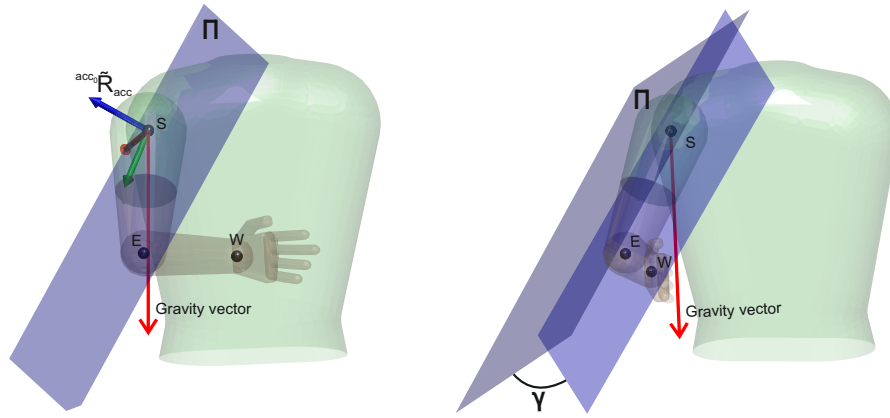
Figure 3.5: Graphic representation of the Π plane *(left)* and the γ angle *(right)*. It is also represented the gravity vector.

where

$$\hat{W} = \frac{(W - S)}{\| (W - S) \|},$$

$$g = \begin{bmatrix} 0 & 0 & -1 \end{bmatrix}^T.$$

Therefore, γ is calculated doing the distance be zero between W and Π as

$$d(W, \Pi) = \frac{|A_\Pi \tilde{W}_x + B_\Pi \tilde{W}_y + C_\Pi \tilde{W}_z + D_\Pi|}{\sqrt{A_\Pi{}^2 + B_\Pi{}^2 + C_\Pi{}^2}} = 0, \tag{3.12}$$

with

$$\begin{bmatrix} A_\Pi \\ B_\Pi \\ C_\Pi \end{bmatrix} = \overline{S\tilde{P}^y_{acc}} \times \overline{\tilde{P}^x_{acc}\tilde{P}^y_{acc}},$$

$$D_\Pi = \begin{bmatrix} A_\Pi & B_\Pi & C_\Pi \end{bmatrix}^T \cdot S,$$

and

$$\tilde{P}^x_{acc} = {}^{acc_0}\tilde{R}_{acc} \begin{bmatrix} 1 & 0 & 0 \end{bmatrix}^T,$$

$$\tilde{P}^y_{acc} = {}^{acc_0}\tilde{R}_{acc} \begin{bmatrix} 0 & 1 & 0 \end{bmatrix}^T,$$

$$\overline{S\tilde{P}^y_{acc}} = \left(\tilde{P}^y_{acc} - S \right),$$

$$\overline{\tilde{P}^x_{acc}\tilde{P}^y_{acc}} = \left(\tilde{P}^y_{acc} - \tilde{P}^x_{acc} \right).$$

From this point, the resolution of γ is computationally expensive and a simplification is needed to online estimate the upper-limb joint movements. Thereby, defining

$$a = A_\Pi \cdot \tilde{W}_x + B_\Pi \cdot \tilde{W}_y, \tag{3.13}$$

$$b = A_\Pi \cdot \tilde{W}_y + B_\Pi \cdot \tilde{W}_x, \tag{3.14}$$

$$c = A_\Pi \cdot S_x + B_\Pi \cdot S_y + C_\Pi \cdot (\tilde{W}_z + S_z) + D_\Pi, \tag{3.15}$$

the equation (3.12) remains

$$a \cdot cos\,(\gamma) - b \cdot sin\,(\gamma) + c = 0. \tag{3.16}$$

Then, multiplying and dividing by the norm of vector $\vec{ab}$, (3.16) yields

$$\sqrt{a^2 + b^2} \left[\frac{a}{\sqrt{a^2 + b^2}} \cdot cos\,(\gamma) + \frac{-b}{\sqrt{a^2 + b^2}} \cdot sin\,(\gamma) \right] + c = 0. \tag{3.17}$$

On the other hand, as the component of a vector divided by its norm varies between ± 1, the following approximation can be assumed

$$cos\,(\eta) = \frac{a}{\sqrt{a^2 + b^2}}, \tag{3.18}$$

$$sin\,(\eta) = \frac{-b}{\sqrt{a^2 + b^2}}. \tag{3.19}$$

Hence, (3.17) can be rewritten as

$$m\,[cos\,(\eta) \cdot cos\,(\gamma) + sin\,(\eta) \cdot sin\,(\gamma)] + c = 0, \tag{3.20}$$

$$m \cdot cos\,(\eta - \gamma) + c = 0, \tag{3.21}$$

being $m = \sqrt{a^2 + b^2}$. Thus, the desired γ value remains solved as

$$\gamma = \eta - arcos\left(\frac{-c}{m}\right), \tag{3.22}$$

where

$$\eta = artg\left(\frac{-b}{a}\right).$$

Finally, two possible γ values are obtained

$$\gamma_1 = artg\left(\frac{-b}{a}\right) - arcos\left(\frac{-c}{\sqrt{a^2 + b^2}}\right), \tag{3.23}$$

$$\gamma_2 = artg\left(\frac{-b}{a}\right) - arcos\left(\frac{-c}{-\sqrt{a^2 + b^2}}\right) - \pi. \tag{3.24}$$

These solutions allows us to solve (3.12) through simple mathematical operations obtaining two possible rotation matrices ${}^{acc_0}R_{acc}^{(j)}$, with $j \in [1, 2]$. Therefore, two elbow positions are derived from these matrices as

$$
{}^{r}P_e^{(j)} = {}^{r}T_{acc}^{(j)} \cdot \begin{bmatrix} 0 & l_u & 0 & 1 \end{bmatrix}^{T}, \tag{3.25}
$$

with

$$
{}^{r}T_{acc}^{(j)} = \begin{bmatrix} {}^{r}R_{acc_0} \cdot {}^{acc_0}R_{acc}^{(j)} & {}^{r}P_s \\ 0 & 1 \end{bmatrix},
$$

being ${}^{r}P_s$ the known shoulder joint position regarding $S0$. However, as the Z-axis of ${}^{acc_0}R_{acc}^{(j)}$ must point the same sense as the result of $\overline{EW} \times \overline{ES}$, only one solution satisfied this constrain. Thus, the elbow joint pose is estimated as

$$
{}^{r}T_e = \begin{bmatrix} {}^{r}R_e & {}^{r}P_e \\ 0 & 1 \end{bmatrix}, \tag{3.26}
$$

with

$$
{}^{r}R_e = {}^{r}R_{acc_0} \cdot {}^{acc_0}R_{acc} \cdot {}^{acc_0}R_e.
$$

Once the location of the elbow joint is estimated, the swivel angle, necessary to compute the augmented Jacobian, can be computed (Kreutz-Delgado et al., 1990). The last step of the algorithm is the estimation of the initial joints, explained in Section 3.4.

3.4   ESTIMATION OF THE INITIAL JOINTS

The initial joint variables are, a priori, unknown. However, it is possible to estimate them through the DH parameters. From Section 3.3, the elbow pose is estimated and, therefore, all the upper-limb joints are known: T_s, T_e, T_w. If the homogeneous transformation matrix is defined as

$$
T = \begin{bmatrix} n_x & n_y & n_z & p_x \\ o_x & o_y & o_z & p_y \\ a_x & a_y & a_z & p_z \\ 0 & 0 & 0 & 1 \end{bmatrix}, \tag{3.27}
$$

the shoulder movements remain

$$T_s = \begin{bmatrix} c_1 s_3 - c_3 s_1 s_2 & -c_2 s_1 & c_1 c_3 + s_1 s_2 s_3 & l_u c_2 s_1 \\ s_1 s_3 + c_1 c_3 s_2 & c_1 c_2 & c_3 s_1 - c_1 s_2 s_3 & -l_u c_1 c_2 \\ -c_2\, c_3 & s_2 & c_2\, s_3 & -l_u s_2 \\ 0 & 0 & 0 & 1 \end{bmatrix}, \qquad (3.28)$$

with $c_k = \cos(q_k)$ and $s_k = \sin(q_k)$, $k \in [1, 2, 3]$. Two possible solutions of the shoulder joint variables are obtained. Expressed following (3.27), the variables yields: (i) if $q_2 \in [0 \quad \pi]$

$$q_1 = \text{sAB-AD} = \text{atan2}\left(-n_y, o_y\right), \qquad (3.29)$$

$$q_2 = \text{sF-E} = \text{atan2}\left(a_y, \sqrt{n_y^2 + o_y^2}\right), \qquad (3.30)$$

$$q_3 = \text{sRot} = \text{atan2}\left(a_z, -a_x\right), \qquad (3.31)$$

and (ii) if $q_2 \in [-\pi \quad 0]$

$$q_1 = \text{atan2}\left(n_y, -o_y\right), \qquad (3.32)$$

$$q_2 = \text{atan2}\left(a_y, -\sqrt{n_y^2 + o_y^2}\right), \qquad (3.33)$$

$$q_3 = \text{atan2}\left(-a_z, a_x\right). \qquad (3.34)$$

The eF-E movement affects the distance $\overline{SW}$ and, therefore, it can be unequivocally estimated through the law of the cosines as

$$q_4 = \text{eF-E} = \arcsin\left(\frac{l_u^2 + l_f^2 - ||W - S||^2}{2 l_u l_f}\right), \qquad (3.35)$$

and T_e remains determined. Since the wrist pose is given by the end effector of the robot, T_w is determined following the same criterion used to solve the shoulder joint variables

$$T_w = (T_s \cdot T_e)^{-1} \cdot {}^r T_w, \qquad (3.36)$$

$$T_w = \begin{bmatrix} c_5 c_7 - s_5 s_6 s_7 & -c_6 s_5 & c_5 s_7 + c_7 s_5 s_6 & 0 \\ c_7 s_5 + c_5 s_6 s_7 & c_5 c_6 & s_5 s_7 - c_5 c_7 s_6 & 0 \\ -c_6 s_7 & s_6 & c_6 c_7 & l_f \\ 0 & 0 & 0 & 1 \end{bmatrix}, \qquad (3.37)$$

and two possible solutions are also obtained, the first solution is

$$q_5 = \text{wP-S} = -\text{atan2}\left(n_y, o_y\right), \tag{3.38}$$

$$q_6 = \text{wDev} = \arcsin\left(a_y\right), \tag{3.39}$$

$$q_7 = \text{wF-E} = -\text{atan2}\left(a_x, a_z\right), \tag{3.40}$$

and the second solution is

$$q_5 = \pi - \text{atan2}\left(n_y, o_y\right), \tag{3.41}$$

$$q_6 = \pi - \arcsin\left(a_y\right), \tag{3.42}$$

$$q_7 = \pi - \text{atan2}\left(a_x, a_z\right). \tag{3.43}$$

Thereby, four solutions, two from each spherical joint, satisfy the kinematic constrains and one solution, at least, accomplishes the anatomical features of the human upper limb. This statement is provable because the human upper-limb joints vary in $[-\pi/2 \quad \pi/2]$ range and each spherical joint solution belongs either $[0 \quad \pi]$ range or $[0 \quad -\pi]$ range. If more than one solution accomplishes the anatomical features, it is selected the closest solution to the center of the joint variables, i. e. the solution with the maximum weight ($w(\vec{q})$), described by Siciliano et al. as

$$w(\vec{q}) = -\frac{1}{2n} \sum_{i=1}^{n} \left(\frac{q_i - \bar{q}_i}{q_{iM} - q_{im}}\right)^2, \tag{3.44}$$

being $n = 7$ and where q_{iM} (q_{im}) denotes the maximum (minimum) joint limits and $\bar{q}_i$ the middle value of each joint range. In conclusion, this method establishes the initial values of the seven joint variables necessary to compute the proposed kinematic reconstruction algorithm.

3.5   VALIDATION IN SIMULATED ENVIRONMENT

Before study the proposed algorithm in a real environment, a simulated scenario was developed in order to test the theoretical development of the algorithm, in which the variables involved are controlled. For this purpose, the simulation of the upper-limb kinematics chain was developed in a Matlab® class, based on Corke (2011) toolbox. This class includes all the kinematic parameters and functions to simulate upper-limb trajectories knowing the joint variables at each point.

In addition, it also had the necessary functions for 3D visualization of the human body in order to represent the movements of the
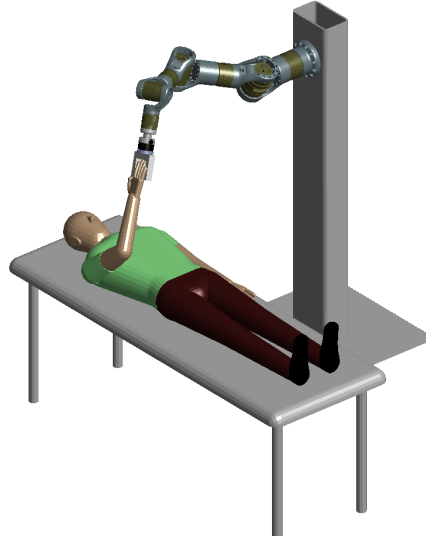
Figure 3.6: Simulated environment developed to test the kinematic reconstruction algorithm. The developed Matlab® class was able to simulate upper-limb movements and an end-effector-based robot.

right and left limbs. Furthermore, a simulation environment of an end-effector-based robot (for more information, please refer to Appendix A.1) was used. The 3D environment is presented in Figure 3.6. Finally, the static acceleration ($^{acc}V_g$) was modeled from the simulated upper-limb joint variables as

$$^{acc}V_g = {}^{e}R_{acc_0}^{-1} \cdot R_s^{-1} \cdot R_r \cdot {}^{acc_0}V_g. \tag{3.45}$$

The simulated joint trajectories of the right upper limb were determined following the *D1* Proprioceptive Neuromuscular Facilitation (PNF) diagonal (Voss et al., 1985), commonly used in neurorehabilitation therapies, guided by a simulated end-effector-based robot. Therefore, knowing the fixed shoulder joint and wrist joint poses along the upper-limb movement, the proposed method was evaluated.

3.5.1 *Results & Discussion*

In this scenario, the simulated upper-limb joint variables are compared against the estimated through the proposed algorithm. Figure 3.7 shows the seven upper-limb joint variables defined, blue smooth line, and the estimated, red dotted line, during the *D1* PNF diagonal. In addition, the root mean square error (RMSE), blue bar, and the maximum error, orange bar, are also shown. Furthermore, the normalized

wrist and elbow trajectories simulated and estimated are also shown as blue smooth and red dotted lines, respectively.
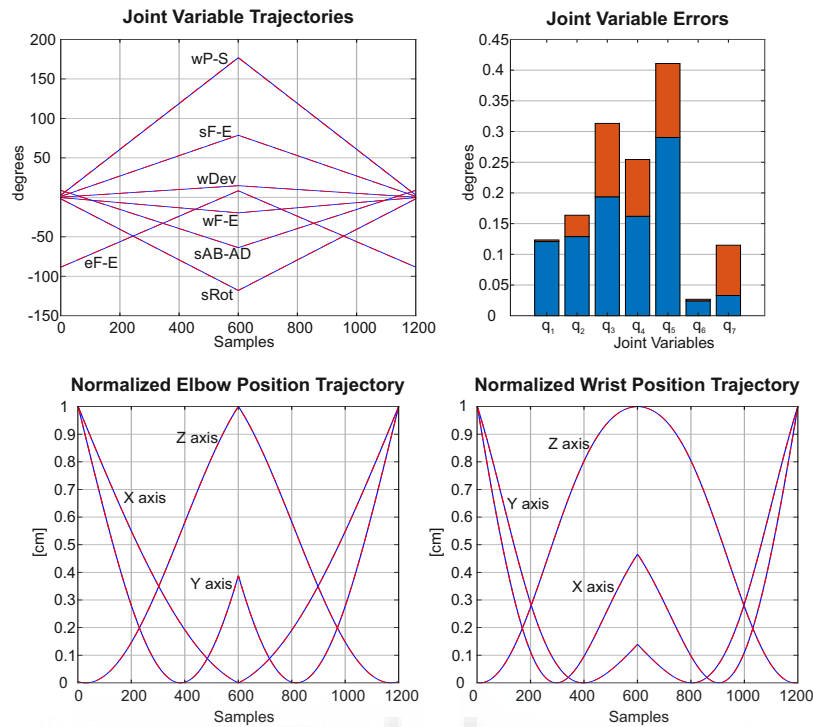
Figure 3.7: Simulation error regarding the joint variables and the normalized elbow and wrist positions. Blue smooth lines represent the defined trajectories and red dotted lines the estimated trajectories. In addition, the RMSE, blue bar, and the maximum error committed, orange bar, in terms of joint variables are shown.

The presented results show high accuracy, less than 1 *mm*, with respect to the two studied joints, at each axis. Regarding the joint variables, the maximum error committed at each joint movement is less than 0.5 *deg* with a mean RMSE of 0.1361 *deg*. This result demonstrates the precision of the proposed algorithm when all the constraints are controlled during the exercise. The next step is to evaluate this method in a real scenario with healthy subjects and an end-effector-based robot.

3.6 VALIDATION IN REAL ENVIRONMENT

Before the proposed algorithm can be used in a clinical environment, it is necessary to study its accuracy in a real environment with healthy subjects. The proposed scenario was composed by an end-effector-based robot with seven DoFs, the same robot used in the simulation scenario, an optoelectronic system, basad on eight six DoFs optical

tracking cameras Optitrack V100: R2 (see Appendix A.5 for more details), and an accelerometer device (see Appendix A.3), as shown in Figure 3.8.
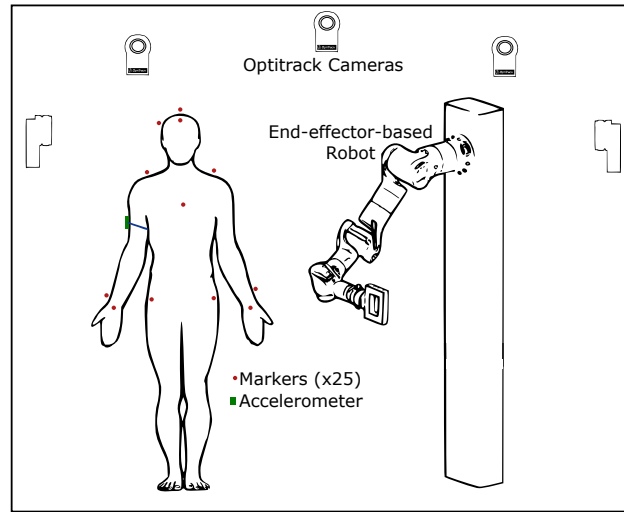
Figure 3.8: Healthy subjects performed arm movements using an end-effector-based robot with seven DoFs, wearing an accelerometer, placed onto the upper arm, and special jacket with 25 passive optoelectronic markers.

The real joint variables, defined as the 'ground truth', were measured through the optoelectronic system following the baseline upper body marker set (NaturalPoint, 2016), placing 25 retro-reflective markers onto a specific jacket as shown in Figure 3.8.

The proposed algorithm was applied with the gain matrix and the damping factor set to $K = diag\{1.5, 1.5, \cdots, 1.5\}$ N/ms and $k^2 = 0.5$, respectively, with a sampling rate of 100 Hz. They were chosen through a 'trial and error' approach, under the exercise conditions. The shoulder joint location was measured with the optoelectronic. However, although this joint is assumed to be fixed, little shoulder displacements may appear during the exercise. Finally, the hand of the user was tightly attached to the end effector of the robot remaining constant and known.

Seven right-handed healthy subjects performed three trials of a point to point task, previously established in the robotic device. Thus, the subjects only have to hold the end effector avoiding jerk and fast upper-limb movements. The main information of the healthy subjects is presented in Table 3.2.

Table 3.2: Demography of the healthy subjects.

ID	1	2	3	4	5	6	7
Age	24	31	24	26	29	24	25
Forearm length [m]	0.25	0.21	0.26	0.26	0.26	0.23	0.26
Upper arm length [m]	0.34	0.30	0.32	0.29	0.31	0.33	0.30

3.6.1 *Results & Discussion*

The accuracy of the proposed algorithm is measured as the difference between the estimated joint variables and the ones measured through the optoelectronic system, namely direct joint variables. Figure 3.9 shows an example of the direct joint variables online measured, blue smooth lines, and the estimated ones, red dotted lines, of a user performing the exercise. Table 3.3 shows the seven joint variables, the elbow joint position and the wrist joint position errors in terms of RMSE, standard deviation (SD), and correlation (R).
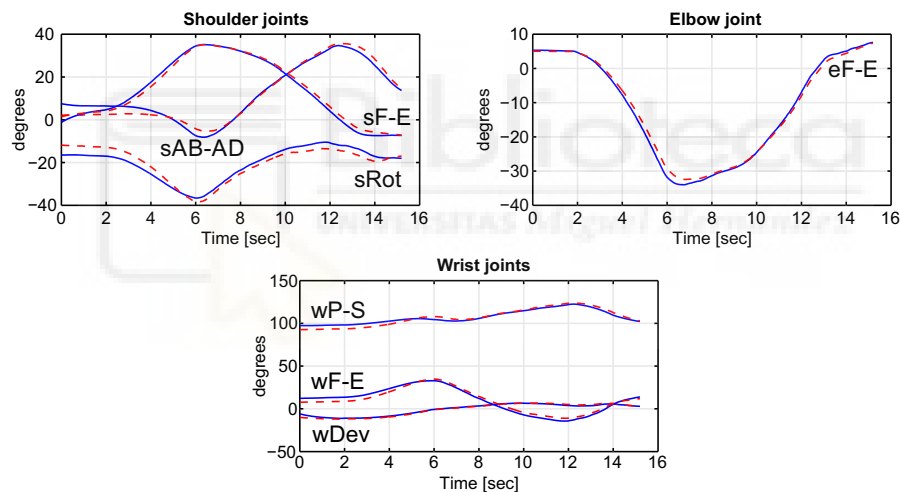
Figure 3.9: Joint variables of one trial performed by a healthy subject. The blue smooth lines represent the direct joint variables and the red dotted lines, the estimated joint variables.

The estimated joint variables show high correlation with respect to the direct joint variables. It must be noted that the elbow and wrist joint positions are accurately estimated, the RMSE is less than 2.5 *cm* in both joints. This error implies a RMSE less than 5 *degrees* in all joint variables with low SD. The minimum error is observed in eF-E movement and the maximum in the most distal movement, the wF-E, the most distal movement. Finally, the simplification performed to estimate the γ angle allowed the algorithm to be performed in real

time. Thus, the mean computational time necessary to estimate the current seven upper-limb joints was 0.9 *ms*, running on an Intel Core i7 3.40GHz computer with Matlab R2017a.

Table 3.3: Estimation error of the joint positions and movements regarding the optoelectronic system, mean of the seven subjects.

	RMSE	SD	R
ELBOW JOINT POSITION [CM]	2.13	1.10	0.977
WRIST JOINT POSITION [CM]	1.89	1.12	0.982
sAB-AD [DEG]	3.55	2.15	0.957
sF-E [DEG]	3.27	2.99	0.977
sROT [DEG]	4.57	3.04	0.966
eF-E [DEG]	1.72	1.54	0.995
wP-S [DEG]	4.51	2.74	0.873
wDEV [DEG]	2.83	2.23	0.899
wF-E [DEG]	4.74	3.28	0.982

From the results, it is concluded that the proposed algorithm is able to accurately estimate the seven upper-limb movements in real time. In addition, this technique do not disturb the normal patient-clinician interaction as it only uses one non-invasive wireless and wearable device placed onto the upper arm.

3.7   STABILITY OF THE ALGORITHM IN CLINICAL ENVIRONMENTS

Once it has been demonstrated that the proposed algorithm is suitable for this application, the last step is to study its stability in patients, where shoulder movements cannot be completely avoided. In this scenario, this algorithm was compared with the previously proposed by Papaleo et al.

This experiment was carried out by three post-stroke patients during a session of their rehabilitation therapy. The affected limb was evaluated through two assessment scales, Ashworth (Bohannon and Smith, 1987) for the elbow joint, and Fugl-Meyer (Fugl-Meyer et al., 1975) for the upper limb. Their scores are shown in Table 3.4.

The end-effector-based robot used was the PUPArm robot, a planar end-effector-based robot (Appendix A.2 contains more details about PUPArm robot). The wF-E and wDev remained fixed during the exercise, being able to estimate the shoulder displacements during the rehabilitation exercise through the algorithm proposed in the following

Table 3.4: Demographic and clinical characteristics of the post-stroke patients. Fugl-Meyer scale for upper extremity was divided in: A) Upper Extremity, B) Wrist, C) Hand, D) Coordination/speed

ID	AFFECTED LIMB	AGE	FOREARM LENGTH [M]	UPPER ARM LENGTH [M]	FUGL-MEYER (A+B+C+D)	ASHWORTH
1	Right	51	0.24	0.30	(33+7+7+2) /66	2
2	Left	58	0.25	0.33	(27+4+3+3) /66	3
3	Left	74	0.24	0.35	(24+2+2+1) /66	3

chapter, due to the optoelectronic system could not be installed in the clinical environment. Therefore, two wearable sensors were necessary to estimate the joint variables, an accelerometer, placed onto the upper arm, and a MARG (see Appendix A.3 for more details), placed onto the shoulder, as shown in Figure 3.10. Detailed explanation regarding the method used to measure the shoulder movements is described in Chapter 4.
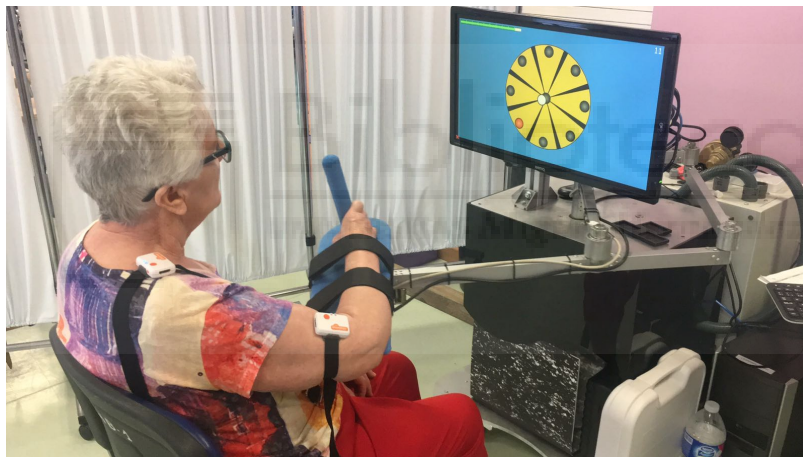
Figure 3.10: Patient performing a point to point exercise with the PUPArm robot, wearing a MARG, placed onto the shoulder, and an accelerometer, placed onto the upper arm.

The patients performed three point to point movements in a roulette activity (Lledó et al., 2016). The algorithm parameters selected for both algorithms were the same used in Section 3.6, also sampled at 100 *Hz*, and online estimating the five joint variables.

3.7.1 *Results & Discussion*

In order to compare both algorithms over shoulder displacements, the algorithm that will be described in Chapter 4 was used. The first

shoulder pose estimated by this algorithm was assumed as the fixed pose. In addition, when the algorithm described by Papaleo et al. could not estimate the joint variables, denoted as instability period, the last known joint variables were assumed. This instability period is marked as a gray color area in Figure 3.11.

The upper limb joint variables estimated from both methods are presented at the top of Figure 3.11. The blue smooth lines represent the kinematic reconstruction obtained from the proposed algorithm, and the estimated joint variables through Papaleo et al. algorithm is presented as red dotted lines. In the middle of Figure 3.11, the shoulder displacements of the three patients during the exercise are shown. Finally, the trajectory followed through the end effector of the robot is presented at the bottom of Figure 3.11, where the red circles denote the eight possible goals in the roulette exercise.

In addition, the measured ROM of each patient, estimated through the proposed algorithm, is presented in Table 3.5. It is observed that Patient #1, the patient with higher Fugl-Meyer and lower Ashworth scores, has the higher ROM, as it was expected. Furthermore, this patient performed the exercise with the higher roulette diameter, 15 *cm*, manually selected to optimize the motor recovery.

Table 3.5: ROM, in degrees, performed by the patients, measured through the proposed algorithm.

ID	sAB-AD	sF-E	sRot	eF-E	wP-S
1	37.5	5.46	43.63	35.8	11.78
2	17.99	11.74	18.04	29.29	9.20
3	18.99	9.47	16.13	26.04	11.38

In summary, it is important to note that shoulder movements cannot be avoided during a rehabilitation exercise with patients. Furthermore, comparing both algorithms, it is observed that the estimated joint variables are very similar outside of the instability areas. In addition, just before the appearance of the instability, the difference between both methods tends to increase. However, as it was not possible to carry the optoelectronic system to the clinic, the error committed with respect to the real joint variables could not be studied in these areas. The instability of the Papaleo et al. algorithm appears due to the strict constrains assumed by this algorithm as it is based on the upper limb lengths. Thus, it can fail with little shoulder displacements, leading a false ROM estimation and, therefore, an error in motor recovery assessment.
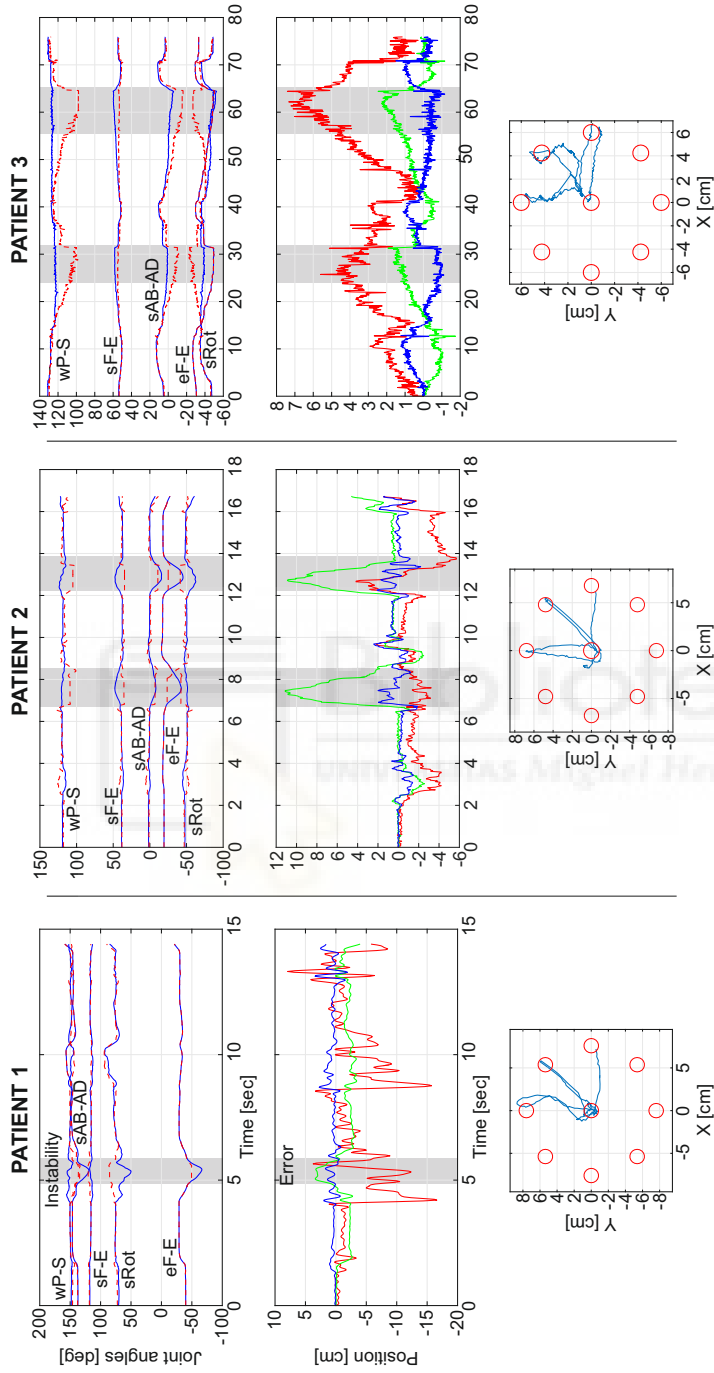
Figure 3.11: *(Up)* Upper limb joint variables estimated through the proposed algorithm (blue smooth line) and with the Papaleo et al. algorithm (red dotted line). The gray area denotes the instability period of the Papaleo et al. algorithm. *(Middle)* Shoulder displacement performed during the therapy by the three patients. The red, green and blue smooth lines denote the right(+)/left(-), forward(+)/backward(-) and up(+)/down(-) movements, respectively. *(Down)* Trajectory followed by the patients during the exercise. The red circles are the possible goals of the proposed exercise.

3.8 CONCLUSIONS

This chapter presented a novel kinematic reconstruction algorithm for the online estimation of a simplified upper-limb model with seven DoFs. The proposed algorithm was developed to be used in robot-aided neurorehabilitation therapies with end-effector-based robot. It only used the static acceleration of the upper arm, acquired through a wireless accelerometer, and the information of the end effector of the robot, where the hand of the patient is attached. It was assumed slow upper-limb movements, to avoid the dynamic component of the acceleration, and that the shoulder remained fixed during the exercise. Furthermore, a protocol to manually measure the length of the upper arm and forearm was introduced. Over these conditions, the proposed method can be easily used in clinical environments without disturbing the patient-clinician interaction.

This algorithm was firstly validated in a simulated environment in order to test the theoretical development of the algorithm. In this scenario, the restrictions of slow movements and fixed shoulder can be controlled complying with the mathematical restrictions. The developed environment simulated a rehabilitatation exercise, the *D1* PNF diagonal, with an end-effector-based robot where the upper-limb trajectory was known and the acceleration at each position could be computed. The results showed an accurate estimation of the seven joint variables, less than 0.5 *deg*, and the wrist and elbow joint positions, less than 1 *mm*, throughout the upper-limb movement.

The next step was to study its precision in a real environment with healthy subjects. Thus, an end-effector-based robot was used to perform a 3D point to point task by seven healthy subjects. The real upper-limb trajectory was measured by an optoelectronic system and compared to the joint variables estimated through the proposed algorithm. Furthermore, the upper-limb lengths were manually measured and an accelerometer was placed onto the upper arm. In this exercise, the error increased with respect to the simulation exercise, as it was expected. However, the measured error remains less than 5 *deg* in all joint variables and less than 2.5 *cm* with respect to the elbow and wrist joint positions. Therefore, the proposed algorithm was able to accurately estimate the joint variables during a rehabilitation exercise, as well as measure the ROM performed by the patients after a therapy session in real time.

Finally, this algorithm was compared to Papaleo et al. algorithm in a clinical environment with three patients, during a rehabilitation exercise using a planar end-effector-based robot. It was observed that when the patients performed shoulder displacements to achieve the goal, due to the motor impairments, the proposed algorithm is stable whilst the other algorithm was unable to determine the kinematic configuration of the upper limb.

Although the proposed algorithm accurately estimates the seven upper-limb joint movements and is stable to shoulder displacements, the main limitation is the assumption that the shoulder is fixed during the exercise. Furthermore, these compensatory movements can have beneficial effects on functional outcomes (Jones, 2017). Therefore, an improvement of this algorithm is explained in Chapter 4, where shoulder displacements are measured together with the joint movements.

ESTIMATION OF JOINT MOVEMENTS AND SHOULDER DISPLACEMENTS IN PATIENTS

The algorithm presented in the previous chapter allows a therapist to assess the motor recovery of the upper limbs through the estimated ROM. However, it is assumed that the shoulder is fixed, a strong constraint that cannot be applied to all patients. Hence, this chapter presents a modification of the previous algorithm in order to also estimate the shoulder displacements, just adding a magneto-inertial device onto the shoulder. Then, the proposed algorithm is validated with healthy subjects performing a rehabilitation execersie in a planar rehabilitation robot. Finally, the algorithm is tested in the worst scenario, when large shoulder displacements appear.

The research presented in this chapter has been previously published in Bertomeu-Motos et al. (2015b).

4.1 KINEMATIC UPPER-LIMB MODEL

The algorithm presented in this chapter performs a five DoFs kinematic reconstruction of the upper limb. Therefore, the corresponding DH parameters has been selected as shown in Table 4.1. The length of the upper arm and forearm are also manually measured following the methodology proposed in Section 3.1.

Table 4.1: DH parameters of the upper limbs ($i \in [1, 7]$).

JOINT MOVEMENT	RIGHT UPPER LIMB				LEFT UPPER LIMB			
	θ_i	d_i	a_i	α_i	θ_i	d_i	a_i	α_i
sAB-AD	$\pi/2 + q_1$	0	0	$\pi/2$	$\pi/2 + q_1$	0	0	$-\pi/2$
sF-E	$3\pi/2 + q_2$	0	0	$\pi/2$	$3\pi/2 + q_2$	0	0	$-\pi/2$
sRot	q_3	l_u	0	$-\pi/2$	q_3	$-l_u$	0	$\pi/2$
eF-E	$\pi/2 + q_4$	0	0	$\pi/2$	$\pi/2 + q_4$	0	0	$-\pi/2$
wP-S	q_5	l_f	0	0	q_5	l_f	0	0

4.2   ELBOW AND SHOULDER JOINTS ESTIMATION

This algorithm uses the same method as proposed in Section 3.2, i.e. through the inverse of the Jacobian. However, it is not necessary to compute the augmented Jacobian as the kinematic chain is composed of five DoFs, a non-redundant chain. Thus, (3.6) remains

$$\dot{\vec{q}} = J^{-1}\left(\vec{q}\right)\left\{\vec{v} + K \cdot \vec{err}\right\}, \tag{4.1}$$

and, therefore, the numerical integration can be applied. On the other hand, the acceleromenter orientation is obtained through the technique presented in Section 3.3. The only difference is that the two known joints are the wrist and the elbow, instead of the wrist and the shoulder. Thus, the elbow position is known from the wrist joint position, provided by the robot, as

$$^{r}P_e = {}^{r}T_w \cdot \begin{bmatrix} 0 & 0 & -lf & 1 \end{bmatrix}^T. \tag{4.2}$$

Then, this algorithm has to estimate the elbow rotation and the shoulder pose. To estimate the elbow rotation and the shoulder position, γ angle must be obtained from the static acceleration of the upper arm. In this case, γ angle is obtained by rotating the Π plane, obtained from (3.10), around the gravity vector (g), placed at the elbow joint (E), forcing to also include the wrist joint (W). Thus, γ angle is also defined as the angle between W and its projection over Π ($\tilde{W}$), where $\tilde{W}$ is determined as

$$\tilde{W} = (g \cdot \hat{W})\, g + \cos\left(\gamma\right)\left(\hat{W} - (g \cdot \hat{W})\, g\right) - \sin\left(\gamma\right)\left(g \times \hat{W}\right), \tag{4.3}$$

where

$$\hat{W} = \frac{(W - E)}{\|(W - E)\|},$$
$$g = \begin{bmatrix} 0 & 0 & -1 \end{bmatrix}^T.$$

Then, γ angle is computed by solving (3.12), i.e. forcing Π to contain W. Thus, two possible accelerometer rotations are also obtained, $^{acc_0}R_{acc}^{(j)}$ with $j \in [1, 2]$. From this two solutions, two shoulder positions are derived

$$^{r}P_s^j = {}^{r}T_e^j \cdot \begin{bmatrix} 0 & lu & 0 & 1 \end{bmatrix}^T, \tag{4.4}$$

with

$$
{}^{r}T_{e}^{j} = \begin{bmatrix} {}^{r}R_{e}^{j} & {}^{r}P_{e} \\ 0 & 1 \end{bmatrix},
$$

$$
{}^{r}R_{e}^{j} = {}^{r}R_{acc_0} \cdot {}^{acc_0}R_{acc}^{j} \cdot {}^{acc_0}R_{e}.
$$

From these two solution, there is only one that meets the restriction that the Z-axis point the same sense as the result of $\overline{EW} \times \overline{ES}$ and, therefore, the shoulder position and the elbow pose are determined.

The last step is to estimate the shoulder orientation. For this reason, a magneto-inertial device is placed onto the shoulder, as shown in Figure 4.1, in order to measure the orientation of the selected device and translate this orientation to the shoulder joint. However, this orientation is not directly obtained.
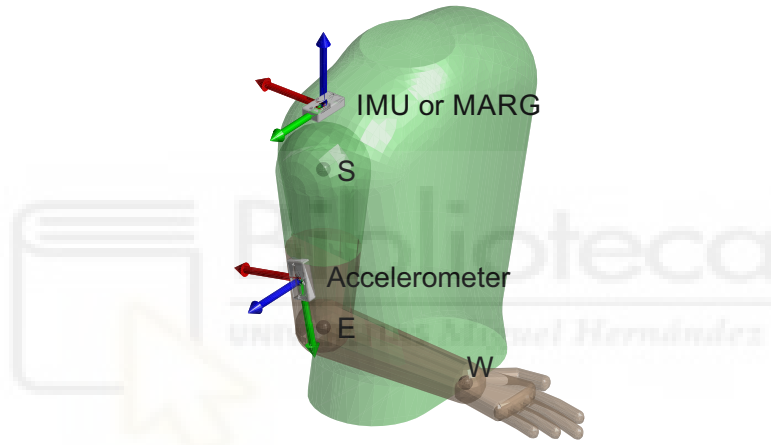
Figure 4.1: Reference orientation of the accelerometer and the magneto-inertial device.

The relation between the device and the shoulder can be computed if the device is initialized in a known orientation regarding $S0$ ($^{r}R_{Dev_0}$). Then, the rotation matrix that relates the device orientation with respect to $S0$ remains

$$
{}^{r}R_{ref} = {}^{r}R_{Dev_0} \cdot {}^{Dev_0}R_{ref}, \tag{4.5}
$$

where $^{Dev_0}R_{ref}$ is the rotation matrix of the device at that initial position. Therefore, the rotation of the device regarding $S0$ remains known as

$$
{}^{r}R_{Dev} = {}^{r}R_{ref} \cdot {}^{Dev}R_{ref}^{-1}, \tag{4.6}
$$

with $^{Dev}R_{ref}$ represents the current rotation of the device. Finally, as the position of this device with respect to the shoulder is known ($^{Dev_0}R_s$), the orientation of the shoulder is determined as

$$^rR_s = {^r R_{Dev}} \cdot {^{Dev_0} R_s},\tag{4.7}$$

and the homogeneous transformation matrix of the shoulder is estimated as

$$^rT_s = \begin{bmatrix} ^rR_s & ^rP_s \\ 0 & 1 \end{bmatrix}.\tag{4.8}$$

From this point, it is necessary to establish the initial position of the upper limb, computed through the same method presented in Section 3.4 and then, the numerical integration proposed through (3.8) and (4.1) can be applied.

4.3   ALGORITHM VALIDATION

The accuracy of the proposed algorithm was studied with the PUPArm robot (detailed in Appendix A.2). In this scenario, a MARG and an accelerometer (refer to Appendix A.3 for detailed information) are placed onto the shoulder and upper arm, respectively, as shown in Figure 4.2. Furthermore, the real joint variables are measured through the six DoFs optical tracking camera Optitrack V120: Trio (for more information, please refer to Appendix A.5).
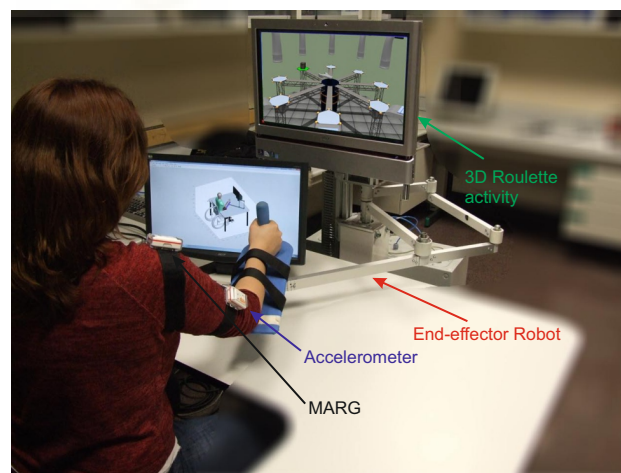
Figure 4.2: Healthy subject performing the 3D roulette activity. She wore an accelerometer and a MARG placed onto the upper arm and shoulder, respectively.

Four healthy right-handed subjects, presented in Table 4.2, performed a rehabilitation exercise, a point to point exercise in a roulette scenario, doing 24 displacements. The algorithm parameters, were set to $K = diag\{1.5, 1.5, ...1.5\}$ N/ms and $k^2 = 0.5$, the gain matrix and the damping factor respectively, with a sampling rate of 100 Hz. Furthermore, the rotation matrix of the MARG placed onto the shoulder was estimated through the Madgwick et al. algorithm.

Table 4.2: Demography of the healthy subjects.

ID	1	2	3	4
AGE	21	51	32	31
FOREARM LENGTH [M]	0.23	0.21	0.25	0.21
UPPER ARM LENGTH [M]	0.32	0.33	0.31	0.33

4.3.1 *Results & Discussion*

The difference between the estimated and the measured upper-limb joint variables and shoulder position are studied in terms of RMSE, SD.

The mean error committed is presented in Table 4.3. It is observed that the error regarding the shoulder movements is less than 2.5 cm. On the other hand, the error with respect to the five joint variables is lower than 5 deg. The maximum error appears in the sF-E, possibly due to the alignment of the accelerometer with respect to the upper-arm segment, a critical point of this algorithm.

Table 4.3: Error committed between the estimated and the real upper-limb variables, mean of the four subjects.

	RMSE	SD
SHOULDER LEFT/RIGHT [CM]	2.13	0.92
SHOULDER BACKWARD/FORWARD [CM]	2.43	1.45
SHOULDER UP/DOWN [CM]	1.55	0.56
sAB-AD [DEG]	1.42	0.91
sF-E [DEG]	4.51	0.34
sROT [DEG]	2.87	0.92
eF-E [DEG]	2.87	0.92
wP-S [DEG]	1.96	0.02

If we compare this error with the algorithm presented in Chapter 3, it is observed that they are very similar. This fact was expected because the used technique was based on the same criterion. In terms of shoulder displacements, the measured error is lower than 2.5 *cm*, an acceptable error for this application.

Figure 4.3 shows an example of the estimated, red dotted lines, and the measured, blue smooth lines, regarding the joint variables and the shoulder displacements during a complete exercise.
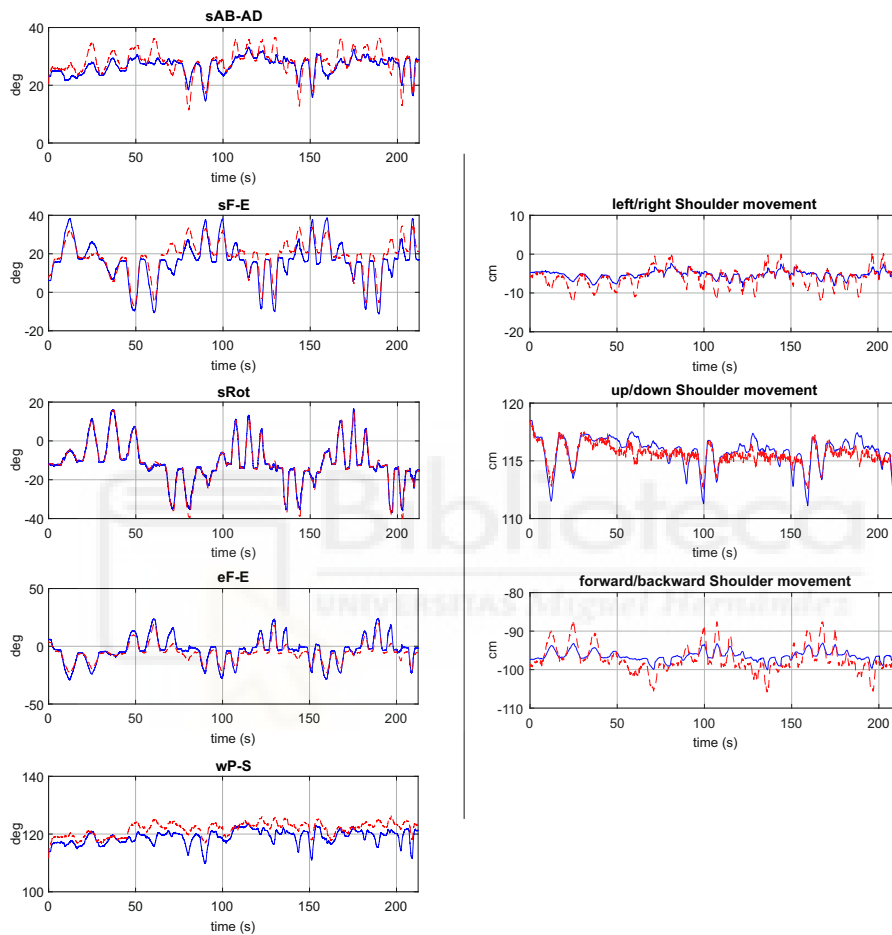
Figure 4.3: Joint variables *(left)* and shoulder movements *(right)* estimated through the proposed algorithm, red dotted lines, and measured through the optoelectronic system, blue smooth lines, of a subject during a complete exercise.

4.4   STUDY OF THE ROM WITH TRUNK COMPENSATION

This algorithm proposes a method to measure shoulder displacements during a rehabilitation exercise. This trunk compensations appear when the patients try to achieve the goals of the proposed exercises due

to the loss of mobility. Therefore, this feature allows the therapist to asses not only the upper-limb ROM, but also movement compensation, directly related to shoulder displacements.

This experiment evaluates the ROM of 51 healthy right-handed subjects, 29 men and 22 women, between 20 and 72 years old. They performed 24 point to point movements in two different scenarios of the same exercise. The first trial they tried not to move the shoulder during the exercise. Then, in the second trial, the subjects were instructed to follow the hand movements with the trunk. The same setup as in the previous section was used, two wearable devices and an optoelectronic system.

4.4.1 *Results & Discussion*

The results are presented in Figure 4.4 as a boxplot of the mean ROM, estimated through the proposed algorithm, at each joint variable in both exercises. The blue boxes represent the exercise without compensation and the orange boxes the exercise with trunk compensation. Both groups were statistically analyzed with the Pearson's linear correlation coefficient. It must be observed that the mean estimated ROMs in the compensation trial are lower than in the trial without compensation, showing significant differences in four of the five joint movements. The ROMs of the wP-S movement are similar in both scenarios, showing a $p - value > 0.05$. This effect is explained due to this specific movement is not affected by the trunk compensation.

Finally, the error committed in the second scenario, in terms of shoulder displacements, is measured in order to study the behavior of the proposed algorithm when high displacements were performed. Figure 4.5 shows the error committed in terms of RMSE and the SD together with an example of the shoulder displacements estimated, red dotted line, and measured, blue smooth line. It must be noted that the lower error is committed in the forward/backward movement and all movement errors are below 5 *cm*, a very good estimation with respect to the real shoulder for the purpose of this application.

4.5 CONCLUSIONS

This chapter improved the algorithm described in the previous chapter. It was able to estimate the shoulder displacements and five upper-limb movements during the rehabilitation exercise in a real clinical environ-
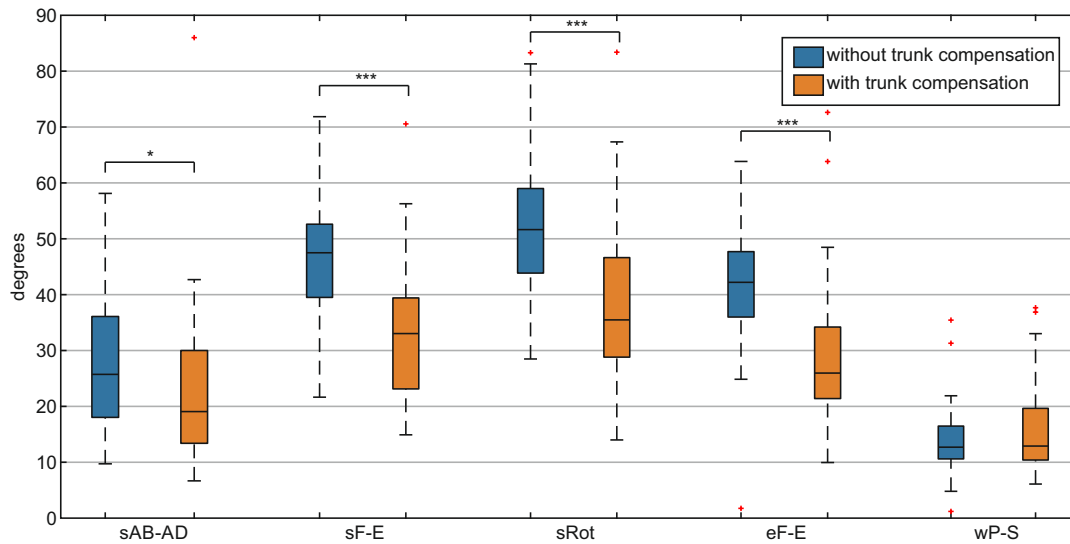
Figure 4.4: Estimated ROM in both scenarios with respect to the five joint variables. The exercise without compensation is shown as blue boxes and the exercise with compensation as orange boxes (*$p <$ 0.05; **$p < 0.01$; ***$p < 0.001$).
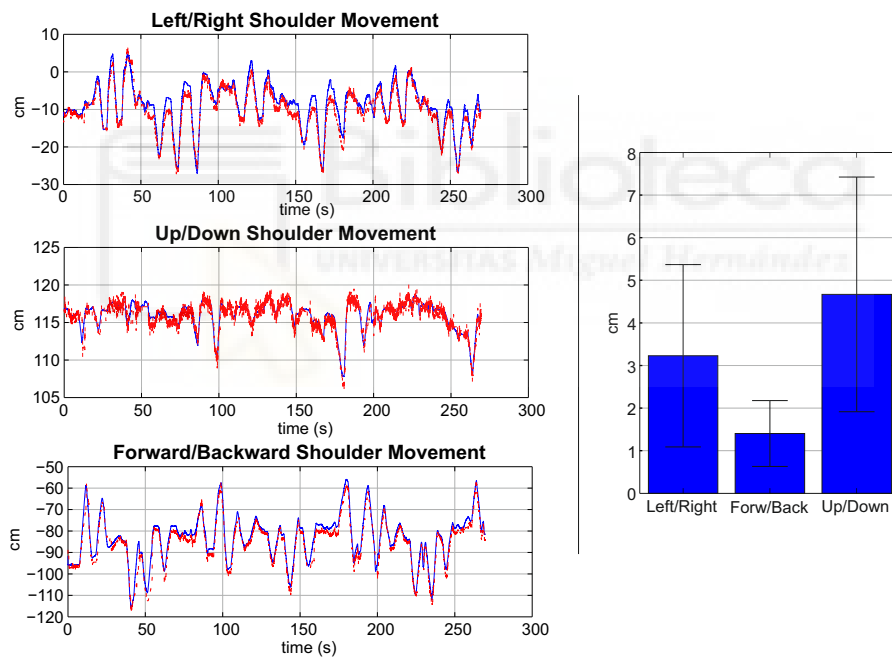
Figure 4.5: *(Left)* Example of the shoulder movements measured, blue smooth line, and estimated, red dotted line. *(Right)* RMSE committed and the SD of all subjects.

ment. Although the joint movements are reduced, from seven to five, this two movements are commonly fixed by the end-effector-based robots used in neurorehabilitation therapies.

It was studied the accuracy of the proposed algorithm obtaining good accuracy, less than 5 *deg* regarding the joint variables and less

than 2.5 *cm* with respect to the shoulder position. While there are extensive technologies applied to the measurement of human limbs for neurorehabilitation purposes, to my knowledge this is the first algorithm that is able to estimate not only the upper-limb joint movements, but also the trunk compensation through non-invasive wearable devices that allow a normal patient-clinician interaction in real rehabilitation environments.

The kinematic analysis of the patient presented here was developed to be used in clinical environments. However, technology solution for home environments can help to improve the neurorehabilitation outcomes and to increase the independence at home for people with severe motor impairments. Thus, the next chapter investigates two intelligent technology solutions for rehabilitation and assistance scenarios.

INTELLIGENT TECHNOLOGY SOLUTIONS FOR REHABILITATION AND ASSISTANCE AT HOME

This chapter presents two novel systems based on artificial intelligent techniques. Section 5.1 proposes a novel system to intelligently assess the quality of a set of upper-limb movements offering a new tool to guide post-stroke patients during a rehabilitation exercise at home. Section 5.2 proposes an intelligent ECI that uses the information of the environment and the behavior of the user to enhance the level of independence at home for people with reduced mobility. Finally, Section 5.3 summarizes and concludes this chapter.

5.1 UPPER-LIMB MOVEMENTS ANALYSIS FOR SELF-MANAGED RE-HABILITATION

After stroke, repetitive and intense therapy improves the rehabilitation progress. However, a discontinuity between therapy in hospital and at home slow down the upper-limb mobility recovery (Demain et al., 2013). Is here where intelligent technology can play an important role offering tools for self-managed rehabilitation, always supervised by a clinician.

This section introduces a method for rehabilitation at home based on the measurement of kinematic configuration of the upper limb fused with machine learning techniques in order to guide the patients during the exercise, according to the quality of the movement performed.

5.1.1 *Estimation of Upper-limb Kinematic Configuration*

In Section 2.2, three different methods to measure the kinematic configuration of the body joints have been introduced. However, as the proposed system has to be affordable, easy to use and precise in the estimation of the joint movements, the wearable inertial-based device systems are the best that fit these conditions. From literature, it has been demonstrated that with only three magneto-inertial devices it is possible to accurately estimate the kinematic configuration of the

upper limbs (de Vries et al., 2010; Bouvier et al., 2015; El-Gohary and McNames, 2015).

The estimation of the orientation of each upper-limb segment was performed through a calibration process in order to know the orientation of the three devices with respect to the reference system $S0$. Thus, as described in Section 4.2, if the devices are initialized in a known orientation, the orientation of each segment is estimated as

$$^{r}R_{upper} = {^{r}R_{Dev_{upper}}} \cdot {^{Dev_0}R_{upper}}, \tag{5.1}$$

$$^{r}R_{fore} = {^{r}R_{Dev_{fore}}} \cdot {^{Dev_0}R_{fore}}, \tag{5.2}$$

$$^{r}R_{hand} = {^{r}R_{Dev_{hand}}} \cdot {^{Dev_0}R_{hand}}, \tag{5.3}$$

where $^{r}R_{Dev_{upper}}$, $^{r}R_{Dev_{fore}}$ and $^{r}R_{Dev_{hand}}$ are the current orientation of the devices obtained through (4.5) and (4.6); and $^{Dev_0}R_{upper}$, $^{Dev_0}R_{fore}$ and $^{Dev_0}R_{hand}$ are the reference position of the three devices with respect to the corresponding segment.

Finally, following the kinematic chain of the upper limbs used in Section 3.1, the matrices related to the seven upper-limb joints remain

$$T_s = \begin{bmatrix} ^{r}R_{upper} & ^{r}P_e \\ 0 & 1 \end{bmatrix}, \tag{5.4}$$

$$T_e = \begin{bmatrix} ^{r}R_{upper}^{-1} \cdot {^{r}R_{fore}} & ^{r}P_e \\ 0 & 1 \end{bmatrix}, \tag{5.5}$$

$$T_h = \begin{bmatrix} ^{r}R_{fore}^{-1} \cdot {^{r}R_{hand}} & ^{r}P_h \\ 0 & 1 \end{bmatrix}, \tag{5.6}$$

being

$$^{r}P_e = {^{r}R_{upper}} \cdot \begin{bmatrix} 0 & l_u & 0 \end{bmatrix}^{T}, \tag{5.7}$$

$$^{r}P_h = T_s \cdot T_e \cdot \begin{bmatrix} 0 & 0 & l_f & 1 \end{bmatrix}^{T}. \tag{5.8}$$

Finally, the online estimation of the joint variables are computed using the integration method proposed in Section 3.2, through (3.6) and (3.8).

5.1.2   *Evaluation of Upper-limb Movements*

The proposed system assesses the quality of the upper-limb movements performed by the patients comparing them to the expert move-

ments, i. e. clinicians. These movements are a set of gestures that goes from simple actions, e. g. touch the head, to complex actions, e. g. draw a circle with the hand, commonly used in neurorehabilitation therapies.

The first step is to present to the patient the gesture that has to be performed. Then, a time series classification model, trained through the expert gestures, classifies the gesture that the patient executes. From literature, it was found an adaptive system able to operate with sequential and multivariate data in noisy environments, a model that perfectly adjust to our data. This model, called Online Infinite Echo-State Gaussian Process (OIESGP), was introduced by Soh and Demiris in 2015. It fuses a class of recursive neural network, the echo-state network (Jaeger, 2001), with Bayesian online learning for Gaussian processes (Csató and Opper, 2002). Furthermore, it can behave as a generative classification model in order to know the confidence about the prediction.

After the classification of the gesture performed, it is complemented by the dynamic time warping (DTW) (Sakoe and Chiba, 1978) as follows:

   a. The patient executed a correct gesture when it is correctly classified and the DTW distance is low at each joint variable.

   b. A false positive can be detected if a desired gesture is correctly classified but the distance between the executed movement and the expert movement is high enough.

   c. If the model classifies an undesired gesture and the DTW distance is low with respect to that gesture, it implies that the patient misunderstood the order and executed that gesture correctly, not the proposed one.

   d. A false negative can be detected if an undesired gesture is classified, the distance with respect to that gesture is high, but the distance with respect to the proposed gesture is low.

   e. The patient could not perform the desired gesture correctly if the model classifies a different gesture and the DTW distance is high with respect to the classified and the proposed gesture.

Finally, according to the previous statements, after each movement the system can make an intelligent decision taking into account the quality of the movement executed. Furthermore, through all the acquired information, such as ROM, joint movements, DTW distance

or gestures correct classified, the therapist can evaluate the patient improvements.

5.1.3 *Experimental Evaluation*

The potential of this system in terms of quality movement was evaluated. Thus, two expert performed ten trials of a set of gestures, with the dominant limb, in order to train the OIESGP model. Then, a healthy subject and two stroke patients executed five trials of these gestures with the dominant and affected limbs, respectively, to study the capability of the trained model to classify the non-expert gestures and evaluate the DTW distance.

All the subjects wore three MARG sensors (see Appendix A.3), placed onto the upper arm, forearm and hand. A sEMG armband (see Appendix A.4 for more details) was placed onto the proximal part of the forearm in the expert subjects, as observed in Figure 5.1. The upper-limb segments of each subject were manually measured as proposed in Chapter 3. Table 5.1 shows the information of the experts, the healthy subject and the patients. In addition, the affected limbs of the patients were evaluated through the Ashworth test (Bohannon and Smith, 1987) for the elbow joint, and the Daniels and Worthingham's Muscle Testing (Hislop et al., 2013).

Figure 5.1: Experimental setup. The subjects wore three magneto-inertial devices placed onto the upper limb. Furthermore, the experts subjects performed the gestures with an sEMG armband. They were sat down in front of a screen where the desired gesture was shown.

Table 5.1: Main information of all the participants

ID	D/A LIMB	AGE	FOREARM LENGTH [M]	UPPER ARM LENGTH [M]	ASWORTH	DWMT
E1	Right	27	0.24	0.310	-	-
E2	Right	28	0.28	0.30	-	-
H1	Right	28	0.27	0.23	-	-
P1	Right	74	0.28	0.29	0	3/5
P2	Right	68	0.27	0.28	0	3/5

E: Expert, H: Healthy Subject, P: Patient.
D/A limb: Dominant (for healthy subjects)/Affected (for patients) limb.

The subjects sat down in front of a screen where the desired gesture was shown. They had five seconds, at most, to complete the corresponding gesture. However, the experts were instructed to perform slow movements and complete the gesture in exactly five seconds. All the devices were sampled at 200 *Hz*. The rotation matrix of each MARG device was estimated through the Madgwick et al. algorithm. The set of gestures determined for this experiment are presented in Table 5.2. The starting position of the corresponding limb was with the hands over the thighs.

Table 5.2: Set of the defined gestures.

NAME	ACTION
Mouth	The participant touches his/her mouth with the fingertips.
Shoulder	The participant touches his/her contralateral shoulder.
Knee	The participant touches his/her contralateral knee.
Ear	The participant touches his/her contralateral ear.
Head	The participant touches the top of the head.
Triangle	The participant draws a triangle with the hand in front of his/her chest.
Square	The participant draws a square with the hand in front of his/her chest.
Circle	The participant draws a circle with the hand in front of his/her chest.

5.1.4 *Results & Discussion*

The acquired data from the experts were used to train three OIESGP models. Figure 5.2 shows a graphic representation of each gesture regarding the seven joint variables. For better visualization, each gestures was normalized with respect to the mean ROM of each
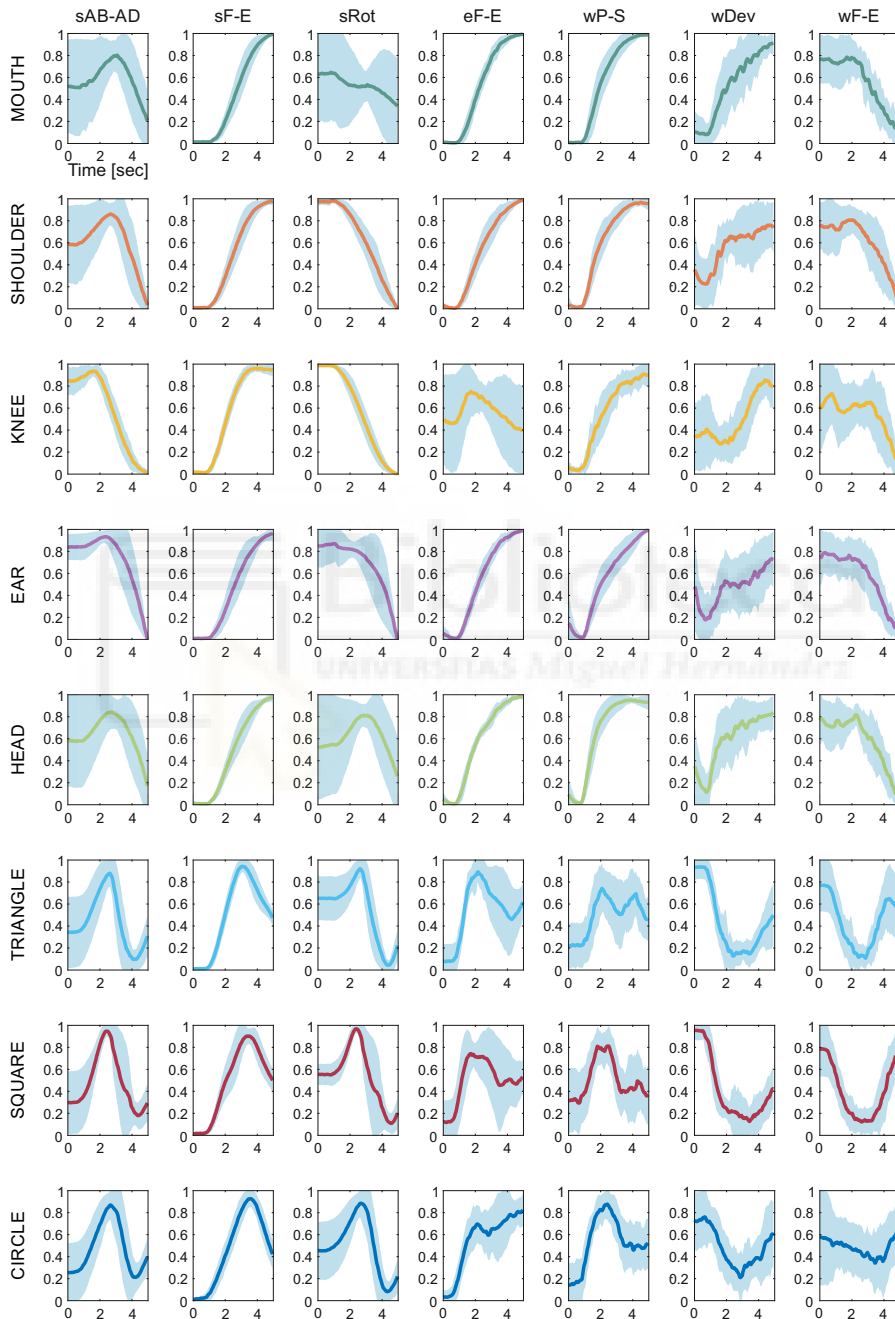
Figure 5.2: Mean joint movements of the gestures performed by the experts. The blue area represents the SD of each joint variable.

joint variable, shown in Table 5.3. The blue area represents the SD of each joint movement.

Table 5.3: Mean ROM of each joint variable regarding the expert gestures.

GESTURE		sAB-AD	sF-E	sRot	eF-E	wP-S	wDev	wF-E
Mouth	RMSE	17.7	43.5	33.1	64.3	94.3	19.5	18.6
	SD	12.6	3.3	10.7	7.4	12	4.6	11.2
Shoulder	RMSE	29.2	46.4	59.4	67.1	71.8	14.6	18.8
	SD	21.2	3.3	30.0	10.6	7.3	6.5	6
Knee	RMSE	15.7	24.9	58	15.2	22.5	7.1	10.1
	SD	5.9	5.5	6.1	6.2	6	2.6	3.2
Ear	RMSE	51.4	57.7	61.6	61.2	109.4	16.3	16.6
	SD	22.1	9.3	34.2	7.9	9.9	6.7	3.1
Head	RMSE	49.5	62.2	58.7	56.8	84.6	18.9	14.4
	SD	30.8	8	23.3	8.1	11.4	7.8	5
Triangle	RMSE	60.1	57.1	80.7	29.3	19.4	17.8	21.4
	SD	12.3	4.7	18.8	11.5	5	8.7	9.8
Square	RMSE	86.7	58.3	100.2	37.2	21.4	19.2	23.9
	SD	28.7	5.9	20.9	13	5	9.2	7.2
Circle	RMSE	73.2	56.5	84	29	22.9	14	14.9
	SD	18.6	4.5	17.2	13.3	7.7	6.6	5

Then, Figure 5.3 shows the confusion matrices obtained through the test set. It presents three different training scenarios: with the seven joint variables, with the eight sEMG sensors and with only five joint variables, skipping the wF-E and wDev joint movements. The training results are studied with only five upper-limb joint movements due to the gestures chosen, since they were focused on gross movements. Furthermore, the patients with high motor disability usually are unable to accurately control the distal joint movements.

From the results, it must be noted that two of the proposed models, using five and seven joint movements, were able to classify the set of gestures over the 80% of success. However, when the model was trained with only the sEMG data, the model poorly classifies the 46% of the gestures.

It should be emphasized that, even though low accuracy was obtained with sEMG training data, three groups can be differentiated, one is composed of the *Face*, *Mouth*, *Shoulder*, *Ear* and *Head* gestures, the second is only the *Knee* gesture, and the third group is the *Triangle*, *Square* and *Circle* gestures. These groups discern gestures performed

SEVEN JOINTS

True Class	Mouth	0.91	0.04	0	0.05	0	0	0	0	0
	Shoulder	0.02	0.91	0.03	0.04	0	0	0	0	0
	Ear	0.04	0.06	0.8	0.1	0	0	0	0	0
	Head	0.03	0	0	0.97	0	0	0	0	0
	Knee	0	0	0	0	1	0	0	0	0
	Triangle	0	0	0	0	0.02	0.67	0.15	0.16	0
	Square	0	0	0	0	0	0.1	0.84	0.06	0
	Circle	0	0	0	0	0	0.07	0.01	0.92	0
	Total	0	0	0	0	0	0	0	0	0.87

Mouth Shoulder Ear Head Knee Triangle Square Circle Total
Predicted Class

FIVE JOINTS

0.86	0.02	0	0.12	0	0	0	0	0
0	0.94	0.04	0.02	0	0	0	0	0
0.08	0.09	0.75	0.08	0	0	0	0	0
0.06	0	0.01	0.93	0	0	0	0	0
0	0	0	0	1	0	0	0	0
0	0	0	0	0	0.69	0.15	0.16	0
0	0	0	0	0	0.16	0.77	0.07	0
0	0	0	0	0	0.16	0.06	0.78	0
0	0	0	0	0	0	0	0	0.83

Mouth Shoulder Ear Head Knee Triangle Square Circle Total

sEMG

0.5	0.18	0.15	0.17	0	0	0	0	0
0.21	0.42	0.22	0.15	0	0	0	0	0
0.06	0.19	0.42	0.31	0.02	0	0	0	0
0.02	0.17	0.12	0.46	0.23	0	0	0	0
0	0.01	0.02	0.1	0.84	0	0	0.03	0
0	0	0	0	0.05	0.35	0.3	0.3	0
0	0	0	0	0.06	0.3	0.43	0.21	0
0	0.02	0.02	0.01	0.14	0.19	0.08	0.54	0
0	0	0	0	0	0	0	0	0.47

Mouth Shoulder Ear Head Knee Triangle Square Circle Total

Figure 5.3: Confusion matrices obtained with the OIESGP model trained through expert data, in three different scenarios: seven joint movements, five joint movements, and sEMG.

around the face, gestures that drew a figure in the air, and the knee gesture.

The next step was to study the classification model and the DTW distance with the healthy subject and patients. The model trained with only five joint variables was chosen, as the classification accuracy of the models trained with five and seven joint variables were very similar. Figure 5.4 presents the confusion matrix of the classification gestures obtained with the healthy user, with an accuracy of 64%. It is observed that the gestures *Shoulder* and *Head* are confused with a very similar gesture, *Mouth*. This effect also occurs with *Circle* gesture, that is confused with *Square*. The success rate of the classification model with the patients are 38% and 8.3%, respectively. This inaccuracy is owed to the motor impairments that, even the DWMT scores shows a full range of motion against gravity, they are unable to perform the desired gestures.

On the other hand, Figure 5.5 shows the classification results of the healthy subject and the patients, regarding the DTW distance to the

Figure 5.4: Confusion matrix obtained with the healthy subject gestures. This data was tested with the OIESGP model trained through the five joint movements scenario.

true and predicted gestures. The DTW is computed as the mean of the five joint movements. It is observed that when a gesture was correctly classified, marked as circle, the distances to the predicted and true gestures are the same, as expected. However, when a gesture was wrongly classified, marked as asterisk, both distances are different. In case the distance to the pred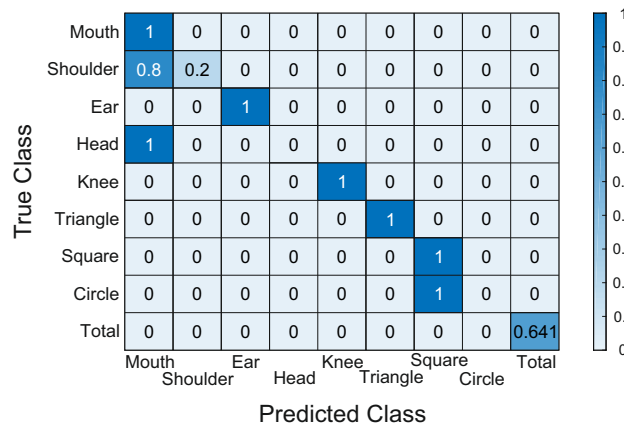icted gestures is greater than the distance to the true gesture, the asterisk appears under the diagonal, otherwise, the asterisk is over the diagonal. The healthy subject is printed in red color, Patient #1 in green color, and Patient #2 in blue color.

From Figure 5.5, it must be noted that the healthy subject obtains the lowest distances, regardless the prediction made, while the DTW distance obtained with the patient gestures are always higher. It is explained as the movement performed by the patients is deficient and, even though the model achieves a correct classification, the quality of the gesture is low regarding the expert joint movements.

In addition, Figure 5.6 presents three of these cases to better understand how to interpret the results of the classification model together with the DTW distances.

The first example, left column, shows the third trial of the *Ear* gesture performed by the healthy subject. The top graph shows the probability over the different gestures throughout the movement, where the corresponding gesture was correctly classified, shown as thick purple line. Under that graph, the left column presents the performed joint movements, purple line, over the desired movement, blue line, computed from the expert data. It is observed that the joint movements were properly executed and, therefore, the aligned signals, right column, are very similar, with low DTW distance computed.
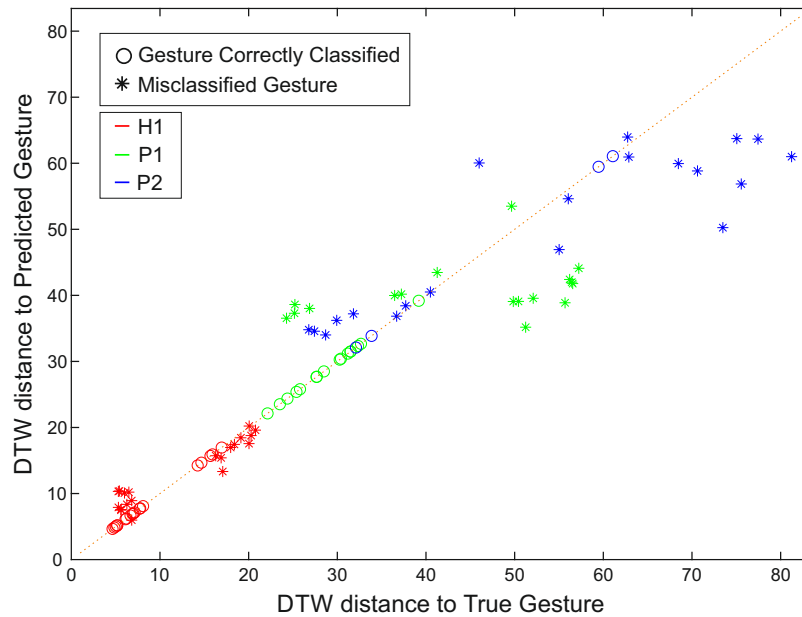
Figure 5.5: Graphic representation of the DTW distance regarding the true and predicted gestures. The DTW is computed as the mean of the five joint movements. The circle represents a correct prediction, whilst the asterisk means a wrong prediction. The healthy subject is printed in red color, Patient #1 in green color, and Patient #2 in blue color.

The second trial is the third *Shoulder* gesture performed by Patient #2. In this case, the gesture was also correctly classified, thick orange line, but the performed joint movements were not properly executed and, therefore, the DTW distance is high. Thus, the system could detect that the patient need to improve the execution of this gesture. The last trial shown is the third *Circle* gesture done by Patient #2. The performed gesture was misclassified by the model and, as it can be observed in the first column, the executed joint movements were very different from the expert movements. Then, two DTW are computed, the distance from the desired gesture, in the second column, obtaining high distances at each joint movement, and the distance from the predicted gesture, third column, computing high distances too. Thus, we can conclude that the gesture performed by the patient was incorrect.
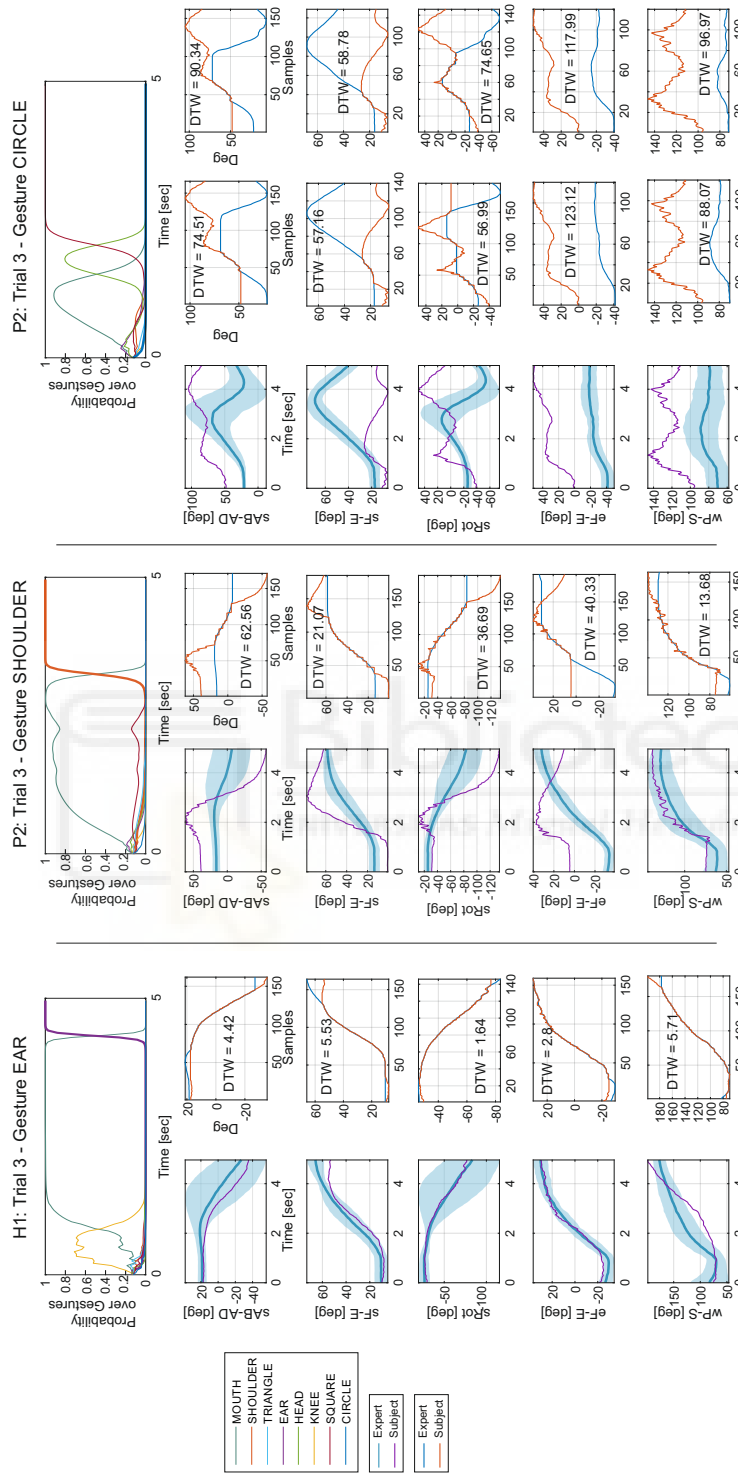
Figure 5.6: Example of three different gestures executed by the healthy subject and the patients. The probability over the gestures was estimated by the OIESGP model (*top*). In addition, the left columns show the executed gestures, purple smooth lines, regarding the expert joint movements, blue smooth lines. Finally, the DTW distances measured from the true gestures, center column, an from the predicted gesture, right column, are shown.

5.1.5   *Conclusions*

This section proposed a novel system for measurement and evaluation of the quality of upper-limb gestures. While three wearable devices online estimate the seven joint movements, an OIESGP model classifies the gesture that the subject is executing. Then, the combination of the model prediction with the measurement of the DTW distance improves the assessment of the joint movements, being able to decide the quality of the performed gesture.

The OIESGP model was trained through a set of eight gesture performed by experts, obtaining high accuracy, more than 80%, in two different scenarios: seven joint variables training and five joint variables training. In addition, a sEMG bracelet with eight sensors was also placed on the forearm in order to study the OIESGP model accuracy with only this information. Even though low precision was obtained, it was found an interesting result. With only the sEMG data, the model was able to differentiate the three working areas of the proposed gestures: the gestures performed near the face, the *Knee* gesture, and the gestures that draw figures in the air.

Then, it was studied the proposed upper-limb movement assessment with a healthy subject and two stroke patients. It has been demonstrated that the fusion of the prediction model, with five joint movements, and the DTW distance offers an intelligent system to assess the quality of an executed movement, taking into account each joint variable independently. Thus, it can be concluded that the proposed system was able to determine the motor capacity over a rehabilitation movement in an intelligent manner. Therefore, it has the potential to become a novel tool for self-managed rehabilitation at home. Furthermore, the acquired information also offers an important data to the therapist in order to enhance the patient assessment.

5.2   USER INTENTION RECOGNITION FOR ECI IMPROVEMENT

In this section the target patients are not just stroke survivors, it is also extend to people with severe motor disabilities, e. g. people who suffered a SCI. The purpose of this section is to develop and test a multimodal system able to recognize the intention of the users, and help them to perform ADL at home through an intelligent ECI mounted on a wheelchair. Furthermore, this system has to adapt to the residual capabilities of each user.

This section's research has been previously published in Bertomeu-Motos et al. (2019).

5.2.1 *Environmental Control Interface*

One of the main parts of this system was the ECI, the interface used for augmentative and alternative communication and for environmental control. It was based on two software components: the GRID3 from Smartbox[1] and the SHX, a specific developed software. This ECI had three different abstraction levels, shown in Figure 5.7. The first one was related to the room, named 'room menu', the second allowed the selection of an activity related to a specific room, named 'activity menu', and the last level was related to the actions regarding a specific activity, named 'ADL menu'. Along this section, a jump between two consecutive levels is named as 'step'.
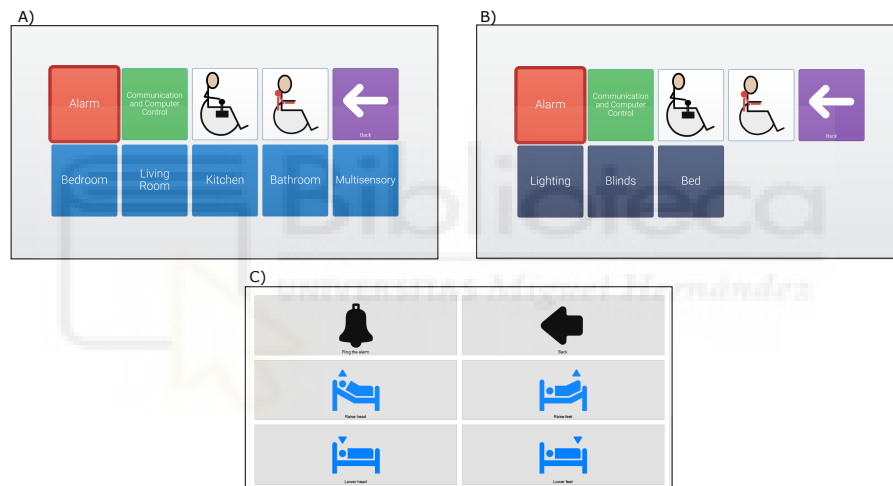
Figure 5.7: The ECI had three different abstraction levels: related to the room, related to the activities that can be performed in a specific room and related to the actions regarding a specific activity. An example menu of each level is shown in (A), (B) and (C), respectively.

Levels one and two were specific grid sets created in GRID3. They included the necessary grids to perform an ADL, a communication grid, a grids for a wheelchair control and one for upper-limb exoskeleton or robotic arm control. The last three grids were out of the scope of this thesis. Furthermore, the following color code had been used to ease the scan: the red color represented the alarm; the green color was used for communication purpose, computer control and digital leisure; white color remarked the wheelchair and arm control; light blue for

---

1 http://thinksmartbox.com/

the rooms; and the dark blue was used for environmental control activities. The dark blue cells linked GRID3 with SHX software. SHX was used to develop the third level, the level for environmental control management. Finally, the developed software allowed the user to scan across the different cells and selected them through different access technology, e. g. EOG, EEG or eye tracking, at the three abstraction levels.

5.2.2 *Prediction Model*

The ECI was developed to combine the information gathered from the environment with the user behavior in order to predict the intention of the user. At home, the remarkable information about an ADL is the room where the activity is being performed, the duration of the task, the brightness of the room, the objects that are part of the activity and where the user is looking at while performing the task.

Under these conditions and due to the difficulty of generating data, the Conditional Random Fields (CRF) model was chosen as it fits our conditions. It is a probabilistic model for labeling and segmentation sequence data, introduced by Lafferty et al. in 2001. This discriminate model uses not only the current state but also the previous states to perform its prediction. Furthermore, as it is a conditional model, it also specifies the probabilities of possible label sequences given an observation sequence.

Finally, the model inputs were: the localization, the objects in the environment, the object that the user is observing, the temperature of the room, the brightness of the room and the time to complete the task. The output of the model was the most probable action, directly linked with a specific 'ADL menu' of the ECI. Table 5.4 shows the proposed ADL and the menus of the third abstraction level.

5.2.3 *Experimental Evaluation*

The evaluation of the proposed system was carried out within the AIDE[2] project. The purpose was to compare the developed ECI with a traditional ECI, i. e. without the prediction of the user intention model. For this purpose and due to the early phase of the project, a virtual house was developed in order to perform the ADL and simulate the input data related to them. The layout of the developed house and a

---

2 https://aideproject.umh.es/

Table 5.4: Correspondence table between the proposed ADL and the ADL menu of the ECI.

ADLs	ADL Menu
Open/close fridge	Drink and Eat
Open/close microwave	Drink and Eat
Eating task	Eat
Drinking task	Drink
Switch on/off Music	Entertainment
Switch on/off PC	Entertainment
Switch on/off TV	TV
Switch on/off air conditioner	Air conditioner
Brushing teeth	Teeth
Washing face	Face
Raise/lower the bed head	Bed
Raise/lower the bed feet	Bed
Open/close the blinds	Blinds
Switch on/off the light	Light

screen shot of the software application while performing an ADL are shown in Figure 5.8. In addition, the software platform was also able to generate the necessary data to train a CRF model.

The experimental evaluation consisted on a two screen layout, as shown in Figure 5.9, where the users had to perform simulated ADL. One screen showed the ECI and the other the virtual environment. The users had to perform a list of ADL in two different modes, randomly selected, during ten minutes each mode:

- *MANUAL* mode: the user had to accomplish the task, showed in top right corner of the virtual environment, navigating through the three abstraction levels. The objects related to the corresponding task were surrounded by a green color.

- *AIDE* mode: in this mode the prediction model was used. Thus, the user had to look at the objects related to the corresponding ADL and, after the model prediction, the ECI directly jumped to the corresponding 'ADL menu'. Then the user had to complete the activity navigating like *MANUAL* mode. In case of wrong prediction, the user had to manually go to the second abstraction level to achieve the desired ADL. In this model, the gaze point of the user were online detected from the Tobbi [3] PCEye go eye

---

3 http://www.tobii.com

tracker (see Appendix A.7 for more information), placed on the virtual environment screen in order to detect the objects that the user was observing. The rest of the input parameters were online simulated.

Figure 5.8: Virtual house developed: layout of the house *(up)*, and screen shot of the software application while performing a specific ADL *(down)*.

Each subject had to perform two experimental sessions in two consecutive days. The user training and the system calibration was performed in the first day. Furthermore, it was performed a familiarization phase with whole system, including the access technology selected. This session lasted around 60-80 minutes. An example of sensorimotor rhythm (SMR) and EOG movements in the training session is shown in Figure 5.10, *C* and *D*, respectively.

The second session lasted a maximum of 60 minutes. The setup and re-familiarization phase took approximately 15 minutes. Then,

Figure 5.9: The experimental setup was composed by two screens: the ECI and the virtual environment. An eye tracking was placed in the virtual environment screen to detect the gaze point.

they had 10 minutes to perform a predefined ADLs list in both mode. There were two kind of ADL: a single action that has a visual effect on the house simulator, e. g. swith on a lamp; or a multiple action that correspond to a complex activity showing a short video about it, e. g. drink from a glass. The order of the modes was randomly selected and during the break, five minutes approximately, and at the end of this session, the subjects answered the NASA task load index questionnaire (Hart and Staveland, 1988).

The proposed ECI was developed to be used with multiple access technologies. In this experimentation, the control of the ECI was performed through a hybrid EEG/EOG-based interface (for more information, please refer to Appendix A.6). Thus, the scan through the ECI was performed with looking-right eye movements (Figure 5.10, *B*) implying a forward displacement of the grid marker (Figure 5.10, *a-e*). After reaching the wanted grid, the user had to wait until the ECI 'switch off' the rest of the grids (Fig. 5.10, *f*) a customized time, chosen in the first session. Finally, the online detection of the SMR-Event-Related Desynchronization (ERD) was used to click at that specific grid, passing to the next abstraction level or completing the activity (Figure 5.10, *A*).

On the other hand, in the phase *f* of the Figure 5.10, the user had the option to cancel the selection of a grid through a looking-left

eye movement, returning the ECI to the phase *a*. When the users performed the desired activity, a visual feedback was presented in the virtual house (Figure 5.10, *g*) and they waited for the next task.
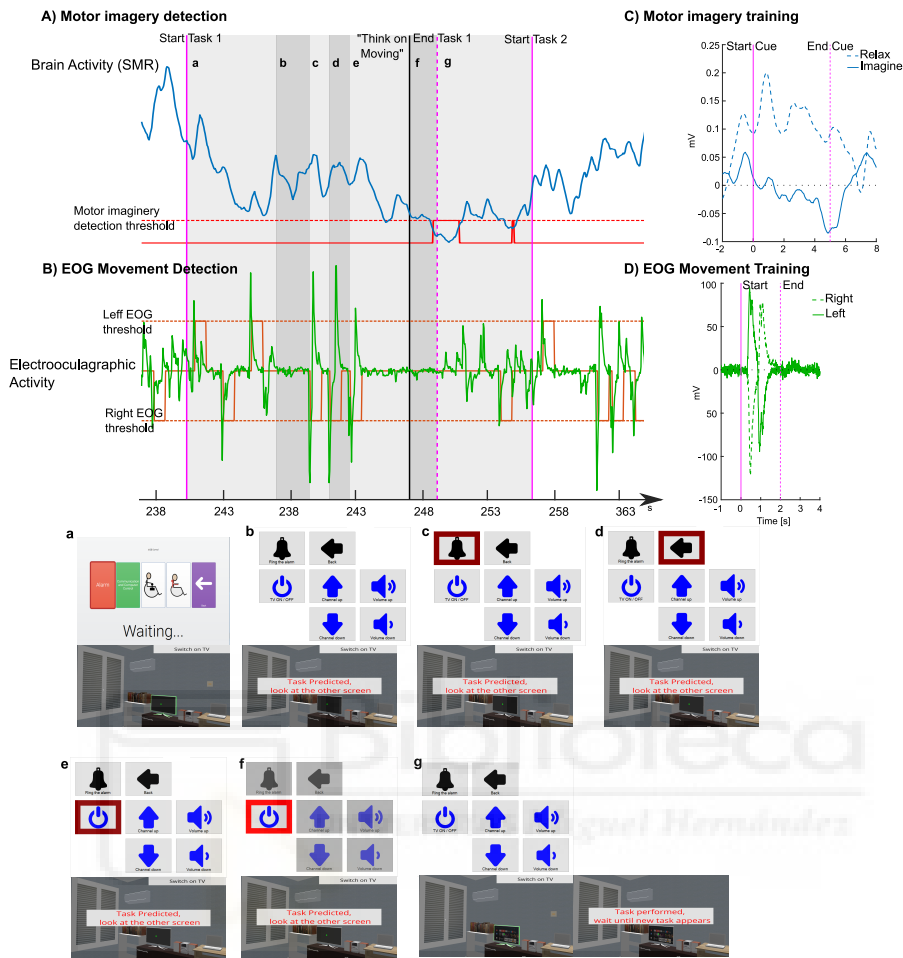
Figure 5.10: The user had to perform different actions in order to execute the corresponding ADL, in this example, the user had to switch on the TV in the *AIDE* mode. Phases a-g show the behavior of both screens during the task. EEG *(A)* and EOG *(B)* signals were acquired to online control the ECI in order to perform ADL in the virtual house. When the task started (vertical purple line), the scan through the ECI was performed by EOG activity detection [orange smooth line in *(B)*], i.e. when HOV activity exceeded the threshold [indicated by the orange dashed line in *(B)*] the grid marker moved forward (phases *a-e*). Once the subject stopped at one grid, a task confirmation was needed [indicated by the vertical black line] and the ECI 'switched off' the rest of the grids indicating this purpose (phase *f*). The confirmation was performed by the detection of SMR-ERD [indicated by red line in *(A)*] and the action was done, so the ADL finished (vertical dotted purple line). This ADL was performed in one step, i.e. the user only needed to navigate through the last abstraction level to complete the task. Before the experimentation, the user was trained in motor imagery *(C)* and EOG movement *(D)* to setup the access technology with the personalized parameters.

This experimental evaluation was performed by 8 subjects with motor disabilities. Table 5.5 shows their demographic and clinical characteristics, and their Barthel scores (Quinn et al., 2011) measured before the experiment. All participants gave informed consent using their standard communication channel prior to participation in the study. The protocol was approved by the Office Research Ethics Northern Ireland - approval granted for project (15/NE/0384).

Table 5.5: Demographic and clinical characteristics of participants.

ID Patient	Sex	Age	Diagnosis	Barthel Score
1	Male	32	C4 SCI	4/20
2	Male	22	Duchenne Muscular Dystrophy	6/20
3	Male	55	Brain stem strokes	16.5/20
4	Male	30	C4/C5 SCI	2/20
5	Female	20	C6/C7 SCI	10/20
6	Male	58	Ischemic Stroke	19/20
7	Male	55	Multiple Systems Atrophy	5/20
8	Male	30	C6/C7 SCI	9/10

5.2.4   *Results & Discussion*

The performance of the users regarding both modes are presented in Figure 5.11. The number of the performed activities with respect to the mean time per activity spent is presented in Figure 5.11, *(A)*. Furthermore, a Support Vector Machine (SVM) model with Gaussian kernel was trained to estimate the boundary between both modes, represented as a yellow smooth line, being able to clearly differentiate both modes. In addition, a statistically significant differences between both modes was obtained through the Wilcoxon test ($p-value <$ 0.001) .

Figure 5.11, *(C)* shows the distribution of the steps performed to successfully achieve the proposed activities. ADL manually omitted during the experimentation, due to the user was blocked during the ECI scan caused by frustration or fatigue, were excluded from the study.

On the other hand, the *AIDE* mode uses the CRF model previously trained with simulated data in order to predict the user intention. Thus, the confusion matrix of the prediction model regarding the ADL
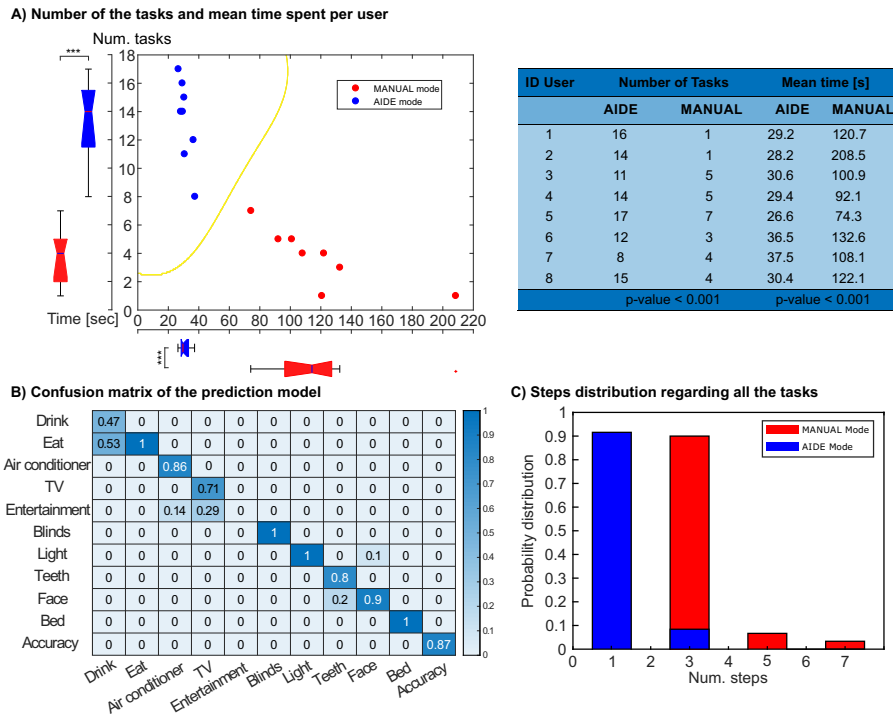
A) Number of the tasks and mean time spent per user

ID User	Number of Tasks		Mean time [s]	
	AIDE	MANUAL	AIDE	MANUAL
1	16	1	29.2	120.7
2	14	1	28.2	208.5
3	11	5	30.6	100.9
4	14	5	29.4	92.1
5	17	7	26.6	74.3
6	12	3	36.5	132.6
7	8	4	37.5	108.1
8	15	4	30.4	122.1
	p-value < 0.001		p-value < 0.001	

B) Confusion matrix of the prediction model

C) Steps distribution regarding all the tasks

Figure 5.11: *(A)* Number of the activities achieved regarding the mean time spent per user. Furthermore, it has been trained a SVM model to find the boundary between both modes, yellow smooth line. *(B)* Confusion matrix of the model, used in the *AIDE* mode. *(C)* Interaction with the ECI, measured by steps.

menus is presented in Figure 5.11 (B). In addition, the results obtained through the NASA-tlx questionnaire are presented in Figure 5.12.

The results show that the *AIDE* mode is more efficient, allowing the user to perform the desired activity using less steps. The users performed one step in the 90% of the activities through the *AIDE* mode, and three steps, at least, were necessary in the *Manual* mode. Furthermore, this fact implies that the users were able to perform the ADL spending less time in the *AIDE* mode. It is important to note that, even though the prediction model fails, only three steps were necessary as the performed prediction is always related to the information gathered from the environment. However, five or seven steps in the *Manual* mode involve a failure in the selection of the abstraction level, that can be caused by lack of practice or system performance.

The *AIDE* mode uses a CRF model to perform the predictions about the user intention. The model uses the information of the virtual home and the object that the user is looking at, acquired thought an eye tracking device. The model was previously trained with simulated data using the same virtual house environment. Thus, Fig. 5.11 *(B)*
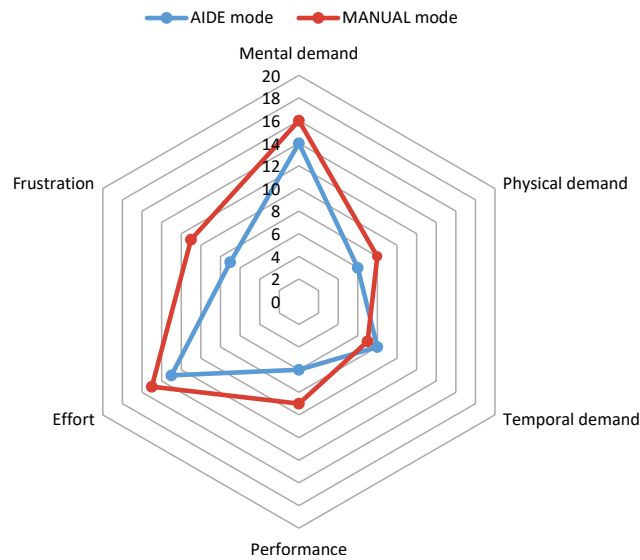
Figure 5.12: Mean scores of the NASA-tlx questionnaire regarding each mode.

shows the confusion matrix of the prediction model, regarding the 'ADL menu', with a global accuracy about 87%. The CRF model, as it takes into account not only the current state but also the previous states to perform its prediction, it could fail in the prediction of task with common features. Therefore, the 50% of the trials related to the *Drink* menu are predicted as the ADL related with the *Eat* menu. In addition, the *TV* and the *Teeth* menus are rarely predicted as the *Entertainment* and *Face* menus, respectively.

Observing the NASA-tlx results, shown in Figure 5.11 there is not statistically significant differences between both modes, unexpectedly. We can say that, as it was the first time that the users handle this complex EEG/EOG interface and multimodal system, both modes were felt very similar. However, a regular use of the proposed system will imply a difference between the modes in terms of task load.

5.2.5 *Conclusions*

The proposed system allows users with motor disabilities to perform ADL in a simulated environment through an ECI controlled by a hybrid EEG/EOG interface. This system uses a prediction model based on CRF in order to detect the user intention and aid in the ECI navigation. Even though the users do not perceive subjective differences between the proposed ECI and the normal ECI, it was observed that the proposed one was more efficient because the users

spent less time to do the desired activity, performing more tasks and doing less steps through the ECI.

We can conclude that the environment analysis and the identification of the user behaviors are a good tool to predict the user intention. Furthermore, it allows to speed up the ECIs scan, opening a new paradigm in the design of these interfaces. Although the developed ECI was only tested in a simulated environment with a specific user interface, it can be easily adapted to a real environment, as the scenario proposed in the AIDE project, and to different interfaces, as switches or voice control commands. Thus, this system demonstrates that assistive technology research can increase the independence at home for people with reduced mobility.

5.3 CONCLUSIONS

This chapter presented two different intelligent technology solutions for home environments. The first scenario proposed a system to intelligently measure independent upper-limb gestures through three MARG devices placed onto the upper arm, forearm and hand. This system uses an OIESGP model, trained through expert data, in order to classify the gesture performed by the patients. In addition, the DTW distance between the performed gesture and the expert gesture was used to assess the quality of the performed gesture and decide the next step in a rehabilitation exercise. This system could allow the patient to rehabilitate not only the motor impairments, but also the cognitive deficits due to the patient must be aware to the indicated actions. These orders can be the execution of simple gestures, complex gestures, a chain of gestures that the patient must complete or a combination of gestures between both upper limbs. In addition, the online feature of this system can allow the system to act at any point of the exercise, guiding the patient to perform a better movement. Finally, all the acquired information can be thoroughly analyzed by the therapist in order to assess the evolution of the patient at home before a therapy session.

On the other hand, the second scenario presented the development of an intelligent ECI that was able to adapt its scan control based on the residual capabilities of the user. Furthermore, it took into account the routine of the subjects and the environmental information facilitating the navigation through the proposed interface. It was demonstrated that learning from the user behaviors and environmental information

is crucial in order to understand their necessities, thus enhancing their independence at home and improving the performance of the ADL.

This chapter has investigated two promising intelligent systems for rehabilitation and assistance at home. However, further developments, discussed in Section 6.2.2 and Section 6.2.3, are necessary before these systems become a powerful tool.

CONCLUSIONS AND FUTURE WORK

This chapter summarizes the contributions that were presented in this thesis and presents the work in progress and future research direction that might emerge from this dissertation.

6.1 OVERVIEW AND CONTRIBUTIONS

This thesis is focused on the development of upper-limb assessment techniques for robot-aided neurorehabilitation therapies at clinical and home environments on the one hand, and on the other for assistance at home when severe motor deficiencies persist after rehabilitation process. The thesis has thus addressed research in various phases and environments that takes part in stroke recovery.

First, it improved the technique presented by Morales Vidal, to online estimate the upper-limb kinematic configuration in neurorehabilitation therapies assisted by end-effector-based robotic devices. It has been demonstrated that the presented algorithm is stable under shoulder displacements, assumed fixed, that can appear due to the motor impairments of the patients. Furthermore, the wearable device attached onto the upper arm, an acceleromenter, does not disturb the normal development of a therapy in which the therapist and the patients are continuously interacting.

To address the issue of the fixed shoulder and bring this tool to a real clinical environment, a second device, attached onto the shoulder, was used to measure the trunk compensations. Thus, a novel algorithm was developed in order to online estimate the upper-limb movements together with the shoulder displacements, and it was successfully validated. Therefore, the proposed algorithm has become an important tool to enhance the assessment of patients during the rehabilitation therapy, as a complement to the clinical assessment scales.

On the other hand, the clinical therapy can be complemented with self-managed rehabilitation systems in order to increase the intensity of the therapy and to improve the rehabilitation outcomes. Thus, this thesis also proposed an intelligent solution, based on the measurement of a set of upper-limb gestures through three wearable devices, to

assess the quality of the exercise performed. The joint movements were assessed through the fusion of two different techniques, one studied the performed movement as a whole, and the other evaluated each joint independently. The promising results suggest that this system could become a new tool to perform motor and cognitive rehabilitation exercises at home as well as endow objective data to the therapist.

Finally, an intelligent environment control interface for ADL assistance at home for people who suffer from severe motor impairments, such as stroke survivors, people with motor disabilities caused by a neurodegenerative disease or a SCI, was developed. This interface was provided with a machine learning model to improve the navigation through it, being able to recognize the intention of the user studying the relevant information of the environment and the user behavior. Furthermore, the scan control of the proposed interface could be adapted to the residual motor capabilities of each individual. Therefore, it is crucial to understand the necessities of each disable person in the development of assistive technology solutions in order to enhance their independence at home.

These contributions focus on both the therapists, providing objective data to perform a better assessments of the patient recovery, and the patients, giving solutions to intensify the therapy at home and improving the rehabilitation outcomes or, in the worst case scenario, offering a tool to increase their independence in daily life.

6.2   FUTURE DIRECTIONS

This section describes some research lines that emerge from the presented work in this thesis which could be addressed in the future.

6.2.1   *Upper-limb Kinematic Reconstruction Algorithm*

This thesis proposes an algorithm to online measure the upper-limb joint variables and the shoulder displacement during a robot-aided neurorehabilitation exercise. However, the upper-limb movements are only used to compute the ROM and the maximum shoulder displacement after the exercise to complement the objective data that the robot itself can provide. One future step is to relate this information with the clinical assessment scales in order to estimates their scores. Furthermore, joint movements can be used to contribute in the user feedback

during the rehabilitation exercises. Thus, the patient can online correct its position and improve the recovery outcomes.

On the other hand, the upper-limb is a complex chain with more than seven DoFs. Thus, the clavicle displacements, omitted in this algorithm, and trunk movements, directly related with shoulder displacements, could be studied and accordingly introduced in the algorithm, in order to enlarge the objective information that the therapist receives.

6.2.2 *Self-managed Rehabilitation System*

The proposed system for self-managed rehabilitation was tested in off-line mode with a healthy subject and two stroke patients. The next step would be to study this system under a specific therapy, online measuring the quality of the gestures performed. Thus, the decisions made by the proposed platform could be analyzed.

Moreover, measuring both limbs and trunk movements would enlarge the therapy options, e. g. to perform a different gesture with each limb, increasing the data offered to the therapist. Indeed, a serious game developed around this system would increase the motivation of the patient and, therefore, the intensity of the therapy.

6.2.3 *Intelligent Environment Control Interface*

The multimodal system proposed was partially simulated due to the complexity in the development of an intelligent house. Furthermore, an hybrid EOG/EEG control system was used to navigate through the proposed ECI. Therefore, this system should be studied in a real environment, with cameras mounted on the user's wheelchair and sensors all around the house. In addition, different control systems could be also tested and compared with the one used in this research, as voice control or eye tracking systems.

ROBOTS, COMPONENTS AND SENSORS

This thesis features several robots, components and sensors, which are described in this appendix for reference.

A.1 HERMES ROBOT

Figure A.1 shows the Hermes robot, a redundant serial robot of seven DoFs. It was designed and built by the Neuro-Bioengineering Research Group (nBio)[1], Miguel Hernández University of Elche, Spain. The workspace of the Hermes robot includes the workspace of the human upper-limb allowing the users to perform three-dimensional movements. It is fully controlled through MatLab®, including forward and inverse kinematic functions, trajectory planning, real time visualization and a simulation environment.
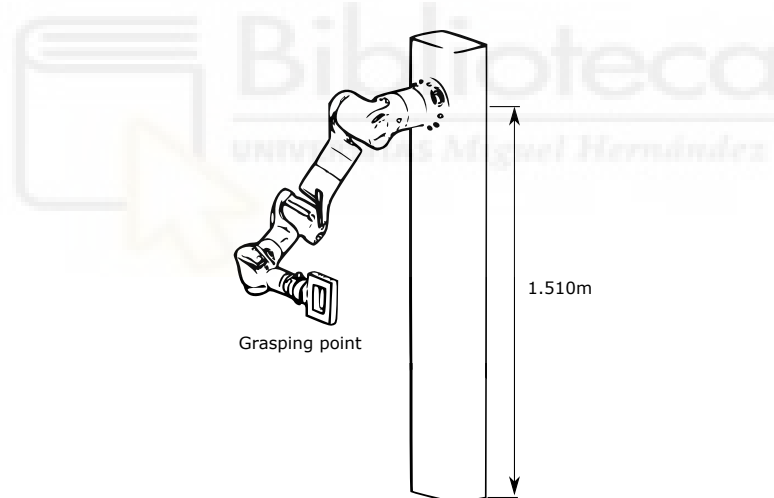
Figure A.1: Hermes Robot.

A.2 PUPARM ROBOT

The PUPArm robot, shown in Figure A.2, is a pneumatic planar robot used in many studies as an end-effector-based neurorehabilitation device (Badesa et al., 2014; Lledó et al., 2016). It was designed and

---

1 http://nbio.umh.es/

built by the Neuro-Bioengineering Research Group (nBio), Miguel
Hernández University of Elche, Spain. It is fully controlled through
Simulink, MatLab®, including real time visualization and a simulation
environment.

Figure A.2: PUPArm Robot.

A.3   MAGNETO-INERTIAL SENSORS

Wearable devices have been used throughout this thesis in order to
measure the acceleration and the orientation of specific upper-limb
segments. Figure A.3 shows the device used with the default axis di-
rections. It is developed by Shimmer™[2] with integrated 9 DoFs inertial
sensing via accelerometer, gyroscope and magnetometer, with a max-
imum sample rate of 1 *kHz*, and a size of 51 *mm x* 34 *mm x* 14 *mm*. It
is a wireless device connected via Bluetooth. This device was used as a
simple accelerometer and as an inertial measurement unit depending
on the needs of each experimentation.
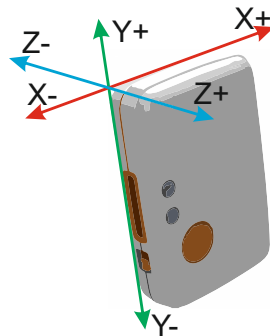
Figure A.3: Wearable device sensor. The default axis directions are marked.

---

2 http://shimmersensing.com/

A.4 SEMG ARMBAND

The Myo Armband[3], developed by Thalmics Labs™, was used in Section 5.1 and it is shown in Figure A.4. It is a wireless sEMG Armband with eight electrodes developed for muscle sensing and equipped with an IMU. The communication is performed via Bluetooth with its own dongle, with a sampling frequency of 200 *Hz*.

Figure A.4: Myo Armband.

A.5 MOTION CAPTURE CAMERAS

Two different motion capture systems were used in the experiments of this thesis. For the validation of the kinematic reconstruction algorithm reported in Chapter 3, a set of eight 6 DoFs optical tracking cameras Optitrack V100: R2, developed by NaturalPoint®[4] was used, shown in

Figure A.5: Optitrack V100: R2 *(up)* and Optitrack V120: Trio *(down)* motion capture cameras.

---

3 https://support.getmyo.com/hc/en-us
4 https://www.naturalpoint.com

Figure A.5, *up*, which relies on the capture of passive markers, with a frame rate from 30 to 100 frames per second, a 640×480 *px* resolution, and an approximate precision of 0.3*mm*.

The Optitrack V120: Trio, also developed by NaturalPoint®, was used in the validation of the proposed algorithm introduced in Chapter 4, shown in Figure A.5, *down*. It is a six DoFs optical tracking with three cameras, with a resolution of 640×480 *px* and a frame rate from 30 to 120 frames per second each one.

A.6   EEG/EOG ACQUISITION SYSTEM

In Section 5.2, the control of the proposed ECI was tested through a hybrid EEG/EOG-based interface (Soekadar et al., 2016). It consists in one acquisition system of eight solid-gel electrodes, placed in F3, C3, Cz, P3, T7 and mastoid with the reference electrode in C4 and the ground in FpZ according to the international 10/20 system, to acquire the SMR, as shown in Figure A.6, *left*. The horizontal eye movements were acquired with two electrodes placed on the outer canthus of the eyes. The EEG/EOG signals were acquired with the Enobio amplifier, developed by Neuroelectrics®[5], Barcelona, Spain, shown in Figure A.6, *right*. It sends the amplified signals to a computer via Bluetooth.
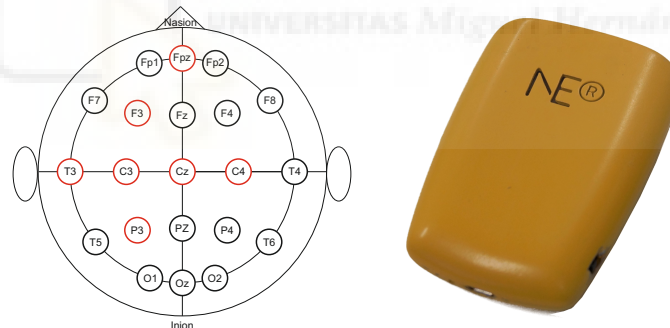
Figure A.6: Position of the electrodes selected, marked as red circles, *(left)* and Enobio amplifier *(right)*.

The real-time SMR-based interface was implemented using BCI2000, a freely distributed software for multipurpose standard BCI platform (Schalk et al., 2004). The sample frequency of the system was set to 500 *Hz*, bandpass filtered at $0.4 - 70$ *Hz* and pre-processed using a Laplacian filter.

---

5 https://www.neuroelectrics.com/

A.7   EYE TRACKER

The Tobii®[6] PCEye Go, shown in Figure A.7, is an eye tracker used in Section 5.2 in order to measure the gaze point of the subjects. Thus, the system was able to detect the objects that the user was observing in the virtual house. It consists in a two infrared illuminators shining light on the user's face, which is then reflected by the cornea. This reflection is registered by a camera in order to estimates the position of each eye over a specific screen. The calibration process is very simple and easy to use by different subjects. The device enables a tracking rate of 30 *Hz* and an accuracy of 0.4 *deg*.

Figure A.7: Eye tracker.

---

6 https://www.tobii.com/

MAIN CONTRIBUTIONS

The presented PhD dissertation is sustained by a compendium of peer-reviewed publications previously published in indexed journals according to the last JCR. Listed are the publications that form the main work of the thesis:

Bertomeu-Motos, **A.**; Lledó, L. D.; Díez, J. A.; Catalan, J. M.; Ezquerro, S.; Badesa, F. J. and Garcia-Aracil, N. (2015b), 'Estimation of Human Arm Joints Using Two Wireless Sensors in Robotic Rehabilitation Tasks', *Sensors* **15**(12), pp. 30571–30583, DOI: `10.3390/s151229818`

- Journal Title: Sensors (ISSN: 1424-8220)

- JCR-SCI Impact Factor (2015): 2.033.

- Category: Instruments & Instrumentation, Quartile Q1 (12/56).

Bertomeu-Motos, **A.**; Blanco, A.; Badesa, F. J.; Barios, J. A.; Zollo, L. and Garcia-Aracil, N. (2018), 'Human arm joints reconstruction algorithm in rehabilitation therapies assisted by end-effector robotic devices', *Journal of NeuroEngineering and Rehabilitation* **15**(1), p. 10, DOI: `10.1186/s12984-018-0348-0`

- Journal Title: J. NeuroEng. Rehabil. (ISSN: 1743-0003).

- JCR-SCI Impact Factor (2018): 3.582.

- Category: Rehabilitation, Quartile Q1 (4/65).

Bertomeu-Motos, **A.**; Ezquerro, S.; Barios, J. A.; Lledó, L. D.; Domingo, S.; Nann, M.; Martin, S.; Soekadar, S. R. and Garcia-Aracil, N. (2019), 'User activity recognition system to improve the performance of environmental control interfaces: a pilot study with patients', *Journal of NeuroEngineering and Rehabilitation* **16**(1), p. 10, DOI: `10.1186/s12984-018-0477-5`

- Journal Title: J. NeuroEng. Rehabil. (ISSN: 1743-0003).

- JCR-SCI Impact Factor (2018[1]): 3.582.

- Category: Rehabilitation, Quartile Q1 (4/65).

Prints of these publications are presented next.

---

1 JCR-SCI Impact Factor corresponding to the year of publication is not available.

Estimation of Human Arm Joints Using Two Wireless Sensors in Robotic Rehabilitation Tasks

Arturo Bertomeu-Motos *, Luis D. Lledó, Jorge A. Díez, Jose M. Catalan, Santiago Ezquerro, Francisco J. Badesa and Nicolas Garcia-Aracil

Neuro-Bioengineering Research Group, Miguel Hernandez University, Avda. de la Universidad W/N, 03202 Elche, Spain; llledo@umh.es (L.D.L.); jdiez@umh.es (J.A.D.); jose.catalan@goumh.umh.es (J.M.C.); sezquerro@umh.es (S.E.); fbadesa@umh.es (F.J.B.); nicolas.garcia@umh.es (N.G.-A.)
* Correspondence: abertomeu@umh.es; Tel.: +34-965-222-505; Fax: +34-966-658-979

Abstract: This paper presents a novel kinematic reconstruction of the human arm chain with five degrees of freedom and the estimation of the shoulder location during rehabilitation therapy assisted by end-effector robotic devices. This algorithm is based on the pseudoinverse of the Jacobian through the acceleration of the upper arm, measured using an accelerometer, and the orientation of the shoulder, estimated with a magnetic angular rate and gravity (MARG) device. The results show a high accuracy in terms of arm joints and shoulder movement with respect to the real arm measured through an optoelectronic system. Furthermore, the range of motion (ROM) of 50 healthy subjects is studied from two different trials, one trying to avoid shoulder movements and the second one forcing them. Moreover, the shoulder movement in the second trial is also estimated accurately. Besides the fact that the posture of the patient can be corrected during the exercise, the therapist could use the presented algorithm as an objective assessment tool. In conclusion, the joints' estimation enables a better adjustment of the therapy, taking into account the needs of the patient, and consequently, the arm motion improves faster.

Keywords: kinematic reconstruction; neuro-rehabilitation; end-effector robots; upper limbs; MARG

1. Introduction

Robot-aided neuro-rehabilitation therapies have become an interesting field in the robotics area. There are several devices, such as exoskeletons, prosthesis or end-effector configuration robots, developed for this purpose [1,2]. They are able to help and assist the shortcomings of human beings. Post-stroke patients usually lose limb mobility due to the impairment in motor activity. Rehabilitation in this field takes an important role when it comes to improving the motor and proprioceptive activity [3,4]. In terms of the activities of daily living (ADL), the total or partial recovery of the upper limbs is the most important part in early rehabilitation. End-effector configuration robots are the most common devices used in these therapies. They are easily adapted to and easy to use by patients with different diseases.

These robots provide objective information about the trajectory followed by the end effector and the improvement in the motor recovery. However, they are not able to measure and control the arm movements. The progress in the arm joints, *i.e.*, the range of motion (ROM), is an important parameter in these kinds of therapies. This estimation requires non-invasive wearable sensors, which must be easy to place onto the patient's arm and must be extended to a clinical environment. Visual feedback of the arm configuration is studied in some rehabilitation therapies, though the arm joints cannot be measured [5,6]. This estimation can be accurately performed with optoelectronic systems based on motion tracking, even though they cannot be adapted to a rehabilitation environment [7,8]. In 2006,

Mihelj developed a method to estimate the arm joints through two accelerometers placed onto the upper arm [9]. Then, Papaleo *et al.* improved this method using a numerical integration through the augmented Jacobian in order to estimate the arm configuration with only one accelerometer [10,11]. This algorithm performs a kinematic reconstruction of the simplified human arm model with seven degrees of freedom (DoFs) assuming that the shoulder is fixed during the therapy. Due to the loss of motor function, shoulder movements cannot be avoided by the patient, and therefore, this assumption cannot be always accomplished. Thus, it is necessary to measure shoulder movements in order to correct the position of the patient during the activity. This compensation can be detected and categorized through the fusion of a depth camera with skeleton tracking algorithms [12]. However, to compute the kinematic reconstruction, the position and orientation of the shoulder with respect to the robot are necessary.

This paper presents a kinematic reconstruction algorithm of human arm joints assuming a simplified model with five DoFs. Furthermore, this method is able to estimate the shoulder movement, *i.e.*, its position and orientation. It is based on the inverse kinematics through the pseudo-inverse of the Jacobian [13]. The end-effector planar robot, called "PUPArm", with three DoFs (see Figure 1), designed and built by Neuro-Bioengineering Research Group (nBio), Miguel Hernández University of Elche, Spain, is used [14]. The accuracy of the estimated joints with respect to the real arm joints, measured through a tracking camera, is studied. In addition, the ROMs on 50 healthy subjects performing a therapy activity are evaluated in two different cases: trying not to move the shoulder during the exercise and following the movement with the trunk to reach the goal.

Figure 1. PUPArm robot.

2. Algorithm Description

2.1. Human Arm Kinematic Chain

The human arm is a complex kinematic chain that can be defined as the contribution of several robotic joints. The arm was defined as a chain of nine rotational joints by Lenarčič and Umek [15]. Only seven DoFs take part in this experiment: a spherical joint in the shoulder; an elbow joint; and a spherical joint in the wrist; as is shown in Figure 2a. On the other hand, the PUPArm robot fixes two kinds of movements: the ulnar-radial deviation and the flexion-extension of the hand; thus, abduction-adduction (q_1), flexion-extension (q_2) and internal-external rotation (q_3) of the shoulder, flexion-extension (q_4) of the elbow and pronation-supination (q_5) of the forearm comprise the kinematic chain linked through two segments: the upper arm (l_u) and the forearm (l_f). The Denavit–Hartenberg (DH) parameters of the arm are shown in Table 1, and their reference systems are shown in Figure 2b.

Table 1. DH parameters of the kinematic arm chain.

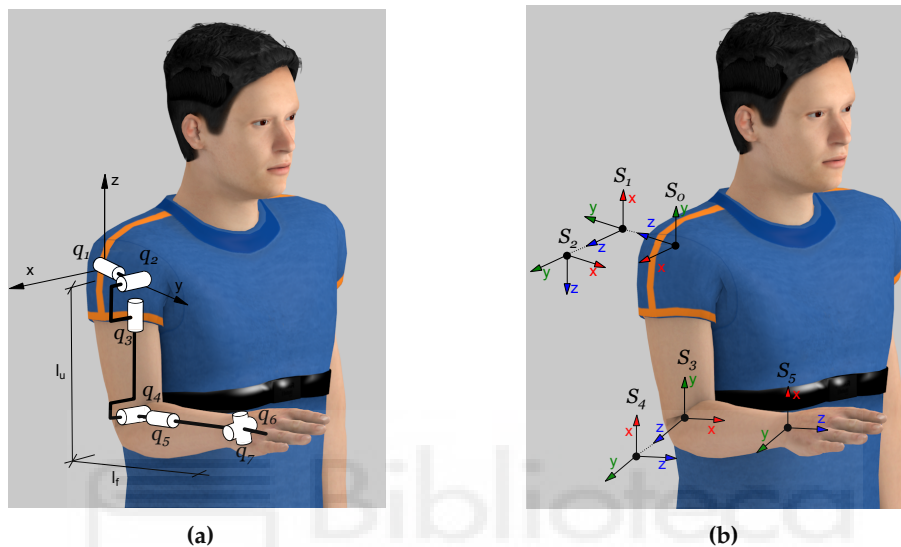| i	θ_i	d_i	a_i	α_i
1	$\pi/2 + q_1$	0	0	$\pi/2$
2	$3\pi/2 + q_2$	0	0	$\pi/2$
3	q_3	l_u	0	$-\pi/2$
4	$\pi/2 + q_4$	0	0	$\pi/2$
5	q_5	l_f	0	0

Figure 2. Human arm joints. (**a**) Simplification of human arm joints with seven DoFs; (**b**) Denavit–Hartenberg (DH) coordinate systems of the arm with five DoFs.

2.2. Integration Method

The inverse kinematics of the human arm during the exercise is based on the numerical integration through the pseudo-inverse of the Jacobian (J) [10]. The necessary devices to estimate the arm joints are: the end-effector robot; an accelerometer placed onto the upper arm and a magnetic angular rate and gravity (MARG) device placed onto the shoulder. Instantaneous joint velocities may be assessed as:

$$\dot{\vec{q}} = J^{-1}(\vec{q})\{\dot{\vec{v}}_d + K \cdot \vec{err}\} \tag{1}$$

being $\dot{\vec{v}}_d$ the Cartesian vector of the hand velocity and $\vec{err}$ the error committed due to the numerical integration. It should be noted that $\dot{\vec{v}}_d$ is the hand velocity vector with respect to the shoulder, estimated through the MARG and the accelerometer. To minimize this error, a 7×7 gain matrix K is added to this Equation [13]. Then, the current arm joints are computed as:

$$\vec{q}(t_{k+1}) = \vec{q}(t_k) + \dot{\vec{q}}(t_k)\Delta t \tag{2}$$

where $\vec{q}(t_k)$ is the previous estimated joints, $\dot{\vec{q}}(t_k)$ is the joint velocity vector obtained through Equation (1) and Δt is the sampling time. On the other hand, the initial arm joints are necessary to begin the integration method; their computation is explained in Section 2.6.

2.3. Accelerometer Orientation

If slow movements are assumed, the orientation of the accelerometer can be estimated in any position of the arm within the reachable workspace of the robot. When joints q_1 to q_5 are equal to zero, the reference position of the arm is set; a visual representation of this position is shown in

Figure 2b. The acceleration acquired in the reference orientation of the accelerometer regarding the gravity, which is shown in Figure 3a, is:

$$^{acc_0}V_g = \begin{bmatrix} 0 \\ 1 \\ 0 \end{bmatrix} \tag{3}$$
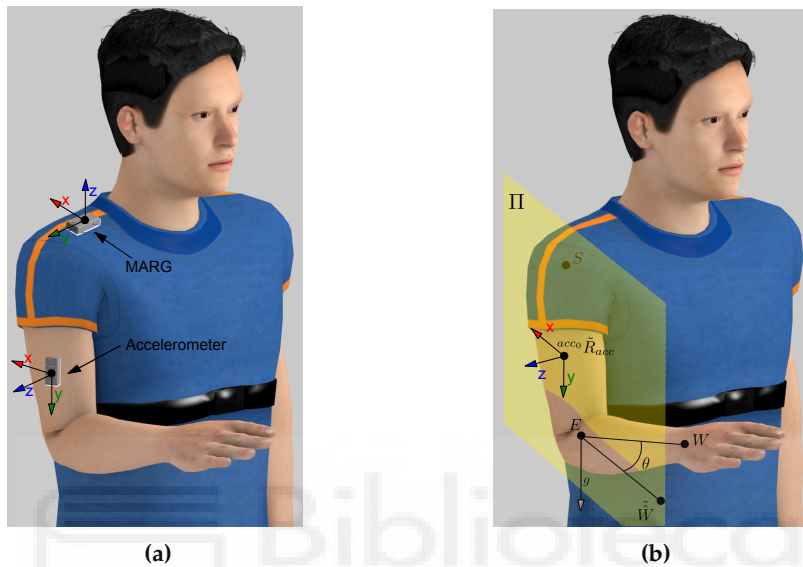
Figure 3. (**a**) Reference orientation of the accelerometer and the MARG. (**b**) Plane Π shaped by the X axis and Y axis of $^{acc_0}\tilde{R}_{acc}$.

Moreover, at any random position of the arm, $^{acc_0}V_g$ can be computed through the applied rotation to the accelerometer ($^{acc_0}R_{acc}$) as:

$$^{acc_0}V_g = {}^{acc_0}R_{acc}{}^{acc}V_g \tag{4}$$

being $^{acc}V_g$ the acceleration at this random position regarding the gravity.

Equation (4) has infinite rotation matrices over the gravity vector, though one possible solution may be computed as:

$$^{acc_0}\tilde{R}_{acc} = I + M + M^2\frac{1 - \cos(\theta)}{\sin^2(\theta)} \tag{5}$$

with:

$$M = \begin{bmatrix} 0 & -V_3 & V_2 \\ V_3 & 0 & -V_1 \\ -V_2 & V_1 & 0 \end{bmatrix}$$

$$V = {}^{acc_0}V_g \times {}^{acc}V_g$$

$$sin(\theta) = \|V\|$$

$$cos(\theta) = {}^{acc_0}V_g \cdot {}^{acc}V_g \tag{6}$$

Thereby, a plane can be shaped by the X axis and Y axis of $^{acc_0}\tilde{R}_{acc}$ (plane Π). This plane only contains the elbow point (E), but the correct orientation of the accelerometer must also contain the shoulder (S) and the wrist (W) points. Thus, the rotation angle (θ) is defined as the angle between the known wrist point and the new wrist point ($\tilde{H}$), contained in the plane Π, when it is rotated

around the gravity vector (g) placed in E (see Figure 3b). Therefore, $\tilde{\bar{H}}$, expressed in terms of θ, can be defined as:

$$\tilde{\bar{W}} = \left(g \cdot \hat{W}\right) g + \cos\left(\theta\right) \left(\hat{W} - \left(g \cdot \hat{W}\right) g\right) - \sin\left(\theta\right) \left(g \times \hat{W}\right) \tag{7}$$

where $\hat{W} = \left(W - E\right) / \left(\|W - E\|\right)$ and $g = \begin{bmatrix} 0 & 0 & -1 \end{bmatrix}^T$. Then, θ can be obtained solving the following equation:

$$d\left(\tilde{\bar{W}}, \Pi\right) = \frac{\left| A_\Pi \tilde{\bar{W}}_x + B_\Pi \tilde{\bar{W}}_y + C_\Pi \tilde{\bar{W}}_z + D_\Pi \right|}{\sqrt{A_\Pi{}^2 + B_\Pi{}^2 + C_\Pi{}^2}} = 0 \tag{8}$$

having the plane Π computed as follows:

$$
\begin{aligned}
\tilde{P}^x_{acc} &= {}^{acc_0}\tilde{R}_{acc} \begin{bmatrix} 1 & 0 & 0 \end{bmatrix}^T \\
\tilde{P}^y_{acc} &= {}^{acc_0}\tilde{R}_{acc} \begin{bmatrix} 0 & 1 & 0 \end{bmatrix}^T \\
\overline{S\tilde{P}^y_{acc}} &= \left(\tilde{P}^y_{acc} - S\right) \\
\overline{\tilde{P}^x_{acc}\tilde{P}^y_{acc}} &= \left(\tilde{P}^y_{acc} - \tilde{P}^x_{acc}\right) \\
\begin{bmatrix} A_\Pi \\ B_\Pi \\ C_\Pi \end{bmatrix} &= \overline{S\tilde{P}^y_{acc}} \times \overline{\tilde{P}^x_{acc}\tilde{P}^y_{acc}} \\
D_\Pi &= \begin{bmatrix} A_\Pi & B_\Pi & C_\Pi \end{bmatrix}^T \cdot S
\end{aligned}
\tag{9}
$$

Two possible solutions are obtained through Equation (8) and, therefore, two values of ${}^{acc_0}R_{acc}$. The correct solution is one for which the Z axis is in the same direction as the cross product between the elbow-wrist segment and elbow-shoulder segment due to the reference position of the accelerometer. Finally, the rotation of the accelerometer regarding the robot is computed as:

$$^r R_{acc} = {}^r R_{acc_0} \cdot {}^{acc_0} R_{acc} \tag{10}$$

being ${}^r R_{acc_0}$ the reference orientation of the accelerometer concerning the robot (see Figure 3a). This orientation is required to estimate the elbow orientation and shoulder position during the exercise.

2.4. MARG Orientation

The orientation of magneto-inertial devices is usually based on Kalman filtering [16]; nevertheless, they can be quite complicated, and an extended Kalman filter is needed to linearize the problem. The orientation filter to measure the rotation of the MARG of Madgwick *et al.* is used in this algorithm [17]. The magnetic distortion that may be introduced by external sources, including metal furniture and metal structures within a building, is performed in this filter [18]. Furthermore, the orientation algorithm requires an adjustable parameter (β) that can be adjusted to the requirements of this exercise. Hence, the value of this parameter ($\beta = 5$) was established after a "trial and error" approach tested before the experiment, taking into account the features of the exercises.

This filter measures the reference quaternion of the device with respect to the Earth reference system, defined by the gravity vector and the Earth's magnetic field lines. However, the rotation of the Earth concerning the robot is unknown. If the MARG is placed in a known orientation with respect to the robot (${}^R_{M_0}\hat{q}$), the acquired transformation defines the Earth frame relative to the sensor frame (${}^{M_0}_E\hat{q}$), and therefore, the reference transformation between the robot and the Earth is known as:

$$^R_E\hat{q} = {}^R_{M_0}\hat{q} \otimes {}^{M_0}_E\hat{q} \tag{11}$$

Therefore, every rotation of the MARG is defined in the workspace as:

$$\underset{M}{\overset{R}{\hat{q}}} = \underset{E}{\overset{R}{\hat{q}}} \otimes \underset{E}{\overset{M}{\hat{q}}}{}^* \tag{12}$$

where $\underset{E}{\overset{M}{\hat{q}}}$ is the current value of the sensor. In this way, the shoulder orientation is estimated during the exercise.

2.5. Elbow and Shoulder Location

The hand, as was said before, is tightly attached to the end effector of the robot, and the ulnar-radial deviation and flexion-extension of the hand remain constant. Hence, the transformation matrix between the hand and the end effector (^rT_w) is known, and therefore, the elbow position may be obtained as:

$$^rP_e = {}^r T_w * \begin{bmatrix} 0 & 0 & -l_f & 1 \end{bmatrix}^T \tag{13}$$

The orientation of the elbow, since the rotation matrix between the elbow and the accelerometer orientation ($^{acc_0}R_e$) is known (see Figure 3a), may be calculated as:

$$^rR_e = {}^r R_{acc} \cdot {}^{acc_0} R_e \tag{14}$$

with $^rR_{acc}$ the rotation matrix computed through Equation (10). Thus, the transformation of the elbow relative to the robot remains:

$$^rT_e = \begin{bmatrix} & {}^rR_e & & {}^rP_e \\ 0 & 0 & 0 & 1 \end{bmatrix} \tag{15}$$

On the other hand, one of the most important points of this algorithm is the ability to estimate the shoulder position and orientation during the exercise. The shoulder position can be processed easily through Equation (15) as:

$$^rP_s = {}^r T_e * \begin{bmatrix} 0 & lu & 0 & 1 \end{bmatrix}^T \tag{16}$$

Whilst the orientation of the MARG relative to the robot is known by Equation (12), its rotation matrix ^rR_M is directly obtained [19]. Thus, the shoulder orientation is estimated as:

$$^rR_s = {}^r R_M \cdot {}^{M_0} R_s \tag{17}$$

where ^rR_M is the current rotation of the sensor with respect to the robot and $^{M_0}R_s$ the reference position of the MARG relative to the shoulder (see Figure 3a). Hence, the transformation of the shoulder relative to the robot remains:

$$^rT_s = \begin{bmatrix} & {}^rR_s & & {}^rP_s \\ 0 & 0 & 0 & 1 \end{bmatrix} \tag{18}$$

Finally, since the elbow and the shoulder location are instantaneously known, the initial conditions and the integration method can be performed.

2.6. Initial Conditions

In this algorithm, since it is based on a numerical integration, the initial conditions are required. The locations of the three main points, namely the shoulder (^rT_s), the elbow (^rT_s) and the wrist (^rT_s), are known. The shoulder joints (q_1, q_2 and q_3) are directly related to the matrix $^sT_e = {}^r T_s^{-1} \cdot {}^r T_e$,

defined in the previous section, and they can be acquired by the spherical joint method [13]. This matrix, in terms of the corresponding joints, can be expressed by DH parameters shown in Table 1 as:

$$
{}^{s_0}T_{s_3} = {}^{s_0}T_{s_1} \cdot {}^{s_1}T_{s_2} \cdot {}^{s_2}T_{s_3} =
\begin{bmatrix}
c_1 s_3 - c_3 s_1 s_2 & -c_2 s_1 & c_1 c_3 + s_1 s_2 s_3 & l_u c_2 s_1 \\
s_1 s_3 + c_1 c_3 s_2 & c_1 c_2 & c_3 s_1 - c_1 s_2 s_3 & -l_u c_1 c_2 \\
-c_2\, c_3 & s_2 & c_2\, s_3 & -l_u s_2 \\
0 & 0 & 0 & 1
\end{bmatrix}
\tag{19}
$$

having $s_i = \sin(q_i)$ and $c_i = \cos(q_i)$, $i = \{1, 2, 3\}$. If the transformation matrix ${}^{s_0}T_{s_3}$ is defined as:

$$
{}^{s_0}T_{s_3}(q_1, q_2, q_3) =
\begin{bmatrix}
n_x & n_y & n_z & p_x \\
o_x & o_y & o_z & p_y \\
a_x & a_y & a_z & p_z \\
0 & 0 & 0 & 1
\end{bmatrix}
\tag{20}
$$

two possible solutions of the shoulder joints are obtained; if $q_2 \in [0 \quad \pi]$:

$$
\begin{aligned}
q_1 &= \text{atan2}\left(-n_y, o_y\right) \\
q_2 &= \text{atan2}\left(a_y, \sqrt{n_y^2 + o_y^2}\right) \\
q_3 &= \text{atan2}\left(a_z, -a_x\right)
\end{aligned}
\tag{21}
$$

and if $q_2 \in [-\pi \quad 0]$:

$$
\begin{aligned}
q_1 &= \text{atan2}\left(n_y, -o_y\right) \\
q_2 &= \text{atan2}\left(a_y, -\sqrt{n_y^2 + o_y^2}\right) \\
q_3 &= \text{atan2}\left(-a_z, a_x\right)
\end{aligned}
\tag{22}
$$

Thereby, the elbow joint (q_4) is directly determined with the cosine law as:

$$
q_4 = \arcsin\left(\frac{l_u^2 + l_f^2 - ||H - S||^2}{2 l_u l_f}\right)
\tag{23}
$$

and its homogeneous matrix remains:

$$
{}^{s_3}T_{s_4} =
\begin{bmatrix}
-\sin(q_4) & 0 & \cos(q_4) & 0 \\
\cos(q_4) & 0 & \sin(q_4) & 0 \\
0 & 1 & 0 & 0 \\
0 & 0 & 0 & 1
\end{bmatrix}
\tag{24}
$$

Thus, the transformation matrix between the systems s_0 and s_4 can be computed. The known matrix ${}^{s}T_h = {}^{r}T_s^{-1} \cdot {}^{r}T_h$ defines the transformation between the system s_0 and s_5. On the other hand, the last joint, q_5, is defined with the DH parameters as:

$$
{}^{s_4}T_{s_5}(q_5) =
\begin{bmatrix}
-\sin(q_5) & \cos(q_5) & 0 & 0 \\
\cos(q_5) & \sin(q_5) & 0 & 0 \\
0 & 0 & 1 & 0 \\
0 & 0 & 0 & 1
\end{bmatrix}
\tag{25}
$$

and therefore, q_5 is estimated as:

$$
q_5 = \text{atan2}\left(-n_x, o_x\right)
\tag{26}
$$

Finally, two possible configurations of the arm joints are found, even though only one solution is possible. Due to the limits of the arm joints, $[-\pi/2 \quad \pi/2]$, only one solution accomplishes this restriction, and the initial position of the arm is assessed. This method can produce abrupt changes in the estimated arm joints caused by possible perturbations in the accelerometer that might lead to a non-anatomical position. Hence, since the new position depends on the latest position and the sample time, the integration method for real-time reconstruction is the best way to overcome the aforementioned drawbacks following Equations (1) and (2).

3. Results and Discussion

3.1. Experimental Exercises

With the aim of studying the arm joint estimation algorithm, with $K = diag\{1.5, 1.5, ...1.5\}$ N/ms (chosen by the "trial and error" approach tested before the experiment), two different experiments were performed. The first exercise was to compute the algorithm accuracy in terms of the arm joints and the position of the shoulder, performed by four healthy subjects. Then, a rehabilitation exercise with two different trials was performed by 50 healthy subject (aged between 20 and 72) to test the behavior of the presented algorithm. In both cases, the length of the upper arm was measured from the lateral side of the acromion to the proximal radius head, in the elbow joint. From the proximal radius head to the radial styloids, the distal part of the radius, the forearm length was measured [20]. Moreover, both experiments are performed under the same activity: 3D roulette, which may be seen in Figure 4. The activity consisted of taking a box from the perimeter and placing it in the center of the screen; hand movements are symbolized as a wrench (see Figure 4). One movement is considered when the subject goes from the center of the roulette to the perimeter and returns again to the center.
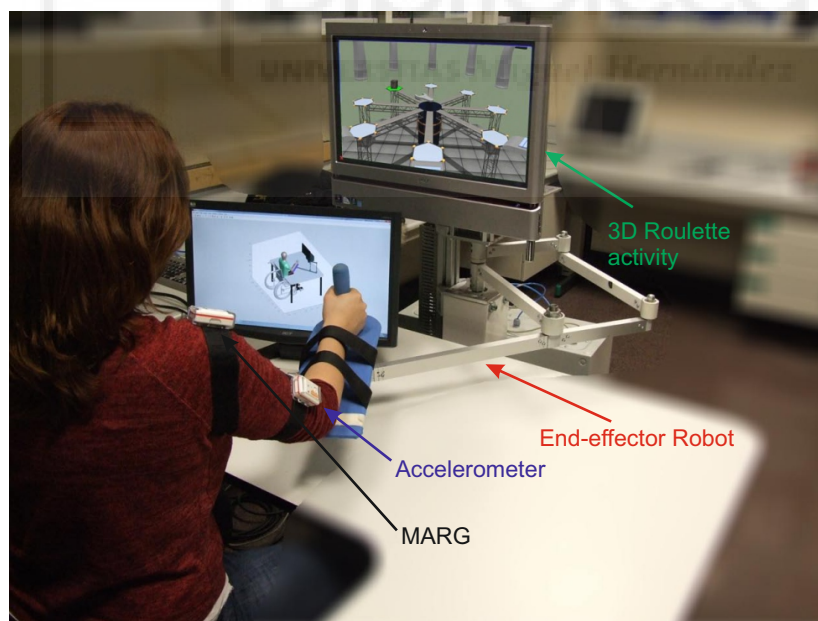
Figure 4. Subject wearing the sensors, the accelerometer and the MARG, grasping the end effector of the robot and performing the 3D roulette activity.

A magneto-inertial sensor, developed by Shimmer$^{©}$, is tightly attached onto the upper arm and onto the shoulder to compute the kinematic reconstruction algorithm. The real position of the arm is computed with a six DoF optical tracking camera Optitrak V120: Trio, developed by NaturalPoint$^{®}$. Specific parts attached to the hand, upper arm and forearm with retro-reflective markers were developed for this purpose. Information about the subjects who carried out the validation experiment are shown in Table 2; they performed three trials of the same exercise.

Table 2. Main subject data from the validation experiment.

ID	Age	Gender	Forearm Length (m)	Upper Arm
1	21	Male	0.23	0.32
2	51	Female	0.21	0.33
3	32	Male	0.25	0.31
4	31	Male	0.21	0.33

In the second experiment, two different trials of the same activity were performed. The first trial was intended not to move the shoulder while the exercise was being conducted, *i.e.*, without compensation with the trunk. However, the participants were asked to follow the hand movements with the shoulder in the second exercise. Each trial consisted of 24 movements.

3.2. Algorithm Validation

The mean error committed, in terms of root mean square error (RMSE) and standard deviation, is shown in Figure 5a. The mean RMSE of the joints is 0.047 rad with a standard deviation of 0.013 rad. Otherwise, the error committed on the shoulder position estimation, which may be found in Figure 5b, shows the mean RMSE committed, less than 0.87 cm, and the standard deviation, around 0.83 cm. The good results show that the error committed is small (it is hardly noticeable by the human eye), and therefore, the accuracy of the presented algorithm with respect to the real arm movements is high. A kinematic reconstruction of the arm joints and the estimation of shoulder position acquired from both methods through the presented algorithm (red dotted line) and the direct reconstruction (blue line) are pictured in Figure 6.
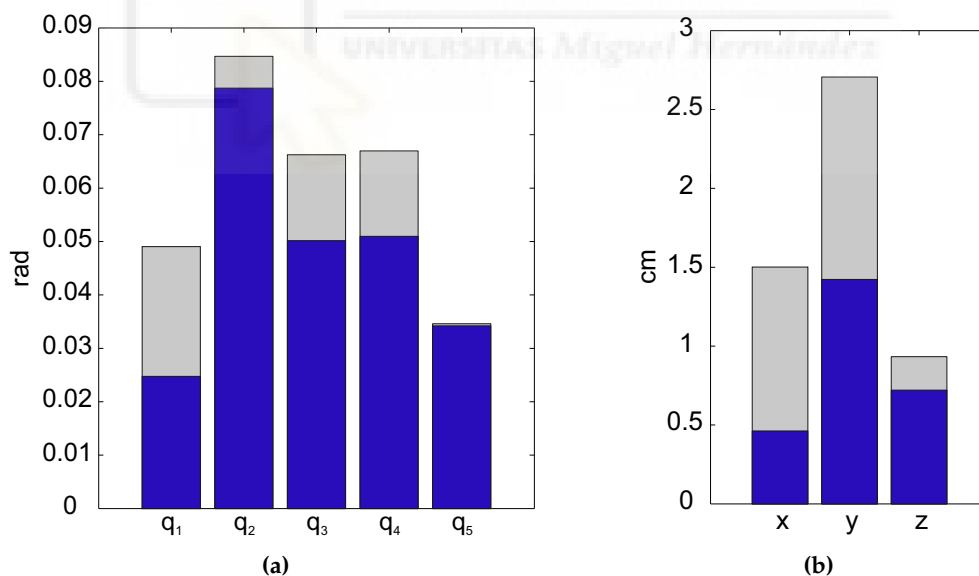

Figure 5. Error committed in the reconstruction algorithm. (**a**) Mean RMSE (blue bar) of the joints committed by the subjects and standard deviation (gray bar); (**b**) Mean RMSE (blue bar) of the shoulder position committed by the subjects and the standard deviation (gray bar): x, left/right movements; y, forward/backward movements; z, up/down movements.
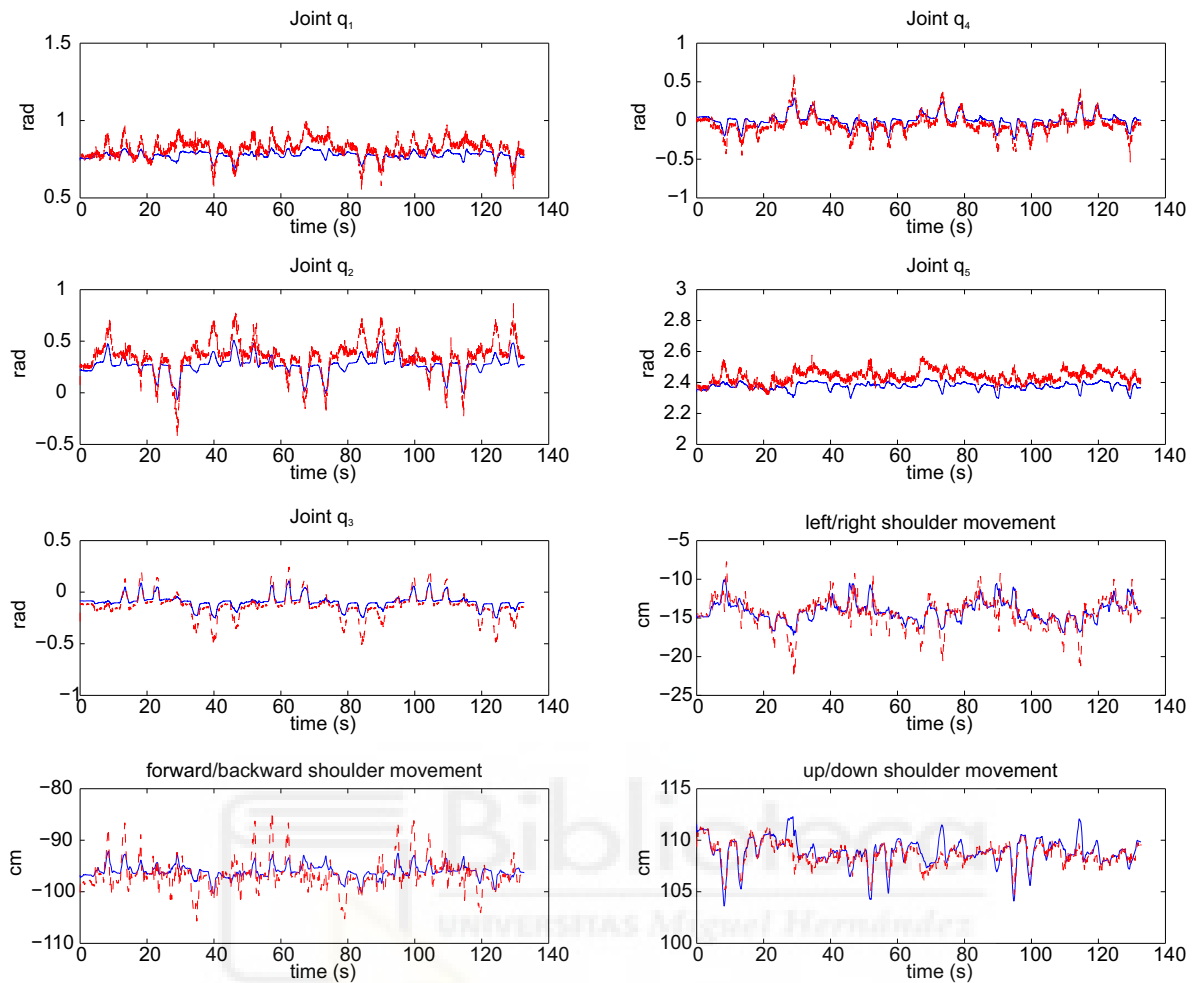
Figure 6. Joints and shoulder movements estimated through the algorithm (dotted red line) and measured through the optoelectronic system (blue line) of a subject during an exercise.

3.3. Arm Joint Range

In this experiment, the ROM between both trials, with and without compensation with the trunk, is studied. Furthermore, the shoulder movement is compared to its real position, acquired with the optoelectronical system mentioned before. To compare both groups, statistical analysis is performed through the *t*-test for paired data for each ROM. Joints 1 to 4 show significant differences ($p \leq 0.05$), but nevertheless, Joint 5, as the subject wrist is attached to the end effector of the robot, does not show significant differences ($p = 0.064$).

The estimated ROM in the exercise without compensation and with compensation is shown in Figure 7a, and the error committed might be seen in Figure 7b. It should be noted that the error committed in each joint for both exercises is smaller than six degrees. On the other hand, the ROM estimated for the trial without compensation is larger than that from the other trial. This result was expected, because the shoulder compensation affects the joint range. However, the ROMs of Joint 5 are similar, because the pronation-supination of the forearm is not affected when the compensation is performed.
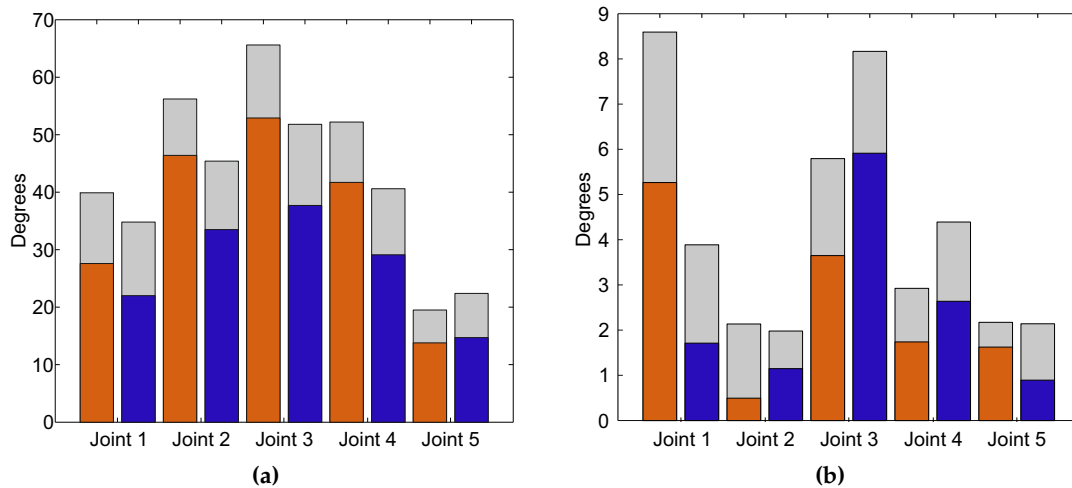
Figure 7. Representation of both trials: without compensation (orange bar) and with compensation (blue bar), and the standard deviation (gray bar) in terms of arm joints. (**a**) Estimated range of motion (ROM); (**b**) Error committed between the real ROM and the estimated ROM.

The accuracy of the shoulder position, taking into account the whole population (N = 51), is shown in Figure 8a. The estimated shoulder position with respect to the real shoulder location in a compensation trial performed by one subject can be seen in Figure 8b.
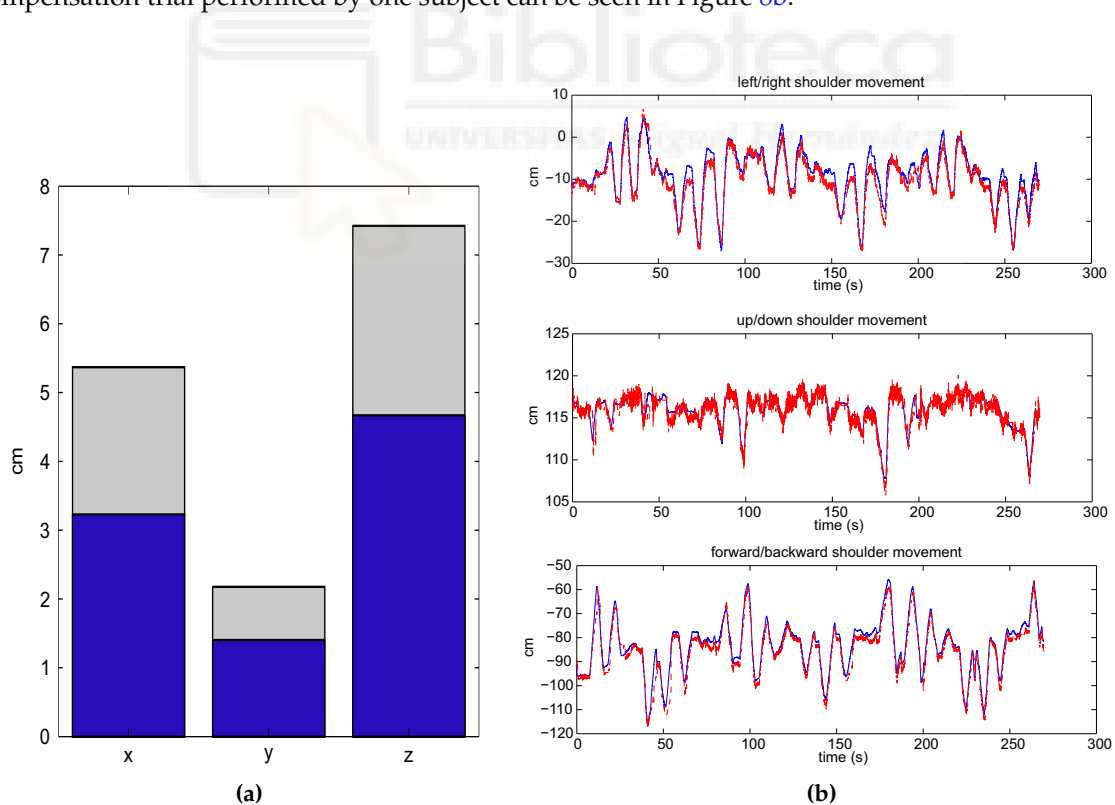
Figure 8. Shoulder movement in the compensation trial. (**a**) Mean RMSE (blue bar) committed by the population and the standard deviation (gray bar): x, left/right movements; y, forward/backward movements; z, up/down movements; (**b**) Estimated movement through the proposed algorithm (dotted red line) and the direct movement (blue line) performed by one subject.

4. Conclusions

In this paper, a kinematic reconstruction of the upper limbs during robot-aided rehabilitation with planar robots taking into account shoulder movements is presented. The estimated arm joints are very accurate with respect to the real position of the arm. Thus, the arm joint improvements of the patient can be measured objectively, and a better adaptation of the therapy to the patient needs can be also performed.

The measurement of the shoulder movement can be also computed accurately. To the best of our knowledge, this feature is not included in the previous algorithms where the shoulder is assumed to be fixed, even when little movements cannot be avoided during the exercise. This feature helps the therapist to correct the patient's posture during exercise for faster improvement in terms of arm mobility.

In summary, the arm joints' improvement may be included as a new objective assessment parameter in addition to the motor and proprioceptive activity and assessments scales, which are, by definition, subjective, as the Fugl–Meyer assessment [21].

Author Contributions: N.G.-A., F.J.B and L.D.L. conceived of and designed the experiments. A.B.-M. and S.E. performed the experiments. A.B.-M. drafted the paper. A.B.-M., J.M.C. and J.A.D. analyzed the data. All authors read and approved the manuscript.

Conflicts of Interest: The authors declare no conflict of interest.

References

1. Nef, T.; Mihelj, M.; Colombo, G.; Riener, R. ARMin-robot for rehabilitation of the upper extremities. In Proceedings of the 2006 IEEE International Conference on Robotics and Automation, Orlando, FL, USA, 15–19 May 2006.
2. Tang, Z.; Zhang, K.; Sun, S.; Gao, Z.; Zhang, L.; Yang, Z. An upper-limb power-assist exoskeleton using proportional myoelectric control. *Sensors* **2014**, doi:10.3390/s140406677.
3. Lum, P.S.; Burgar, C.G.; Shor, P.C.; Majmundar, M.; der Loos, M.V. Robot-assisted movement training compared with conventional therapy techniques for the rehabilitation of upper-limb motor function after stroke. *Arch. Phys. Med. Rehabil.* **2002**, *83*, 952 – 959.
4. Badesa, F.; Morales, R.; Garcia-Aracil, N.; Alfaro, A.; Bernabeu, A.; Fernandez, E.; Sabater, J. Robot-assisted rehabilitation treatment of a 65-year old woman with alien hand syndrome. *Biomed. Robot. Biomech.* **2002**, doi:10.1109/BIOROB.2014.6913809.
5. Cameirao, M.; Badia, S.; Oller, E.; Verschure, P. Neurorehabilitation using the virtual reality based Rehabilitation Gaming System: methodology, design, psychometrics, usability and validation. *J. NeuroEng. Rehabil.* **2010**, doi:10.1186/1743-0003-7-48.
6. Wittmann, F.; Lambercy, O.; Gonzenbach, R.R.; van Raai, M.A.; Hover, R.; Held, J.; Starkey, M.L.; Curt, A.; Luft, A.; Gassert, R. Assessment-driven arm therapy at home using an IMU-based virtual reality system. *Rehabil. Robot.* **2015**, doi:10.1109/ICORR.2015.7281284.
7. Klopčar, N.; Lenarčič, J. Kinematic model for determination of human arm reachable workspace. *Meccanica* **2005**, *40*, 203–219.
8. Rab, G.; Petuskey, K.; Bagley, A. A method for determination of upper extremity kinematics. *Gait Posture* **2002**, doi:10.1016/S0966-6362(01)00155-2.
9. Mihelj, M. Human arm kinematics for robot based rehabilitation. *Robotica* **2006**, *24*, 377–383.
10. Papaleo, E.; Zollo, L.; Garcia-Aracil, N.; Badesa, F.; Morales, R.; Mazzoleni, S.; Sterzi, S.; Guglielmelli, E. Upper-limb kinematic reconstruction during stroke robot-aided therapy. *Med. Biol. Eng. Comput.* **2015**, *53*, 815–828.
11. Kreutz-Delgado, K.; Long, M.; Seraji, H. Kinematic analysis of 7 DOF anthropomorphic arms. *Robot. Autom.* **1990**, doi:10.1109/ROBOT.1990.126090.

12. Taati, B.; Wang, R.; Huq, R.; Snoek, J.; Mihailidis, A. Vision-based posture assessment to detect and categorize compensation during robotic rehabilitation therapy. *Biomed. Robot. Biomech.* **2012**, doi:10.1109/BioRob.2012.6290668.

13. Siciliano, B.; Sciavicco, L.; Villani, L.; Oriolo, G. *Robotics: Modelling, Planning and Control*; Springer-Verlag London: London, UK, 2009.

14. Badesa, F.J.; Llinares, A.; Morales, R.; Garcia-Aracil, N.; Sabater, J.M.; Perez-Vidal, C. Pneumatic planar rehabilitation robot for post-stroke patientes. *Biomed. Eng. Appl. Basis Commun.* **2014**, doi:10.4015/S1016237214500252.

15. Lenarčič, J.; Umek, A. Simple model of human arm reachable workspace. *IEEE Trans. Syst. Man. Cybern.* **1994**, *24*, 1239–1246.

16. Kalman, R.E. A new approach to linear filtering and prediction problems. *J. Basic Eng.* **1960**, *82*, 35–45.

17. Madgwick, S.; Harrison, A.; Vaidyanathan, R. Estimation of IMU and MARG orientation using a gradient descent algorithm. *Rehabil. Robot.* **2011**, doi:10.1109/ICORR.2011.5975346.

18. Bachmann, E.; Yun, X.; Peterson, C. An investigation of the effects of magnetic variations on inertial/magnetic orientation sensors. *Robot. Autom.* **2004**, doi:10.1109/ROBOT.2004.1307974.

19. Kuipers, J.B. *Quaternions and Rotation Sequences*; Princeton University Press: Princeton, NJ, USA, 1999.

20. Mazza, J.C. Mediciones antropométricas. Estandarización de las Técnicas de medición, Actualizada según Parámetros Internacionales. Available online: http://g-se.com/es/journals/publice-standard/articulos/mediciones-antropometricas.-estandariza-cion-de-las-tecnicas-de-medicion-actualizada-segun-parametros-internacionales-197 (accessed on 9 October 2015).

21. McCrea, P.H.; Eng, J.J.; Hodgson, A.J. Biomechanics of reaching: Clinical implications for individuals with acquired brain injury. *Disabil. Rehabil.* **2002**, *24*, 534–541.

RESEARCH

Open Access

Human arm joints reconstruction algorithm in rehabilitation therapies assisted by end-effector robotic devices

Arturo Bertomeu-Motos[1]* , Andrea Blanco[1], Francisco J. Badesa[2], Juan A. Barios[1], Loredana Zollo[3] and Nicolas Garcia-Aracil[1]

Abstract

Background: End-effector robots are commonly used in robot-assisted neuro-rehabilitation therapies for upper limbs where the patient's hand can be easily attached to a splint. Nevertheless, they are not able to estimate and control the kinematic configuration of the upper limb during the therapy. However, the Range of Motion (ROM) together with the clinical assessment scales offers a comprehensive assessment to the therapist. Our aim is to present a robust and stable kinematic reconstruction algorithm to accurately measure the upper limb joints using only an accelerometer placed onto the upper arm.

Methods: The proposed algorithm is based on the inverse of the augmented Jaciobian as the algorithm (Papaleo, et al., Med Biol Eng Comput 53(9):815–28, 2015). However, the estimation of the elbow joint location is performed through the computation of the rotation measured by the accelerometer during the arm movement, making the algorithm more robust against shoulder movements. Furthermore, we present a method to compute the initial configuration of the upper limb necessary to start the integration method, a protocol to manually measure the upper arm and forearm lengths, and a shoulder position estimation. An optoelectronic system was used to test the accuracy of the proposed algorithm whilst healthy subjects were performing upper limb movements holding the end effector of the seven Degrees of Freedom (DoF) robot. In addition, the previous and the proposed algorithms were studied during a neuro-rehabilitation therapy assisted by the 'PUPArm' planar robot with three post-stroke patients.

Results: The proposed algorithm reports a Root Mean Square Error (RMSE) of 2.13*cm* in the elbow joint location and 1.89*cm* in the wrist joint location with high correlation. These errors lead to a RMSE about 3.5 *degrees* (mean of the seven joints) with high correlation in all the joints with respect to the real upper limb acquired through the optoelectronic system. Then, the estimation of the upper limb joints through both algorithms reveal an instability on the previous when shoulder movement appear due to the inevitable trunk compensation in post-stroke patients.

Conclusions: The proposed algorithm is able to accurately estimate the human upper limb joints during a neuro-rehabilitation therapy assisted by end-effector robots. In addition, the implemented protocol can be followed in a clinical environment without optoelectronic systems using only one accelerometer attached in the upper arm. Thus, the ROM can be perfectly determined and could become an objective assessment parameter for a comprehensive assessment.

Keywords: Neuro-rehabilitation therapy, End-effector robots, Kinematic reconstruction, Upper limbs

---

*Correspondence: abertomeu@umh.es
[1]Miguel Hernández University of Elche, Av. Universidad w/n, Ed. Innova, 03202
Elche, Spain
Full list of author information is available at the end of the article

Bertomeu-Motos *et al. Journal of NeuroEngineering and Rehabilitation*   (2018) 15:10

Page 2 of 11

Background

Robot-assisted therapies have become a new tool in post-stroke upper limb treatments [1, 2]. One of the most common consequences of stroke, brain cells damage caused by an interruption of the blood flow to the brain, is the hemiparesis, a loss of physical strength on one side of the body, as well as memory problems that they directly affect the realization of the Activities of Daily Living (ADL) [3]. The main goal in these kind of therapies is the effective use of neuroplasticity of the brain performing several exercises assisted by a robotic device which can be adapted to the tasks regarding his/her residual motor capabilities. This technology aims to maximize the patient's recovery, minimize the rehabilitation period and encourage the motivation of patients [4–6].

Rehabilitation robotic devices for upper limbs can be classified into two types: exoskeletons devices [7], have robot axes aligned with the anatomical axes of the upper limb segments providing direct control of individual joints, and end-effector devices [8], work by applying mechanical forces to the distal segments of limbs (see Fig. 1). Though exoskeletons allow the total control of the arm joints, they are difficult to adapt and attach to the patient arm [9, 10]. Moreover, the attachment process takes a long time in order to avoid misalignment between the robot and the arm that can injure the patient. However, end-effector robots can be easily adapted and used by several patients with different pathologies [11–14]. Nevertheless, these robots provide information about the end effector trajectory followed during the therapy and the interaction forces between the hand and the end effector, by which the therapist can perform an objective assessment and customize the therapy based on patients' needs [15–17], but they are not able to know the upper limb joints of the patient.

On the other hand, monitoring joint angles enables human posture to be analyzed in a wide range of application and disciplines, such as physical and neuro-rehabilitation, sports medicine or virtual training. The Range of Motion (ROM) in upper limb neuro-rehabilitation therapy offers a comprehensive assessment together with the clinical assessment scales [18–20]. Standard motion analysis instruments are widely used in these fields that can be mainly divided into three groups: opto-electronic systems, inertial measurement units (IMUs) systems, and wearable goniometers. The former system is often very expensive and difficult to adapt into a clinic environment, it requires a large and controlled area without camera obstruction [21]. The latter is an emerging technology that aims to measure the angle joints by the deformation of a specific sensor or by optical-based goniometers [22–24]. However, they are able to measure only simple joints as a flexo-extension of the knee or the elbow, not a combination of upper limb joints. The IMUs systems, based on the integration of accelerometers, gyroscopes and magnetometers, have gained the reputation of being the cutting edge of wearable motion tracking systems [25, 26]. IMUs estimate the orientation of the body segments where they are attached by combining multi-sensor information through dedicated optimal sensor fusion algorithms. However, the calibration of these sensors is sometimes very difficult to achieve with post-stroke patient due to a specific body configuration requirements, as with the well known XSens MVN system [27], or the system need a fusion of many sensors placed onto the body [28].

There are several studies which have produced arm reconstruction through motion tracking cameras to estimate the position of the arm and implement a visual feedback on rehabilitation activities [29, 30]. However, they do not perform an accurate measurement of the arm joints during the rehabilitation therapy. A new tool capable to compute the arm joints through two non-invasive accelerometers placed onto the upper arm was introduced by Mihelj [31]. Papaleo et al. improved this method by integrating the joint kinematic reconstruction through the inverse of the augmented Jacobian being able to accurately estimate the human upper limb joints using only one accelerometer [32]. Although this algorithm presents a low error with respect to the real arm, it is unstable when a small shoulder movement is done due to the inevitable trunk compensation performed by patients. Furthermore,
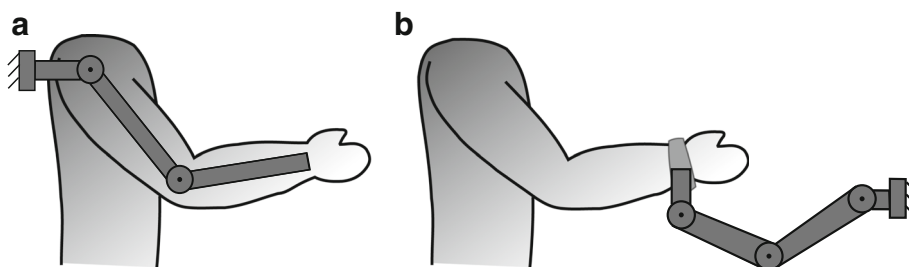

Fig. 1 Robotic devices for upper limb rehabilitation: **a** Exoskeletons, **b** End effector

Bertomeu-Motos *et al. Journal of NeuroEngineering and Rehabilitation*   (2018) 15:10

Page 3 of 11

the system uses the information of an optoelectronic system to measure the upper arm and forearm lengths, the shoulder position, and the initial position.

In this paper, an upper limb kinematic reconstruction algorithm, based on the same criterion presented in [32], is developed. It uses the information provided by one accelerometer placed onto the upper arm and by the end effector of the robot. This algorithm solves the instability in the upper limb joints estimation, proposing a protocol to manually measure the upper arm and forearm lengths and we present a technique to estimate the initial upper limb joints. The main difference between the proposed and the previous algorithm is that the estimation of the elbow joint location is done through computation of the accelerometer rotation after an arm displacement. The end-effector robot with seven Degrees of Freedom (DoF), designed and built by the Neuro-Bioengineering Research Group (nBio), Miguel Hernández University of Elche, Spain, was used to carry out the experimental validation of the proposed algorithm [33]. Furthermore, a comparative analysis of both algorithms in a neuro-rehabilitation therapy with post-stroke patients is performed, studying their behavior when shoulder movements cannot be avoided by patients but measured through the method proposed in [34] using the 'PUPArm' robot.

Methods
Kinematic model of the human arm
The human arm is a complex kinematic chain that can be simplified into seven DoF arm model, connected through two links: upper arm (l_u) and forearm (l_f), as can be seen in Fig. 2a) [35]. The shoulder has been modeled as a spherical joint composed of abduction-adduction (q_1), flexion-extension (q_2) and internal-external rotation (q_3) movements. The double-hinge elbow joint comprises the flexion-extension (q_4) and pronation-supination (q_5) of the forearm. Though q_5 anatomically belongs to the elbow joint, it is considered as a wrist DoF. Thereby, the wrist joint is a spherical joint composed of q_5, ulnar-radial deviation (q_6) and flexion-extension (q_7) of the hand. The Denavit-Hartenberg (DH) parameters [36] of the arm and the reference systems of each joint were established as are shown in Table 1 and in Fig. 2b, respectively.

Inverse kinematics with augmented Jacobian
The kinematic reconstruction algorithm is based on the augmented Jacobian introduced by Kreutz-Delgado [37]. The analysis of a seven DoF manipulator with revolute joints was performed to uniquely determine the joint angles for a given end-effector location. The redundancy is catheterized by the swivel angle (α), the angle between the arm plane formed by the shoulder, elbow and wrist points and a reference plane SVW, shown in Fig. 3.

Then, the augmented Jacobian can be expressed as

$$J_A(\vec{q}) = \begin{bmatrix} J_g(\vec{q}) \\ J_\alpha(\vec{q}) \end{bmatrix},$$

where $J_g(\vec{q})$ is the geometric Jacobian matrix of the arm and $J_\alpha(\vec{q})$ is the swivel angle Jacobian, providing the joint velocities with respect to the amount of change of α. Thus,
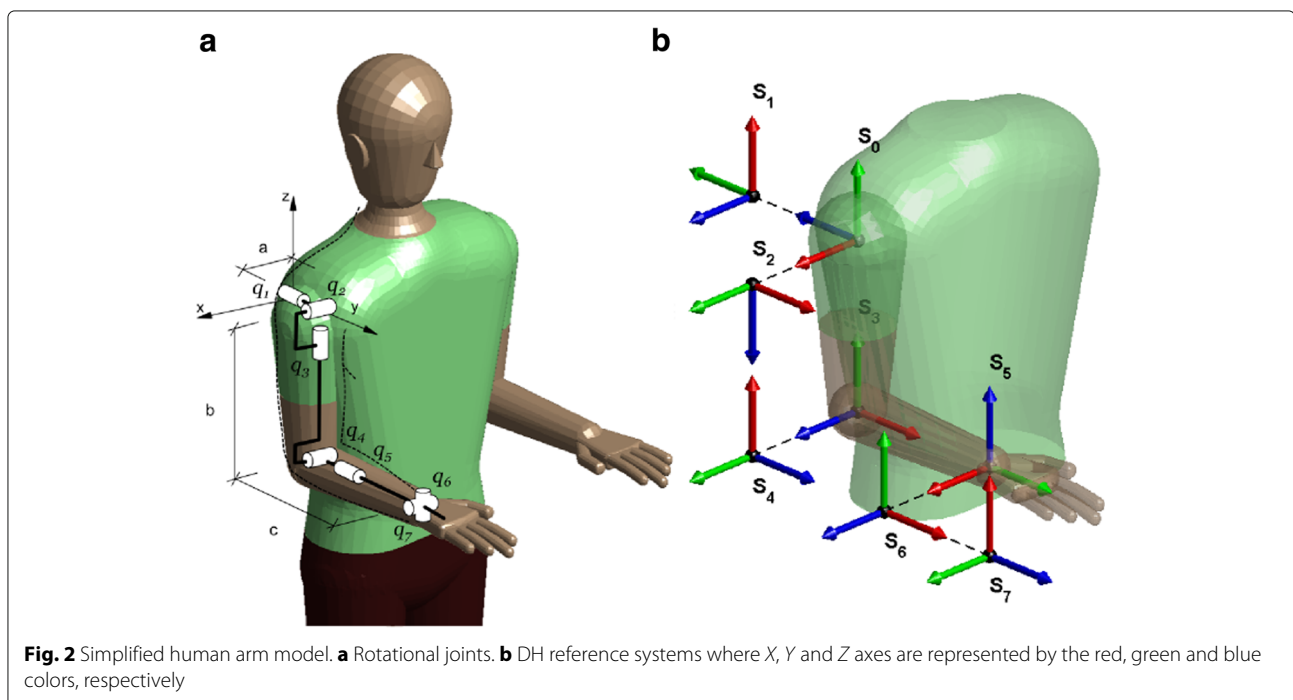

Fig. 2 Simplified human arm model. **a** Rotational joints. **b** DH reference systems where *X*, *Y* and *Z* axes are represented by the red, green and blue colors, respectively

Bertomeu-Motos *et al. Journal of NeuroEngineering and Rehabilitation* (2018) 15:10

Page 4 of 11

Table 1 DH Parameters of the human arm

i	θ_i	d_i	a_i	α_i
1	$\pi/2 + q_1$	0	0	$\pi/2$
2	$3\pi/2 + q_2$	0	0	$\pi/2$
3	q_3	l_u	0	$-\pi/2$
4	$\pi/2 + q_4$	0	0	$\pi/2$
5	$\pi/2 + q_5$	l_f	0	$\pi/2$
6	$\pi/2 + q_6$	0	0	$\pi/2$
7	$\pi/2 + q_7$	0	0	$\pi/2$

the arm joint velocities are computed through the inverse of the augmented Jacobian with respect to the upper limb joints ($\vec{q}$) as

$$\dot{\vec{q}} = J_A^{-1}(\vec{q}) \left\{ \begin{bmatrix} \dot{\vec{v}}_d \\ \dot{\alpha} \end{bmatrix} + K \cdot \vec{err} \right\}, \tag{1}$$

being $\dot{\vec{v}}_d$ the hand velocity vector and $\dot{\alpha}$ the swivel angle velocity. The error produced by the discrete integration is
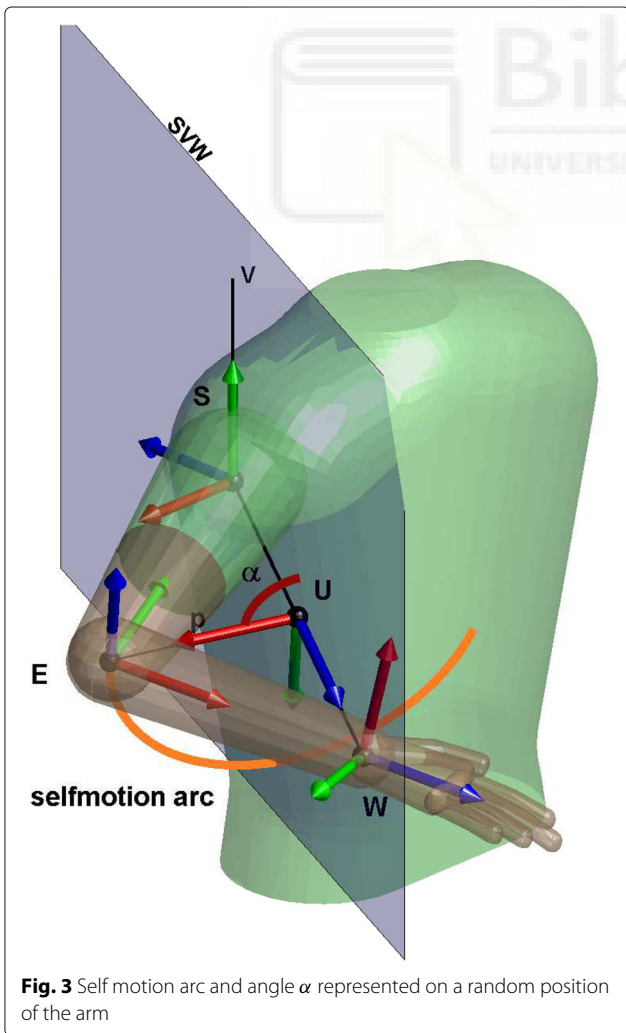

Fig. 3 Self motion arc and angle α represented on a random position of the arm

minimized with the vector error ($\vec{err}$) multiplied by a suitable gain matrix K [38]. The Jacobian matrix can induce high joint speed in the regions close to kinematic chain singularities. Thereby, the damped least-square approach [38] was applied to the augmented Jacobian matrix as

$$J_A^* = J_A^T \left(J_A \cdot J_A^T + k^2 \cdot I \right)^{-1},$$

where k^2 is the damping factor that, chosen properly, performs an accuracy approach to the singularity area, and I is the identity matrix. Therefore, the Jacobian matrix J_A^* is introduced in (1) instead of J_A.

Thus, the arm joints at time t_k are estimated as

$$\vec{q}(t_k) = \vec{q}(t_{k-1}) + \dot{\vec{q}}(t_k)\Delta t,$$

being $\vec{q}(t_{k-1})$ the previous arm joints, $\dot{\vec{q}}$ computed from (1) and Δt the sampling rate.

Elbow estimation

The estimation of the elbow joint pose is the key of the proposed inverse kinematic reconstruction. It is computed through the orientation of the accelerometer placed onto the upper arm. This orientation can be estimated assuming slow movements during the exercise, to erase the dynamic component of the acceleration.

Starting from the reference position of the arm and the accelerometer, shown in Fig. 4, the value of the accelerometer at this position, normalized with respect to the gravity acceleration, is

$$^{acc_0}V_g = \begin{bmatrix} 0 \\ 1 \\ 0 \end{bmatrix}.$$

The acceleration value in a random upper limb position can be expressed as a combination of the reference value and the rotation applied ($^{acc_0}R_{acc}$) as

$$^{acc}V_g = \left(^{acc_0}R_{acc} \right)^{-1} {}^{acc_0}V_g.$$

The rotation matrix $^{acc_0}R_{acc}$ is unknown, however one possible solution might be computed as

$$^{acc_0}\tilde{R}_{acc} = I + M + M^2 \frac{1 - \cos(\theta)}{\sin^2(\theta)},$$

with

$$M = \begin{bmatrix} 0 & -V(3) & V(2) \\ V(3) & 0 & -V(1) \\ -V(2) & V(1) & 0 \end{bmatrix},$$

$$V = {}^{acc_0}V_g \times {}^{acc}V_g,$$

$$sin(\theta) = \|V\|,$$

$$cos(\theta) = {}^{acc_0}V_g \cdot {}^{acc}V_g.$$

From this rotation, it is possible to find the proper arm position making the plane XY of $^{acc_0}\tilde{R}_{acc}$ to include the known shoulder and wrist joints position, shown as Π
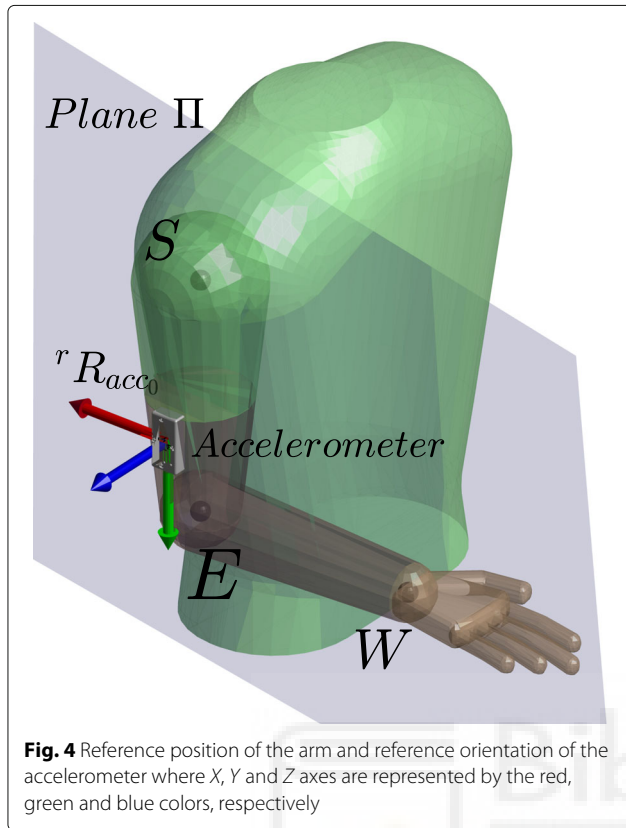
Bertomeu-Motos *et al. Journal of NeuroEngineering and Rehabilitation* (2018) 15:10

Page 5 of 11

Fig. 4 Reference position of the arm and reference orientation of the accelerometer where *X*, *Y* and *Z* axes are represented by the red, green and blue colors, respectively

plane in Fig. 4. Hence, it is necessary to rotate the matrix $^{acc_0}\tilde{R}_{acc}$ around the gravity vector a γ angle to accomplish this restriction. The computation of this angle is explained in the Additional file 1. The simplification performed in order to obtain this angle allows the algorithm to be performed in real time (average time in the computation of the mathematical operations: ≈ 0.9 *ms* running on the Intel Core i7 3.40GHz with Matlab R2017a).

Two solutions of angle γ are found, each solution computes a different rotation matrix $^{acc_0}R_{acc}^{(i)}$, with $i \in \{1, 2\}$, in which the *Z* axis point to each normal vector of the plane Π. Thus, two elbow positions with respect to the robot ($^r P_e$) are obtained as

$$^r P_e = ^r T_{acc} \cdot \begin{bmatrix} 0 & lu & 0 & 1 \end{bmatrix}^T, \text{with}$$

$$^r T_{acc} = \begin{bmatrix} ^r R_{acc_0} \cdot {}^{acc_0}R_{acc}^{(i)} & ^r P_s \\ 0 & 1 \end{bmatrix},$$

being $^r T_{acc}$ the homogeneous matrix of the accelerometer regarding the robot, $^r R_{acc_0}$ the rotation matrix between the robot and the accelerometer in the reference position of the arm and $^r P_s$ the shoulder joint position regarding the robot. Therefore, the correct elbow position is the one which the *Z* axis of the $^{acc_0}R_{acc}^{(i)}$ points the same direction as the cross product between the segment $\overline{EW}$ and

$\overline{ES}$ being *S*, *E* and *W* the shoulder, elbow and wrist joint position.

Finally, the elbow location regarding the robot is estimated as

$$^r T_e = \begin{bmatrix} ^r R_e & ^r P_e \\ 0 & 1 \end{bmatrix}, \text{with} \tag{2}$$

$$^r R_e = ^r R_{acc_0} \cdot {}^{acc_0}R_{acc} \cdot {}^{acc_0}R_e$$

being $^{acc_0}R_e$ the rotation matrix of the elbow regarding the accelerometer in the reference arm position. Once the location of the elbow joint is estimated, the swivel angle, necessary to compute the augmented Jacobian, can be computed [37].

Initial conditions

The initial upper limb joints are necessary to the kinematic reconstruction algorithm. The following locations with respect to the robot are initially known: the shoulder $^r T_s$, obtained at the beginning of the therapy; the wrist $^r T_w$, known through the end effector of the robot; and the elbow $^r T_e$, estimated as explained in the previous section. Thus, the initial joint angles can be estimated using the DH parameters [39] shown in Table 1.

The known matrix that determines the shoulder movement regarding its joints (q_1, q_2, q_3) is defined as

$$^r T_s = {}^{s_0}T_{s_3} = {}^{s_0}T_{s_1} \cdot {}^{s_1}T_{s_2} \cdot {}^{s_2}T_{s_3} \simeq \begin{bmatrix} n_x & n_y & n_z & p_x \\ o_x & o_y & o_z & p_y \\ a_x & a_y & a_z & p_z \\ 0 & 0 & 0 & 1 \end{bmatrix};$$

and two possible solutions of the shoulder joints are obtained as

(i) if $q_2 \in [0 \quad \pi]$:

$q_1 = \text{atan2} \left(-n_y, o_y \right)$

$q_2 = \text{atan2} \left(a_y, \sqrt{n_y^2 + o_y^2} \right)$

$q_3 = \text{atan2} \left(a_z, -a_x \right)$

(ii) if $q_2 \in [0 \quad \pi]$:

$q_1 = \text{atan2} \left(-n_y, o_y \right)$

$q_2 = \text{atan2} \left(a_y, -\sqrt{n_y^2 + o_y^2} \right)$

$q_3 = \text{atan2} \left(-a_z, a_x \right)$

On the other hand, the flexion-extension of the elbow, joint q_4, affects the distance $\overline{SW}$ and, therefore, it can be unequivocally computed through the law of the cosines as

$$q_4 = \arcsin \left(\frac{l_u^2 + l_f^2 - ||W - S||^2}{2 l_u l_f} \right).$$

Finally, since the wrist location is given by the robot end-effector pose, its transformation matrix $^r T_w = {}^{s_0}T_{s_7}$ is known. Thus, the wrist joints can be also estimated following the criterion used to solve the shoulder joints as

$$^{s_4}T_{s_7} = \left({}^{s_0}T_{s_3} \cdot {}^{s_3}T_{s_4} \right)^{-1} \cdot {}^{s_0}T_{s_7} \simeq \begin{bmatrix} n_x & n_y & n_z & p_x \\ o_x & o_y & o_z & p_y \\ a_x & a_y & a_z & p_z \\ 0 & 0 & 0 & 1 \end{bmatrix};$$

Bertomeu-Motos *et al. Journal of NeuroEngineering and Rehabilitation*   (2018) 15:10

Page 6 of 11

with $^{s_3}T_{s_4}$ the homogeneous matrix of the joint q_4, and two possible solutions can be also obtained as

(iii) if $q_6 \in [-\pi/2 \quad \pi/2]$:   (iv) if $q_6 \in [\pi/2 \quad 3\pi/2]$:

$q_5 = -\text{atan2}\left(n_y, o_y\right)$ $q_5 = \pi - \text{atan2}\left(n_y, o_y\right)$

$q_6 = \arcsin\left(a_y\right)$ $q_6 = \pi - \arcsin\left(a_y\right)$

$q_7 = -\text{atan2}\left(a_x, a_z\right)$ $q_7 = \pi - \text{atan2}\left(a_x, a_z\right)$

Thereby, four solutions, two due to the shoulder joints and two due to the wrist joints, can satisfy the kinematic constraints. However, only one solution accomplishes the anatomical features of the human upper limb. This statement is provable because the human arm joints vary in $[-\pi/2 \quad \pi/2]$ and each solution belongs either $[0 \quad \pi]$ range or $[0 \quad -\pi]$ range and, therefore, the initial arm joints remain defined. An extensive explanation of the estimation of the initial conditions is presented in Additional file 2.

Experimental protocol

Two different experiments were performed, in the first experiment was intended to measure the accuracy of the proposed algorithm with respect to an optoelectronic system, taken as a ground truth, and the second was intended to study the behaviour of the algorithm in a rehabilitation therapy and compare its stability with respect to the previous algorithm presented in [32]. Data recordings have been approved by the ethics committee of the Miguel Hernández University of Elche, Spain. All the subjects provided written informed consent.

The first experimental exercise was carried out by seven right-handed healthy subjects performing three trials, their main information is presented in Table 2. The subjects wore a specific jacket with 25 markers attached to it using the baseline upper body marker set [40] in order to measure the 'ground truth' joints. Thus, the location of the upper arm, forearm and hand were directly obtained through the optoelectronic system and therefore the arm joints were computed as explained in the previous section. In order to estimate the upper limb joints through the proposed algorithm, a magneto-inertial sensor was tightly attached to the upper arm and the wrist joint location

Table 2 Main information of the healthy subjects

ID	Age	Forearm length [m]	Upper arm length [m]
1	24	0.25	0.34
2	31	0.21	0.30
3	24	0.26	0.32
4	26	0.26	0.29
5	29	0.26	0.31
6	24	0.23	0.33
7	25	0.26	0.30

was obtained with the end-effector robot with seven DoF, designed and built by the Neuro-Bioengineering Research Group (nBio), Miguel Hernández University of Elche, Spain [33]. The shoulder joint location was only measured at the beginning of the experimentation through the optoelectronic system as the shoulder and the trunk are fixed during the exercise. The trajectory was previously established in the end-effector robot, a point to point task.

The second experimental exercise was carried out by three post-stroke patients, the scores of two assessment scales are shown in Table 3, Ashworth [41], for the elbow joint, and Fugl-Meyer [42]. Two magneto-inertial sensors were used, one attached to the upper arm and the other onto the shoulder (see Fig. 5). The wrist joints location was computed during the exercise with the end-effector robot called 'PUPArm', designed and built by the Neuro-Bioengineering Research Group (nBio), Miguel Hernández University of Elche, Spain; and the shoulder joint location, as the flexion-extension and ulnar-radial deviation of the wrist joint is fixed by the robot, the algorithm proposed in [34] can be used and the shoulder location remains estimated during the exercise. The subjects performed three movements in the roulette activity [43].

In both exercises, the length of the upper arm was manually measured from the lateral side of the acromion to the proximal radius head, in the elbow joint; and the forearm length was measured from the proximal radius head to the radial styloid, the distal part of the radius [44]. Furthermore, the upper limb joints were on-line estimated. The main parameters of the kinematic reconstruction algorithm, the gain matrix and the damping factor, were set to $K = diag\{1.5, 1.5, \ldots 1.5\}\,N/ms$ and $k^2 = 0.5$ respectively. They were chosen through a "trial and error" approach under the exercise conditions. The magneto-inertial sensors used were developed by Shimmer™ and sampled at $100\,Hz$. The optoelectronical system was composed by 8 6DoF optical tracking cameras Optitrack V100: R2, developed by NaturalPoint®. This camera has a $640 \times 480\,px$ resolution with an approximate precision of $0.3\,mm$ and frame rate of $30 - 120$ frames per second.

Results

Validation of the proposed algorithm

This algorithm was previously studied in a simulated environment with a 7 DoF robot, being able to avoid shoulder movements and misalignment between the accelerometer and the upper arm, in [45]. The accuracy of the proposed algorithm was measured as the difference between the values acquired through the optoelectronic system and estimated by the proposed algorithm in terms of Root Mean Square Error (RMSE), Standard Deviation (SD) and correlation coefficient (R), shown in Table 4. It can be observed that the correlation between both upper limb joints reconstruction is high with low error. In addition,

Bertomeu-Motos *et al. Journal of NeuroEngineering and Rehabilitation* (2018) 15:10

Page 7 of 11

Table 3 Main information of the post-stroke patients

ID	Affected arm	Age	Forearm length [m]	Upper arm length [m]	Fugl-Meyer (A+B+C+D)[*]	Ashworth
1	Right	51	0.24	0.30	(33+7+7+2) /66	2
2	Left	58	0.25	0.33	(27+4+3+3) /66	3
3	Left	74	0.24	0.35	(24+2+2+1) /66	3

[*]Fugl Meyer scale for upper extremity is divided in: A) Upper Extremity, B) Wrist, C) Hand, D) Coordination/speed

the reconstructed kinematic joints of a subject while performing a trial is shown in Fig. 6.

Experimental results with patients

The proposed kinematic reconstruction algorithm was tested in a clinic environment with post-stroke patients during a robot-aided neuro-rehabilitation therapy with the 'PUPArm' robot. In addition, the previous algorithm presented by Papaleo et al. was also studied [32]. Figure 7 shows the upper limb joints estimated with the proposed algorithm and with the previous algorithm. Furthermore, the shoulder displacement of the patients and the trajectory followed with the end effector of the robot are also shown. The gray area denote the instability of the previous algorithm, i.e. the time in which the upper limb joints cannot be estimated with the previous algorithm. In these areas the arm joints were set to the last known value estimated through the previous algorithm. The trajectory followed with the end effector of the robot is also shown in the figure together with the eight possible goals of the roulette exercise [43]. In this case the exercise performed was to achieve three goals. It can be observed that the diameter of the roulette is higher in the user one,

15 *cm*, than in the user two and three, 13 *cm* and 12 *cm* respectively, implying higher estimated ROM in joints q_1 and q_3 (see Table 5), as it was expected due to the high Fugl-Meyer score (see Table 3).

Discussion

The aim of this study was to develop a robust kinematic reconstruction algorithm of the human upper limb joints being able to perform a real-time joint estimation during a neuro-rehabilitation therapy assisted by robots with only one accelerometer placed onto the upper arm. Furthermore, the previous algorithm, presented in [32], the initial upper limb joints; the upper arm and the forearm length; and the shoulder position were measured by the optoelectronic system, not used in a clinical environment. Therefore, we have defined a protocol to manually measure the upper arm and forearm lengths; we have introduced a mathematical method to estimate the initial upper limb joints; and the presented algorithm, as it is based on the computation of the accelerometer rotation, is always able to estimate the upper limb joints.

The kinematic reconstruction algorithm proposed shows high correlation with respect to the real upper arm.
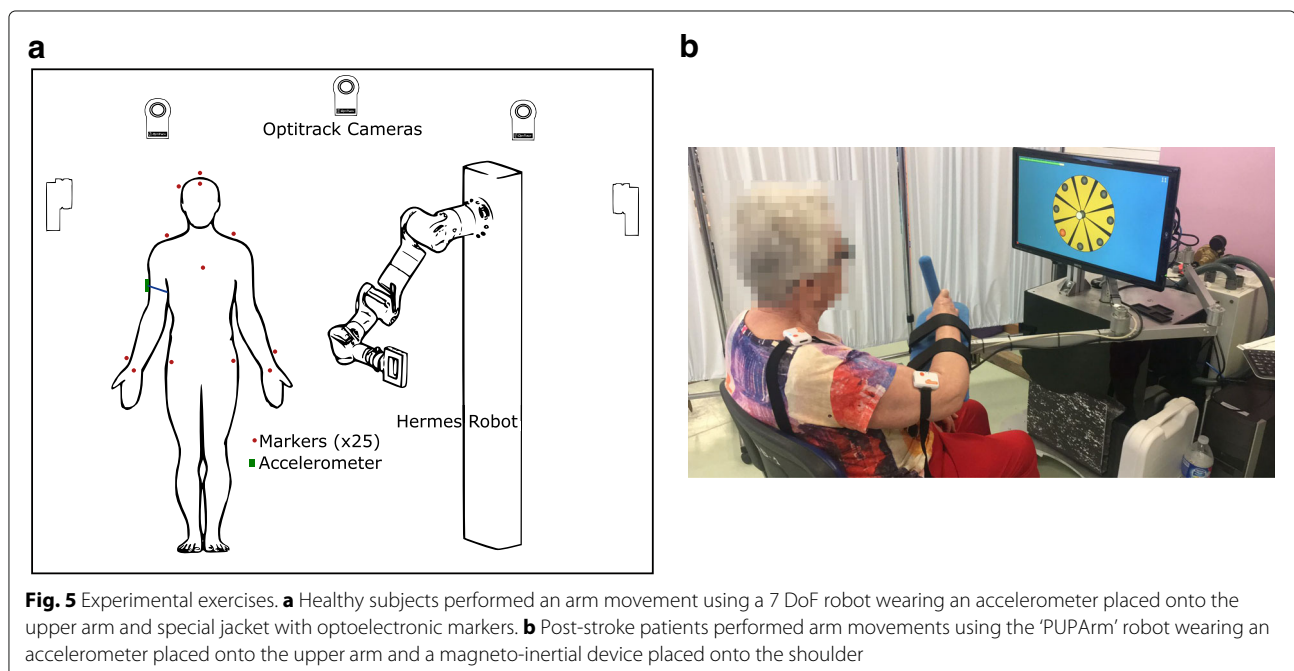

Fig. 5 Experimental exercises. **a** Healthy subjects performed an arm movement using a 7 DoF robot wearing an accelerometer placed onto the upper arm and special jacket with optoelectronic markers. **b** Post-stroke patients performed arm movements using the 'PUPArm' robot wearing an accelerometer placed onto the upper arm and a magneto-inertial device placed onto the shoulder

Bertomeu-Motos *et al. Journal of NeuroEngineering and Rehabilitation* (2018) 15:10

Page 8 of 11

Table 4 RMSE of the proposed algorithm regarding the optoelectronic system reconstruction (grand mean of the seven subjects)

	RMSE	SD	R	*p*-value
Elbow joint position [cm]	2.13	1.1	0.977	< 0.001
Wrist joint position [cm]	1.89	1.12	0.982	< 0.001
q_1 [deg]	3.548	2.148	0.957	< 0.001
q_2 [deg]	3.271	2.992	0.977	< 0.001
q_3 [deg]	4.569	3.041	0.966	< 0.001
q_4 [deg]	1.719	1.542	0.995	< 0.001
q_5 [deg]	4.506	2.741	0.873	< 0.001
q_6 [deg]	2.825	2.226	0.899	< 0.001
q_7 [deg]	4.742	3.279	0.982	< 0.001

Although the error committed in the estimation of the wrist and shoulder position is low, $2cm$ approximately, it implies an upper limb joints RMSE about 3.5 *degrees* (mean of the seven joints) with high correlation in all joints. It must be noticed that q_5 and q_6 joints have low correlation with respect to the others, it may be due to these joints are in the distal part of the arm where the error between the real arm and the estimated arm is maximum and the estimation could differ slightly.

The second experiment was intended to study the behavior of the proposed and previous algorithms in patients during a neuro-rehabilitation therapy assisted by end-effector robots, being able to estimate the shoulder movements using the method proposed in [34] and assuming the joints q_6 and q_7 fixed by the robot. Figure 7 shows that the previous algorithm is unstable when shoulder movements appear, areas marked in gray, whilst the

proposed not. Although the shoulder is assumed fixed in both methods, it is very difficult to fix the shoulder and avoid little displacements with patients. It must be noticed that, before the error appears, the difference between both algorithms increases and, after the instability, the previous algorithm tends to follow the proposed estimated joints. Therefore, we can say that in the areas when the previous algorithm fails the proposed kinematic reconstruction performs a correct estimation. This error appears due to the method employed in the estimation of the elbow joint location because it is based on the strict constrains of the human upper limb which, a little movement of the shoulder assumed fixed, can lead to the algorithm failure. Furthermore, this error is closely related to the ROM estimation, a very important parameter in these therapies, and could lead a false ROM improvement [17]. Therefore, it is very important the stability of the kinematic reconstruction algorithm during the exercise.

On the other hand, the estimation of the ROM together with the assessments scales proposed and the trajectory performed by the user with the end effector of the robot encompasses an objective and comprehensive assessment of the patient condition during a robot-aided neuro-rehabilitation therapy. Thus, it can be observed that subject 3 performed worse trajectories than the other two subjects as it was expected due to the low score on the Fugl-Meyer scale with high Ashworth score. Furthermore, the patient with higher Fugl-Meyer and less Ashworth scores has the highest estimated ROM.

Conclusions

The presented kinematic reconstruction algorithm of the human upper limbs has a low error regarding the real arm acquired through an optoelectronic system. This
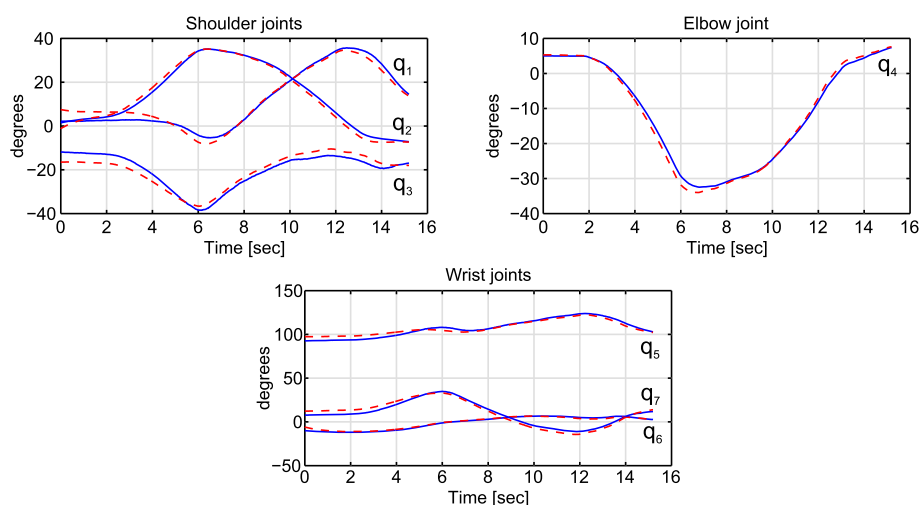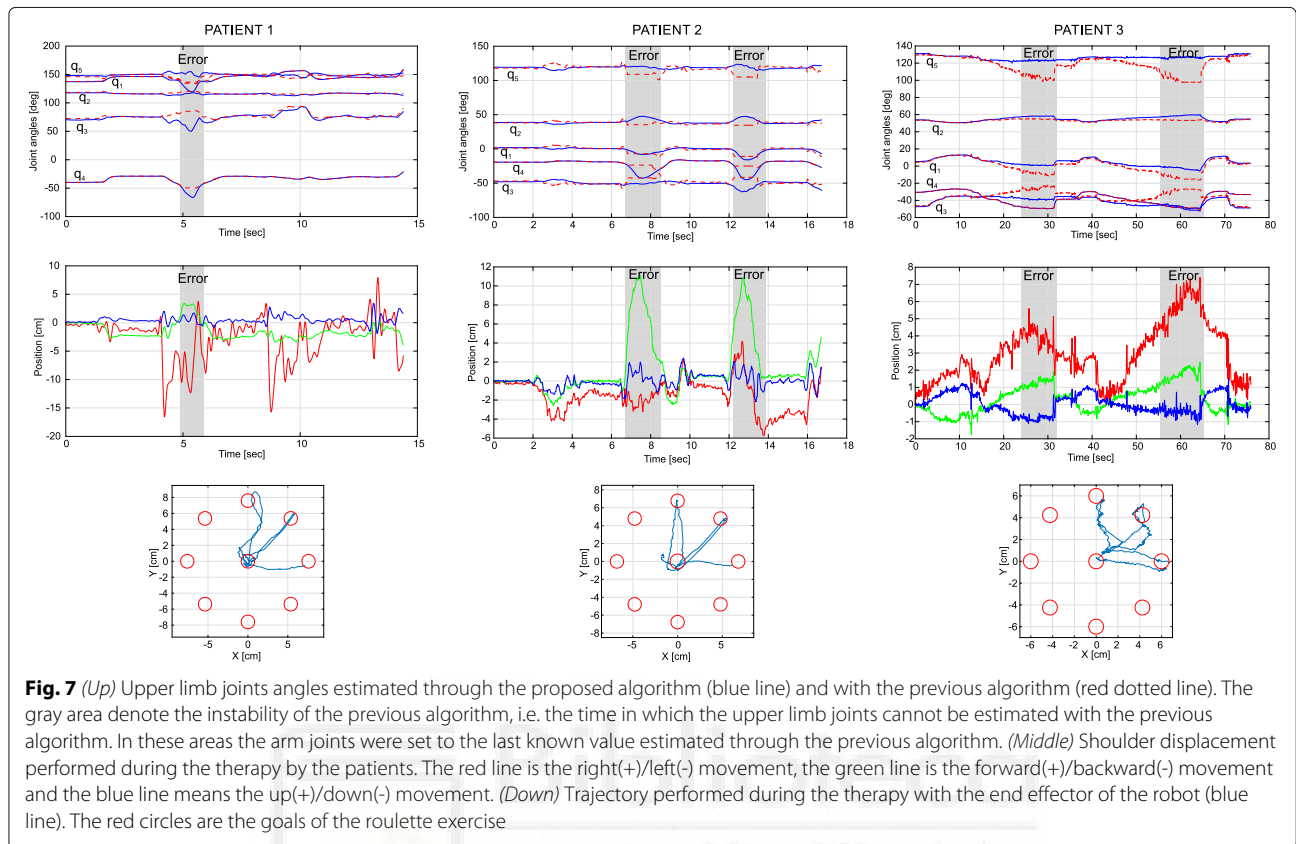

Fig. 6 Reconstructed upper limb joints estimated by the proposed algorithm (blue smooth line) and acquired through the optoelectronic system (red dotted line) of one trial performed by a healthy subject

Bertomeu-Motos *et al. Journal of NeuroEngineering and Rehabilitation* (2018) 15:10

Page 9 of 11

Fig. 7 *(Up)* Upper limb joints angles estimated through the proposed algorithm (blue line) and with the previous algorithm (red dotted line). The gray area denote the instability of the previous algorithm, i.e. the time in which the upper limb joints cannot be estimated with the previous algorithm. In these areas the arm joints were set to the last known value estimated through the previous algorithm. *(Middle)* Shoulder displacement performed during the therapy by the patients. The red line is the right(+)/left(-) movement, the green line is the forward(+)/backward(-) movement and the blue line means the up(+)/down(-) movement. *(Down)* Trajectory performed during the therapy with the end effector of the robot (blue line). The red circles are the goals of the roulette exercise

algorithm performs the kinematic reconstruction during the exercise allowing the therapist to correct, in real time, wrong upper limb position. Furthermore, compared to the previous algorithm, it is stable; proposes a protocol to manually measure the upper arm and forearm length; and estimates the initial upper limb joints being able to be used in a clinic environment. In addition, the study of the kinematics in the 'normal' model, performed by healthy subjects, during robot-aided rehabilitation tasks could be directly applied in the evaluation of the patients. Finally, the ROM estimation of the upper limb joints together with the assessment scales, as Fugl-Meyer or Ashworth, and the trajectory performed by the patient allows the therapist to have a comprehensive assessment during the therapy.

Table 5 ROM, in degrees, estimated through the proposed algorithm during the therapy

ID	Joint q_1	Joint q_2	Joint q_3	Joint q_4	Joint q_5
1	37.5	5.46	43.63	35.8	11.78
2	17.99	11.74	18.04	29.29	9.20
3	18.99	9.47	16.13	26.04	11.38

Additional files

Additional file 1: Solution of γ angle. (PDF 104 kb)

Additional file 2: Estimation of the initial conditions. (PDF 107 kb)

Abbreviations
DH: Denavit-hartenberg; DoF: Degree of freedom; MSE: Root Mean square error; ROM: Range of motion; SD: Standard deviation

Availability of data and materials
Data and materials can be made available upon request to the corresponding author.

Authors' contributions
ABM and FJB conceived of and designed the experiments. ABM and AB performed the experiments. ABM and JAB analyzed the data. ABM drafted the

Bertomeu-Motos *et al. Journal of NeuroEngineering and Rehabilitation* (2018) 15:10

Page 10 of 11

Publisher's Note

Author details
[1]Miguel Hernández University of Elche, Av. Universidad w/n, Ed. Innova, 03202
Elche, Spain. [2]Universidad de Cadiz, Avenida de la Universidad n 10, 11519
Puerto Real, Spain. [3]Research Unit of Biomedical Robotics and
Biomicrosystems, Università Campus Bio-Medico di Roma, via Álvaro del
Portillo, 21, 00128 Roma, Italy.

References

1. Lo AC, et al. Robot-assisted therapy for long-term upper-limb impairment after stroke. N Engl J Med. 2010;362(19):1772–83. https://doi.org/10.1056/NEJMoa0911341. PMID: 20400552.
2. Krebs HI, et al. Rehabilitation robotics: Performance-based progressive robot-assisted therapy. Autonomous Robots. 2003;15(1):7–20. https://doi.org/10.1023/A:1024494031121.
3. Donnan GA, Fisher M, Macleod M, Davis SM. Stroke. The Lancet. 2008;371(9624):1612–23. https://doi.org/10.1016/S0140-6736(08)60694-7.
4. Miller EL, et al. Comprehensive overview of nursing and interdisciplinary rehabilitation care of the stroke patient: A scientific statement from the american heart association. Stroke. 2010;41(10):2402–48. https://doi.org/10.1161/STR.0b013e3181e7512b.
5. Riener R, Nef T, Colombo G. Robot-aided neurorehabilitation of the upper extremities. Med Biol Eng Comput. 2005;43(1):2–10. https://doi.org/10.1007/BF02345116.
6. Novak D, Nagle A, Keller U, Riener R. Increasing motivation in robot-aided arm rehabilitation with competitive and cooperative gameplay. J NeuroEng Rehabil. 2014;11(1):64–79. https://doi.org/10.1186/1743-0003-11-64.
7. Lo HS, Xie SQ. Exoskeleton robots for upper-limb rehabilitation: State of the art and future prospects. Medical Eng Phys. 2012;34(3):261–8.
8. Chang WH, Kim YH. Robot-assisted therapy in stroke rehabilitation. J stroke. 2013;15(3):174.
9. Vitiello N, Lenzi T, Roccella S, De Rossi SMM, Cattin E, Giovacchini F, Vecchi F, Carrozza MC. Neuroexos: A powered elbow exoskeleton for physical rehabilitation. IEEE Trans Robot. 2013;29(1):220–35. https://doi.org/10.1109/TRO.2012.2211492.
10. Lenzi T, De Rossi SMM, Vitiello N, Carrozza MC. Intention-based emg control for powered exoskeletons. Trans Biomed Eng. 2012;59(8):2180–90. https://doi.org/10.1109/TBME.2012.2198821.
11. Burgar CG, Lum PS, Shor PC, Van der Loos HM. Development of robots for rehabilitation therapy: the palo alto va/stanford experience. J Rehab Res Dev. 2000;37(6):663–74.
12. Krebs HI, Volpe BT, Ferraro M, Fasoli S, Palazzolo J, Rohrer B, Edelstein L, Hogan N. Robot-aided neurorehabilitation: from evidence-based to science-based rehabilitation. Top Stroke Rehabil. 2002;8(4):54–70.
13. Reinkensmeyer DJ, Kahn LE, Averbuch M, McKenna-Cole A, et al. Understanding and treating arm movement impairment after chronic brain injury: progress with the arm guide. J Rehab Res Dev. 2000;37(6):653.
14. Coote S, Stokes E, Murphy B, Harwin W. The effect of GENTLE/S robot-mediated therapy on upper extremity dysfunction post stroke.

15. Proceedings of the 8th International Conference on Rehabilitation Robotics. 2003, pp. 23–5.
16. Zollo L, Rossini L, Bravi M, Magrone G, Sterzi S, Guglielmelli E. Quantitative evaluation of upper-limb motor control in robot-aided rehabilitation. Med Biol Eng Comput. 2011;49(10):1131.
17. de los Reyes-Guzmán A, Dimbwadyo-Terrer I, Trincado-Alonso F, Monasterio-Huelin F, Torricelli D, Gil-Agudo A. Quantitative assessment based on kinematic measures of functional impairments during upper extremity movements: A review. Clin Biomech. 2014;29(7):719–27.
18. Nordin N, Xie SQ, Wünsche B. Assessment of movement quality in robot-assisted upper limb rehabilitation after stroke: a review. J Neuroengineering Rehab. 2014;11(1):137.
19. Lum PS, Burgar CG, Shor PC, Majmundar M, Van der Loos M. Robot-assisted movement training compared with conventional therapy techniques for the rehabilitation of upper-limb motor function after stroke. Arch Phys Med Rehabil. 2002;83(7):952–9.
20. Winstein CJ, Rose DK, Tan SM, Lewthwaite R, Chui HC, Azen SP. A randomized controlled comparison of upper-extremity rehabilitation strategies in acute stroke: a pilot study of immediate and long-term outcomes. Arch Phys Med Rehabil. 2004;85(4):620–8.
21. Kwakkel G, Kollen BJ, Krebs HI. Effects of robot-assisted therapy on upper limb recovery after stroke: A systematic review. Neurorehabil Neural Repair. 2007. https://doi.org/10.1177/1545968307305457.
22. Kirk AG, O'Brien JF, Forsyth DA. Skeletal parameter estimation from optical motion capture data. 2005 IEEE Computer Society Conference on Computer Vision and Pattern Recognition (CVPR'05). 2005;2:782–8. https://doi.org/10.1109/CVPR.2005.326.
23. Tognetti A, Lorussi F, Carbonaro N, De Rossi D. Wearable goniometer and accelerometer sensory fusion for knee joint angle measurement in daily life. Sensors. 2015;15(11):28435–55.
24. Stupar DZ, Bajic JS, Manojlovic LM, Slankamenac MP, Joza AV, Zivanov MB. Wearable low-cost system for human joint movements monitoring based on fiber-optic curvature sensor. IEEE Sensors J. 2012;12(12):3424–31.
25. Mengüç Y, Park YL, Pei H, Vogt D, Aubin PM, Winchell E, Fluke L, Stirling L, Wood RJ, Walsh CJ. Wearable soft sensing suit for human gait measurement. Int J Robot Res. 2014;33(14):1748–64.
26. Leardini A, Lullini G, Giannini S, Berti L, Ortolani M, Caravaggi P. Validation of the angular measurements of a new inertial-measurement-unit based rehabilitation system: comparison with state-of-the-art gait analysis. J Neuroengineering Rehab. 2014;11(1):136.
27. Seel T, Raisch J, Schauer T. Imu-based joint angle measurement for gait analysis. Sensors. 2014;14(4):6891–909.
28. Roetenberg D, Luinge H, Slycke P. Xsens mvn: full 6dof human motion tracking using miniature inertial sensors. Xsens Motion Technologies BV, Tech. Rep. 2009.
29. Novak D, Goršič M, Podobnik J, Munih M. Toward real-time automated detection of turns during gait using wearable inertial measurement units. Sensors. 2014;14(10):18800–22. https://doi.org/10.3390/s141018800.
30. Klopčar N, Lenarčič J. Kinematic model for determination of human arm reachable workspace. Meccanica. 2005;40(2):203–19. https://doi.org/10.1007/s11012-005-3067-0.
31. Cameirao M, Badia S, Oller E, Verschure P. Neurorehabilitation using the virtual reality based rehabilitation gaming system: methodology, design, psychometrics, usability and validation. J NeuroEng Rehab. 2010;7(1):48–62. http://doi.org/10.1186/1743-0003-7-48.
32. Mihelj M. Human arm kinematics for robot based rehabilitation. Robotica. 2006;24(3):377–83. https://doi.org/10.1017/S0263574705002304.
33. Papaleo E, et al. Upper-limb kinematic reconstruction during stroke robot-aided therapy. Med Biol Eng Comput. 2015;53(9):815–28. https://doi.org/10.1007/s11517-015-1276-9.
34. Badesa FJ, Morales R, Garcia-Aracil N, Sabater JM, Perez-Vidal C, Fernandez E. Multimodal interfaces to improve therapeutic outcomes in robot-assisted rehabilitation. IEEE T Syst Man Cy C. 2012;42(6):1152–8. https://doi.org/10.1109/TSMCC.2012.2201938.
35. Bertomeu-Motos A, Lledó LD, Díez JA, Catalan JM, Ezquerro S, Badesa FJ, Garcia-Aracil N. Estimation of human arm joints using two wireless sensors in robotic rehabilitation tasks. Sensors. 2015;15(12):30571–83. https://doi.org/10.3390/s151229818.
36. Lenarčič J, Umek A. Simple model of human arm reachable workspace. IEEE T Syst Man Cyb. 1994;24(8):1239–46. https://doi.org/10.1109/21.299704.

36. Denavit J. A kinematic notation for lower-pair mechanisms based on matrices. J Appl Mech, ASME. 1955;22:215–21.
37. Kreutz-Delgado K, Long M, Seraji H. Kinematic analysis of 7 dof anthropomorphic arms. In: Proc 1990 IEEE Int Conf Robot Autom. p. 824–30. https://doi.org/10.1109/ROBOT.1990.126090.
38. Siciliano B. Kinematic control of redundant robot manipulators: A tutorial. J Intell Robot Syst. 1990;3(3):201–12. https://doi.org/10.1007/BF00126069.
39. Siciliano B, Sciavicco L, Villani L, Oriolo G. Robotics: Modelling, Planning and Control. London: Springer-Verlag; 2009. https://doi.org/10.1007/978-1-84628-642-1.
40. Baseline Upper Body (25) Markerset. https://v20.wiki.optitrack.com/index.php?title=Baseline_Upper_Body_(25). Accessed 28 Nov 2017.
41. Charalambous CP. Interrater reliability of a modified ashworth scale of muscle spasticity. Classic Papers in Orthopaedics. London: Springer; 2014, pp. 415–7. https://doi.org/10.1007/978-1-4471-5451-8_105.
42. Fugl-Meyer AR, Jääskö L, Leyman I, Olsson S, Steglind S. The post-stroke hemiplegic patient. 1. a method for evaluation of physical performance. Scand J Rehabil Med. 1975;7(1):13–31.
43. Lledo LD, Diez JA, Bertomeu-Motos A, Ezquerro S, Badesa FJ, Sabater-Navarro JM, Garcia-Aracil N. A comparative analysis of 2d and 3d tasks for virtual reality therapies based on robotic-assisted. Front Aging Neurosci. 2016;8:205. https://doi.org/10.3389/fnagi.2016.00205.
44. Mazza JC. Mediciones antropométricas. estandarización de las técnicas de medición, actualizada según parámetros internacionales. Revista de Actualización en Ciencias del Deporte. 1993;1(2):197.
45. Bertomeu-Motos A, Morales R, Lledó LD, Díez JA, Catalan JM, Garcia-Aracil N. Kinematic reconstruction of the human arm joints in robot-aided therapies with hermes robot. In: 2015 37th Annual International Conference of the IEEE Engineering in Medicine and Biology Society (EMBC). 2015. p. 1190–3. https://doi.org/10.1109/EMBC.2015.7318579.

CrossMark

User activity recognition system to improve the performance of environmental control interfaces: a pilot study with patients

Arturo Bertomeu-Motos[1]* , Santiago Ezquerro[1], Juan A. Barios[1], Luis D. Lledó[1], Sergio Domingo[2],
Marius Nann[4], Suzanne Martin[3], Surjo R. Soekadar[5] and Nicolas Garcia-Aracil[1]

Abstract

Background: Assistive technologies aim to increase quality of life, reduce dependence on care giver and on the long term care system. Several studies have demonstrated the effectiveness in the use of assistive technology for environment control and communication systems. The progress of brain-computer interfaces (BCI) research together with exoskeleton enable a person with motor impairment to interact with new elements in the environment. This paper aims to evaluate the environment control interface (ECI) developed under the AIDE project conditions, a multimodal interface able to analyze and extract relevant information from the environments as well as from the identification of residual abilities, behaviors, and intentions of the user.

Methods: This study evaluated the ECI in a simulated scenario using a two screen layout: one with the ECI and the other with a simulated home environment, developed for this purpose. The sensorimotor rhythms and the horizontal oculoversion, acquired through BCI2000, a multipurpose standard BCI platform, were used to online control the ECI after the user training and system calibration. Eight subjects with different neurological diseases and spinal cord injury participated in this study. The subjects performed simulated activities of daily living (ADLs), i.e. actions in the simulated environment as drink, switch on a lamp or raise the bed head, during ten minutes in two different modes, *AIDE* mode, using a prediction model, to recognize the user intention facilitating the scan, and *Manual* mode, without a prediction model.

Results: The results show that the mean task time spent in the *AIDE* mode was less than in the *Manual*, i.e the users were able to perform more tasks in the *AIDE* mode during the same time. The results showed a statistically significant differences with $p < 0.001$. Regarding the steps, i.e the number of abstraction levels crossed in the ECI to perform an ADL, the users performed one step in the 90% of the tasks using the *AIDE* mode and three steps, at least, were necessary in the *Manual* mode. The user's intention prediction was performed through conditional random fields (CRF), with a global accuracy about 87%.

Conclusions: The environment analysis and the identification of the user's behaviors can be used to predict the user intention opening a new paradigm in the design of the ECIs. Although the developed ECI was tested only in a simulated home environment, it can be easily adapted to a real environment increasing the user independence at home.

Keywords: Environment control interface, Brain-computer interface, User intention prediction, Multimodal system, Brain injury, Spinal-cord injury

*Correspondence: abertomeu@umh.es
[1] Miguel Hernández University of Elche, Av. Universidad w/n, Ed. Innova, 03202 Elche, Spain
Full list of author information is available at the end of the article

BMC

Background

It is estimated that one in six people in the world are diagnosed with a neurological disorder and this number is expected to rise considerable due to extensions of life expectancy [1]. A neurological condition is a damage to the brain, spinal column or nerves due to illness or injury such as spinal cord injury, acquired brain damage, stroke, motor neurons disease and locked in syndrome. Neurological disorders are considered the primary cause of disability in modern society [1, 2]. The debilitating consequences of neurological disorders include communication difficulties, impaired memory, inappropriate behavior, physical disability, restricted independence, social isolation and poor quality of life.

Assistive technologies aim to increase quality of life [3–6], reduce dependence on care giver [7] and reduce dependence on the long term care system [8]. Several studies have demonstrated the effectiveness in the use of environment control interfaces (ECI) for environment control or communication through voice commands [9], scan interfaces based on grid structure, eye tracking [10–12] or brain-computer interface (BCI) based on P300 [13], among others. These software platforms actively aid during the Activities of Daily Living (ADL) improving the independence both at home and outside. However, these platforms are based in a manual scan over the different abstraction levels of the ECIs and the scan speed only depends on the users familiarization with the system and the configuration of the grids over the different menus. Thus, introducing the user environment and behavior into this loop will help the navigation agility in the ECIs.

On the other hand, The progress of BCI research together with exoskeleton enables a person with motor impairment to interact with new elements of the environment [14, 15]. Thus, this progress will deliver new scenarios to BCI systems out of laboratories and move BCI into the domestic environment. The AIDE project[1] aims to create new shared-control paradigm for assistive devices that integrates information from identification of residual abilities, behaviors, emotional state and intentions of the user on one hand and analysis of the environment and context factors on the other hand. In this context, a hybrid BCI model was chosen to control the ECI. It was developed as a fusion between non-invasive electroencephalography (EEG) and electrooculography (EOG) system [16]. The EEG records the sensorimotor rhythms (SMR) called event-related desynchronization (ERD) and event-related synchronization (ERS) during a motor imagery (MI) task [17] whilst the EOG records the horizontal oculoVersion (HOV).

This paper aims to evaluate the ECI developed under the AIDE project conditions, a multimodal system developed to assist people with acquired brain damage or neurodegenerative diseases that need a wheelchair and has low or any upper limbs mobility in their ADLs, in a simulated environment able to detect the user intention through the environment analysis and the identification of the user's behaviors, based on a conditional random fields (CRF) model [18]. Thus, the handling of the interface was studied in two different ways, with and without the prediction of the user's intention. Users with neurological and muscular diseases and spinal cord injury (SCI) tested the system on a virtual home due to the early phase of the project.
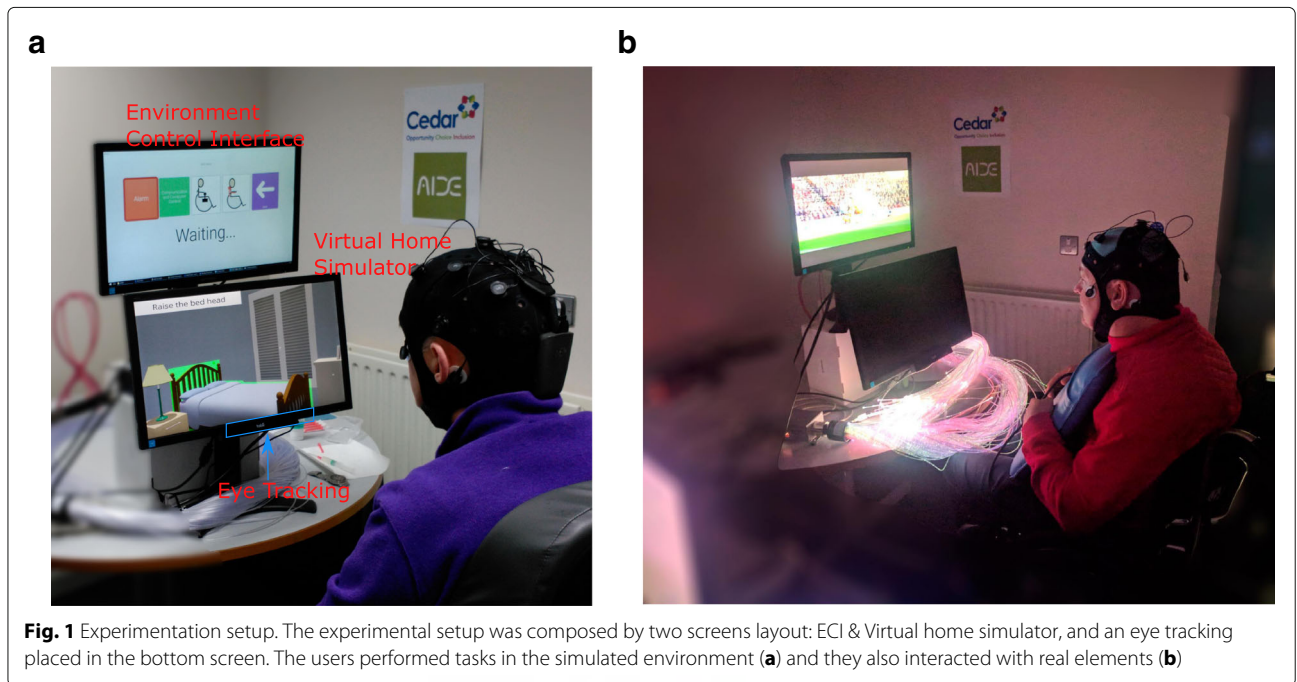
Methods

This study evaluated the ECI in a simulated scenario under the AIDE project conditions, a multimodal interface able to analyze and extract relevant information from the environments as well as from the identification of residual abilities, behaviors, and intentions of the user. It consisted in a two screen layout: ECI and simulated room, with an EEG and EOG data acquisition system (see Fig. 1).

Environment control interface

The environment control system used in this experimentation was based in two main software components: GRID3 from Smartbox[2], a commercial augmentative and alternative communication (AAC) solution, and SHX, a specific developed software, presented in Fig 2. The ECI had three different abstraction levels: 1) related with the room (room menu), 2) related to the activities that can be performed in a specific room (activity menu), and 3) related to the actions regarding a specific activity (ADL menu). The jump between two consecutive abstraction levels will be named as *step*.

Levels one and two were specific grid sets, created in GRID3, to be used in the context of the experimentation. They include grids for the different rooms, communication, control a wheelchair and control an exoskeleton arm. In all grids, a color code has been used: red for the alarm; green for communication, computer control and digital leisure; white for wheelchair and arm control (not used in this experimentation); light blue for the rooms; dark blue for environmental control activity. The dark blue cells are referred to environmental control activities and linked Grid3 with the SHX application. The user could scan across the different cells, select one, and then confirm or cancel the selection using the chosen signals (EOG, EEG, eye tracking, etc.).

SHX is a custom build solution for environmental control management, level three. It allowed the user to easily configure and select the actions programmed for a specific activity. Different scenes for each of the possible activities in every room were created. Here too, the user could scan across the different cells, select one, and then confirm or cancel the selection using the chosen signals (EOG, EEG, eye tracking, etc.).
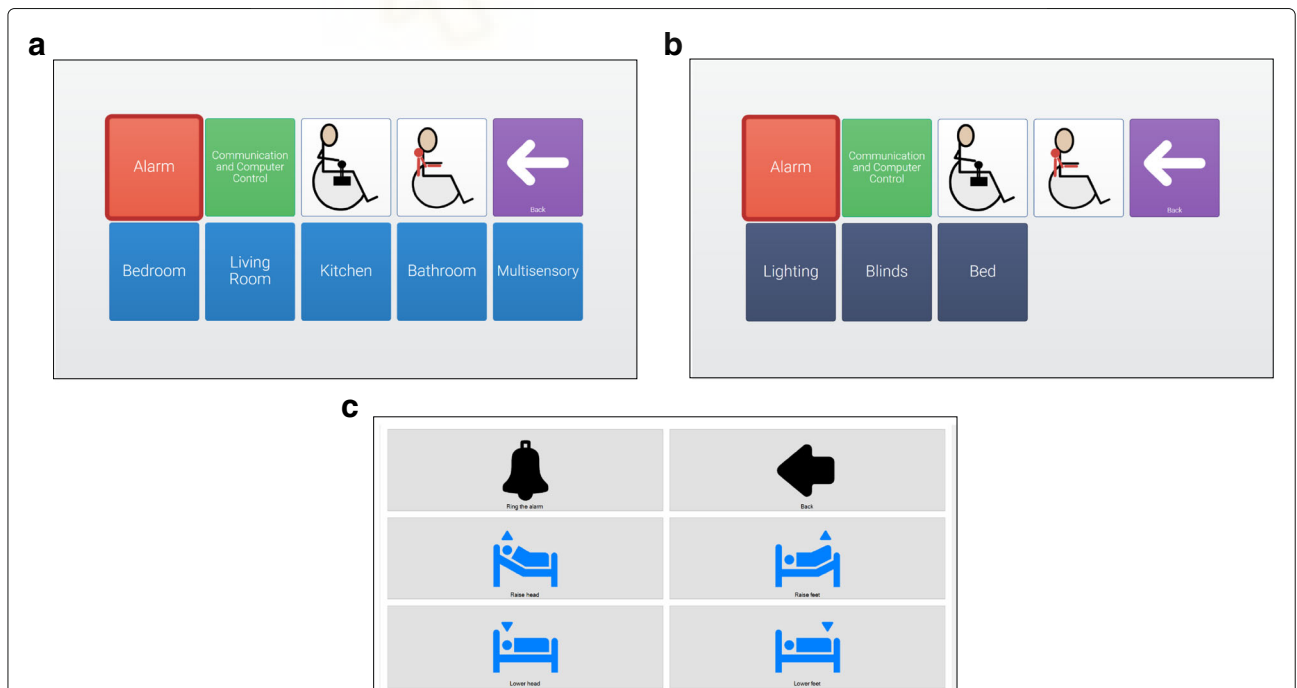
Fig. 1 Experimentation setup. The experimental setup was composed by two screens layout: ECI & Virtual home simulator, and an eye tracking placed in the bottom screen. The users performed tasks in the simulated environment (**a**) and they also interacted with real elements (**b**)

Data acquisition

The acquisition of the brain activity was performed with eight solid-gel electrodes placed according to international 10-20 system placed at F3, C3, Cz, P3, T7 and Mastoid, a reference electrode was placed on C4 and the ground on FpZ. Furthermore, two electrodes were placed on the outer canthus of the eyes to the EOG signal recording. The EEG/EOG signal was acquired via Bluetooth through the Neuro-electrics amplifier (Enobio, Neuroelectrics, Barcelona, Spain). Skin/electrode resistance was kept below 12 kOhm.

Fig. 2 Environment Control Interface. The ECI had three different abstraction levels: 1) related with the room, 2) related to the activities that can be performed in a specific room and 3) related to the actions regarding a specific activity. An example menu of each level is shown in (**a**), (**b**) and (**c**) respectively

A real-time SMR-based BCI was implemented using BCI2000, a freely distributed software for multipurpose standard BCI platform [19]. EEG and EOG were recorded at a sampling rate of 500 Hz, bandpass filtered at 0.4-70 Hz and pre-processed using a small Laplacian filter. Based on the maximum values for basal ERD, the ongoing EEG signal associated with the specified SMR rhythm frequency range (11-14 Hz) calculated from C3 electrode, a subject's individual motor imagery discrimination threshold were set. The EOG discrimination thresholds were calculated regarding the average amplitudes of horizontal saccades. These individual parameters were obtained from the training session and used for later online BCI control [20].

Prediction model

The proposed ECI combines the environmental information and context factors together with user's behaviors in order to detect the user intention. Thus, the input information of the prediction model was a sequence of data, the user is moving and looking at the environment, that had to be labeled. In this context, different models were tested (time-delay neural networks, decision trees, hidden markov model (HMM)...) and the CRF model was chosen, showing the best results. The CRF model is a probabilistic model for segmentation and labeling sequence data. This discriminate model takes into account not only the current state but also the previous states to perform its prediction. A conditional model specifies the probabilities of possible label sequences given an observation sequence in contras of the generative models that make very strict independence assumptions on the observation, for instance conditional independence given the labels as HMM [21].

In our case, the inputs of the system were: localization, objects in the environment, object that the user is looking at, temperature of the room, brightness of the room and day time; the output was the ADL menu, i.e. the most probable action that the user wanted to perform that were directly linked with a specific ADL (see Table 1.

Participants

Eight persons with different neurological pathology and spinal cord injury participated in this study (37 ± 15 years old), their demographic and clinical characteristics are listed in (Table 2). The subjects were evaluated before the experiment with the barthel index [22]. All participants gave informed consent using their standard communication channel prior to participation in the study. The protocol was approved by the Office Research Ethics Northern Ireland - approval granted for project (15/NE/0384).

Table 1 Correlation between the ADLs and ADL menu name, in the third abstraction level

ADLs	ADL menu	ADLs	ADL menu
Open/close fridge	Drink or eat	Switch on/off air conditioner	Air conditioner
Open/close microwave	Drink or eat	Brushing teeth	Teeth
Eating task	Eat	Washing face	Face
Drinking task	Drink	Raise/lower the bed head	Bed
Switch on/off Music	Entertainment	Raise/lower the bed feet	Bed
Switch on/off PC	Entertainment	Open/close the blinds	Blinds
Switch on/off TV	TV	Switch on/off the light	Light

Experimental protocol

Subjects were sitting in his/her own wheelchair in front of a table with two screens, as shown in Fig. 1. The screens were used to show the ECI and the virtual home simulator. Subjects used the AIDE multimodal interface, hybrid EEG EOG system, to online control the ECI and preform specific ADLs. Two modes were tested:

A) *MANUAL* mode: the user had to navigate through the three abstraction levels in order to accomplish the task showed in the virtual house. The objects related with the corresponding task were surrounded by a green color in the virtual house environment and the task appeared in the right top corner.

B) *AIDE* mode: in this mode the prediction model was used. The user had to look at the objects related to the specific ADL, showed like in the other mode, and, after the user's intention prediction, the ECI directly jumped to the corresponding ADL menu. Then the user had to navigate like *MANUAL* mode. In case of

Table 2 Demographic and clinical characteristics of participants

ID Patient	Sex	Age	Diagnosis	Barthel score
1	Male	32	C4 SCI	4/20
2	Male	22	Duchenne Muscular Dystrophy	6/20
3	Male	55	Brain stem strokes	16.5/20
4	Male	30	C4/C5 SCI	2/20
5	Female	20	C6/C7 SCI	10/20
6	Male	58	Ischemic Stroke	19/20
7	Male	55	Multiple Systems Atrophy	5/20
8	Male	30	C6/C7 SCI	9/10

wrong prediction, the user had to manually go back, the second abstraction level, and complete the corresponding ADL. The observed objects were online detected from the eye tracking Tobbi[3] PCEye go, placed on the virtual environment screen, and the rest of the inputs were online simulated.

Each subject performed two experimental sessions in two consecutive days. The first session was for training and calibration purpose as well as for the familiarization with the systems to be controlled. This session lasted around 60-80 min. In the last part of this session the user learned how to use the hybrid EEG/EOG interface in order to control the ECI. An example of MI and EOG movements in the training session are shown in Fig. 3c and d, respectively.

The second session lasted a maximum of 60 min. The setup and familiarization phase took approximately 15 min (subjects have already tested the system in the first session). They had 10 min to perform a predefined ADLs list in both *AIDE* and *Manual* modes (all ADLs can be observed in Table 1). Each ADL can be a single action, it has a visual effect on the house simulator, e.g. swith on a lamp, or an exoskeleton action, the simulator play a short video showing the corresponding action, e.g. drink from a glass. The order of the modes was randomly selected and, before each mode, a baseline of 3 min was acquired. During the break (5 min) and at the end of this session the subjects answered the NASA task load index (tlx) questionnaire [23].

The scan in the ECI was performed through looking-right eye movements (Fig. 3b) implying a forward displacement of the grid marker (Fig. 3a-e). Once the subject stopped at one grid a customized time, chosen in the first session, the ECI 'switch off' the rest of the grids (Fig. 3f). Then, the next level or the action in the ECI was achieved by on-line ERD detection, like the subjects learned during the first session (Fig. 3a). On the other hand, if the user did not want to click on this specific grid, in the phase Fig. 3f, a looking-left eye movement returns the ECI to the phase Fig. 3a. When the user performs an action, a visual feedback is presented in the virtual home regarding to the action performed (Fig. 3g) and he/she waited for the next task.

After both modes, they were instructed to interact with real elements through the ECI and watch a video using objects of a multi-sensory room, as can be observed in Fig. 1b.

Results
The users performed simulated ADLs during 10 min in a virtual home using an ECI in both *Manual* and *AIDE* modes. The number of the performed tasks with respect to the mean time spent per user is presented

in Fig. 4a. Furthermore, it has been trained a Support Vector Machine (SVM) model with Gaussian kernel to estimate the boundary between both modes (yellow line in Fig. 4a). It should be noted that statistically significant differences between both modes in terms of number of tasks and mean tasks time is shown ($p - value < 0.001$ using Wilcoxon test). The steps distribution that the users performed in both modes are shown in Fig. 4c. ADLs manually omitted tasks were excluded from the study due to the subject was blocked during the ECI scan caused by frustration or fatigue over a specific task.

On the other hand, the *AIDE* mode uses a CRF model, previously trained with simulated data using the same virtual home, to predict the user intention. Thus, the confusion matrix of the prediction model regarding the ADL menus is presented in Fig. 4b. In addition, the results obtained through the NASA tlx questionnaire are presented in Fig. 5.

Discussion
The AIDE project aims to develop a multimodal system in order to help people with neurological diseases wearing a wheelchair. The presented environment allowed the user to navigate through a virtual house and perform several ADLs using a developed ECI. Two modes were estudied, the *AIDE* mode, that used a CRF model to predict the user intention and ease the ECI scan, and the *Manual* mode, that needed a complete scan through the ECI to perform a specific ADL. The ECI was online controlled using the AIDE multimodal system based on a combination of EEG and EOG wireless acquisition system [17].

The results presented in Fig. 4a show the mean time per task spent in the AIDE mode is less than in the Manual mode being able to perform more tasks in the same time, both modes show statistically significant differences ($p < 0.001$). Furthermore, both modes can be easily classified by training a SVM model with Gaussian kernel, the boundary is presented with a yellow line in Fig. 4a.

On the other hand, Fig. 4c shows the difference between both groups in terms of steps, i.e. the ECI abstraction levels that the user had to cross in order to perform a specific ADL. It must be noticed that in the *AIDE* mode, the users performed one step in the 90% of the tasks and three steps, at least, were necessary in the *Manual* mode. Regarding the *AIDE* mode, three steps were necessary only when the CRF model realized a wrong prediction and, therefore, the user had to return to the activity menu and select the proper ADL menu. Although a bad prediction is sometimes performed, the multimodal system helps in terms of location, i.e. the activity that the system predicts is always related with the room where the user is, facilitating the navigation. Perform five or seven steps in the *Manual* mode implies that a wrong abstraction level was selected,
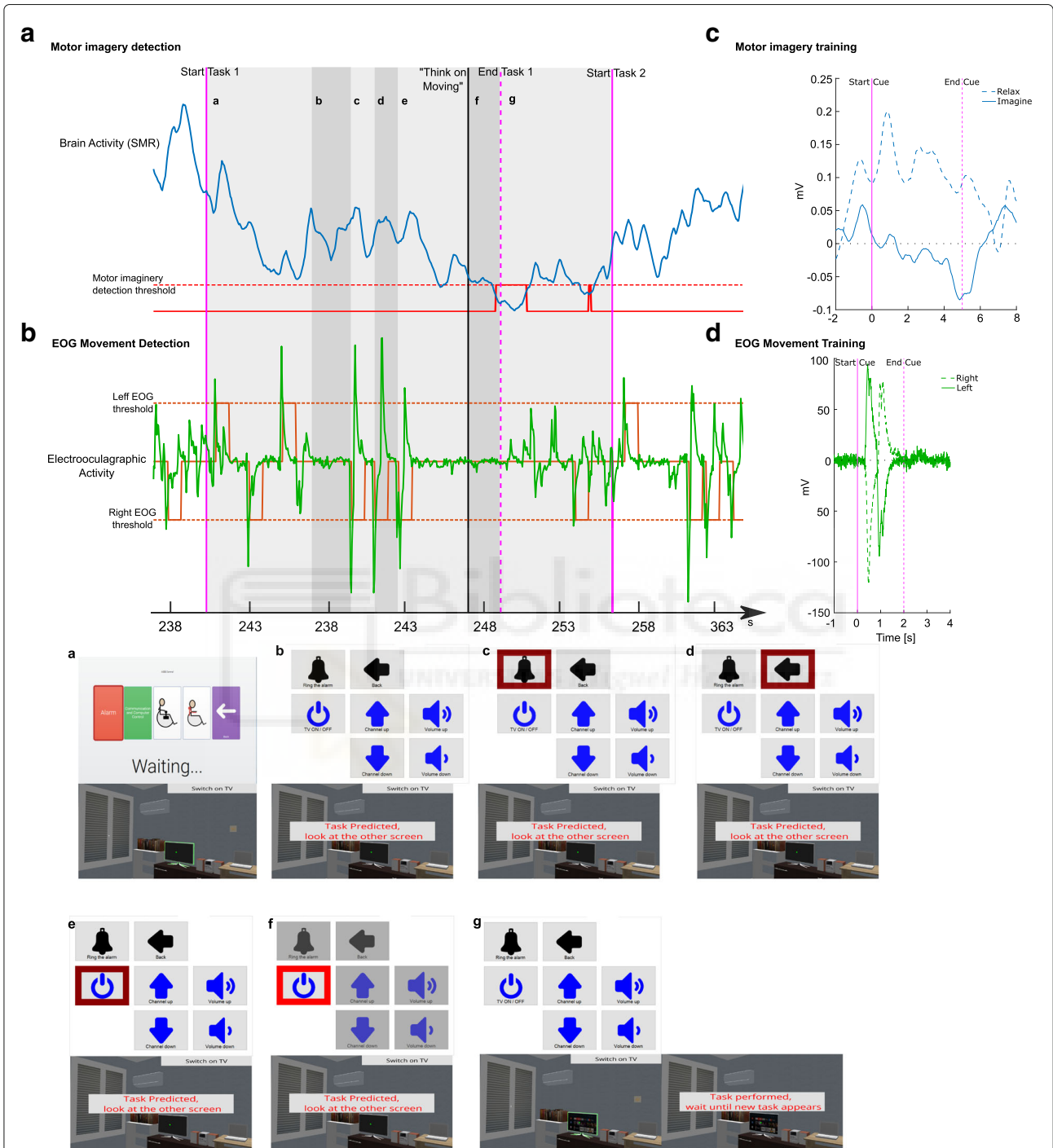
Fig. 3 Multimodal system processing for one ADL in *AIDE* mode. The user had to perform different actions in order to execute the corresponding ADLs, in this example, the user had to switch on the TV, phases a-g show the behavior of both screens during the task. EEG (**a**) and EOG (**b**) signals were acquired to online control the ECI in order to perform ADLs in a virtual house. When the task started (vertical purple line), the scan through the ECI was performed by EOG activity detection [orange line in (**b**)], i.e. when HOV activity exceeded the threshold [indicated by the orange dashed line in (**b**)] the grid marker moved forward (phases a-e). Once the subject stopped at one grid, a task confirmation was needed [indicated by the vertical black line] and the ECI 'switched off' the rest of the grids indicating this purpose (phase f). The confirmation was performed by the detection of SMR-ERD [indicated by red line in (**a**)] and the action was done, so the ADL finished (vertical dotted purple line). This ADL was performed in one step, i.e. the user only needed to navigate through the last abstraction level to complete the task. Before the experimentation, the user was trained in motor imagery (**c**) and EOG movement (**d**) to the set up the control system with the personalized parameters
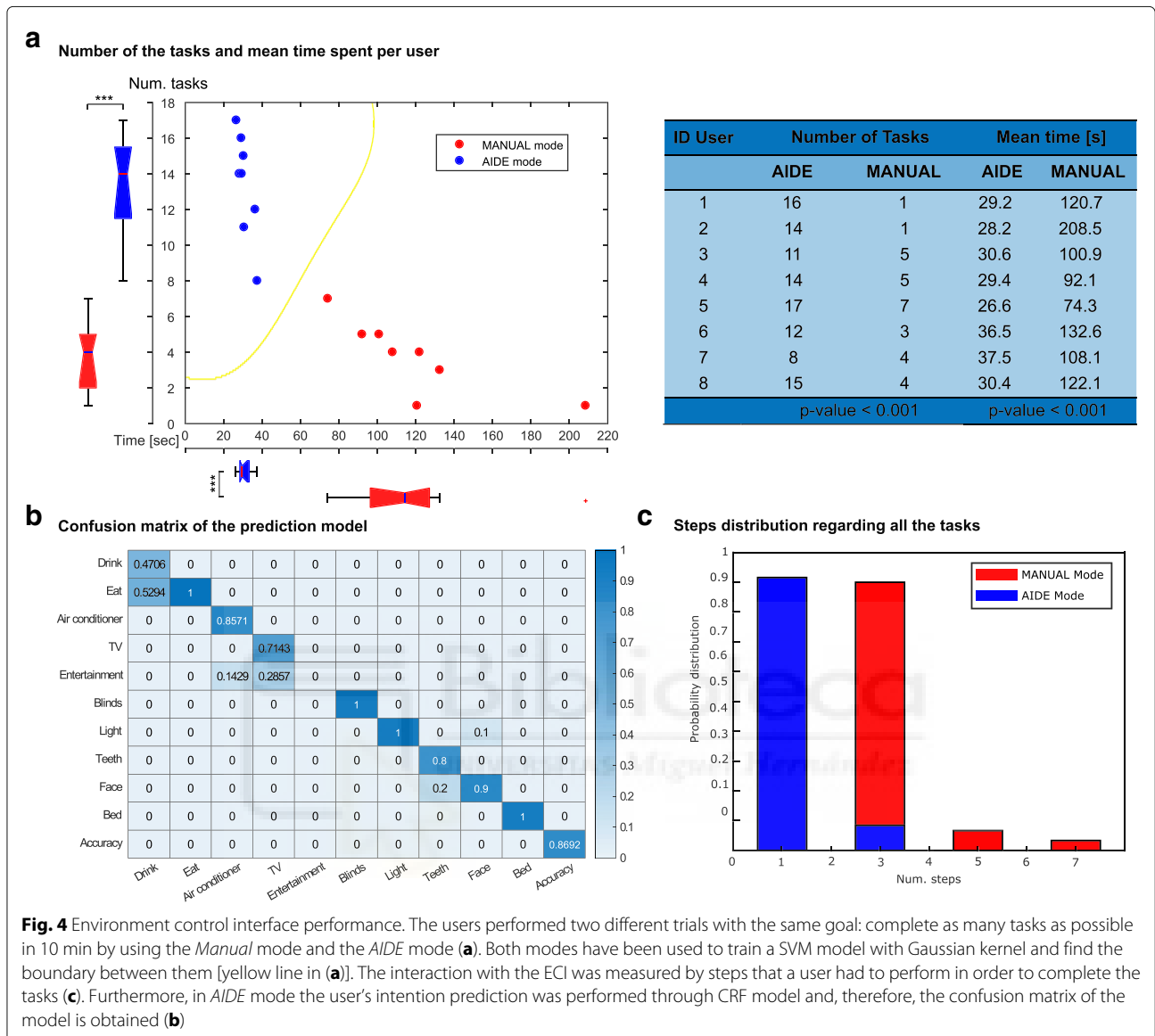
Fig. 4 Environment control interface performance. The users performed two different trials with the same goal: complete as many tasks as possible in 10 min by using the *Manual* mode and the *AIDE* mode (**a**). Both modes have been used to train a SVM model with Gaussian kernel and find the boundary between them [yellow line in (**a**)]. The interaction with the ECI was measured by steps that a user had to perform in order to complete the tasks (**c**). Furthermore, in *AIDE* mode the user's intention prediction was performed through CRF model and, therefore, the confusion matrix of the model is obtained (**b**)

due to user confusion or lack of practice, and the user had to go back in the ECI.

The *AIDE* mode uses a CRF model to perform the predictions about the user's intention. The model uses the information of the virtual home and the object that the user is looking at, acquired thought an eye tracking device. The model was previously trained with simulated data using the same virtual house environment. Thus, Fig. 4b shows the confusion matrix of the prediction model, regarding the ADL menu, with a global accuracy about 87%. The CRF model, as it takes into account not only the current state but also the previous states to perform its prediction, it could fail in the prediction of task with common features. Therefore, the ADLs related to the *Drink* menu are sometimes predicted as the ADLs related

with the *Eat* menu, in this case around the 50% of the trials. In addition, *TV* and the *Teeth* menus are rarely selected as *Entertainment* and *Face* menu, respectively, by the prediction model.

After each mode, the subjects answered the NASA tlx questionnaire in order to assess the workload between the modes, showed in Fig. 5. Unexpectedly, it has not statistically significant differences, so we can say that the users do not notice subjective differences between both modes in terms of workload. It can be explained because it was the first time that the users handle the complex multimodal control system (EEG+EOG) with this ECI. We assume that, observing the results presented in Fig 4, the workload should decrease, at least, in the AIDE mode.
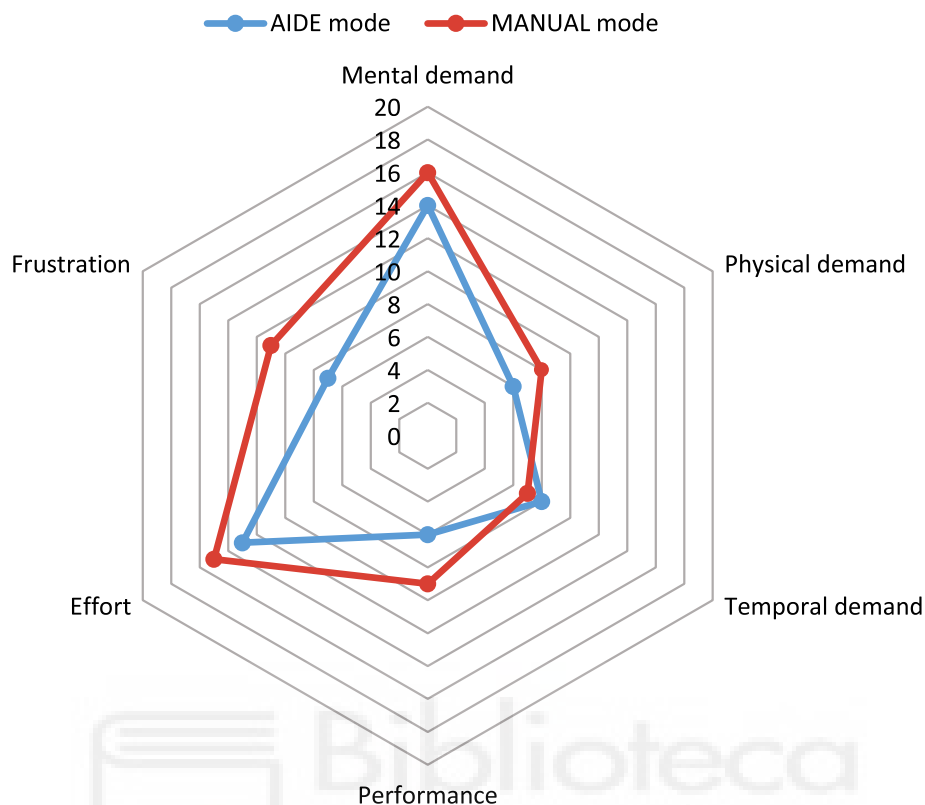
Fig. 5 NASA task load index. The subjects answered the NASA tlx questionnaire after each mode

Conclusion

The presented ECI allowed the users to perform simulated ADLs with a multimodal control system. The platform was tested in two different scenarios: *Manual* and *AIDE* mode. The first one was presented as a simple ECI where the user had to achieve the corresponding ADL. The second mode used a CRF model to predict the user's intention through the environment analysis and identification of the user's behaviors. We conclude that, even the users do not perceive subjective differences between both modes in terms of workload, the *AIDE* mode helps the user to perform mode ADLs, spending less time per task, showing statistically significant differences with respect to the *Manual* mode. This effect is caused by the user's intention prediction as the ECI jumps directly to the last abstraction level of the ECI. The environment analysis and the identification of the user's behaviors can be used to predict the user intention and will allow to speed up the ECIs scan opening a new paradigm in the design of these interfaces. Although the developed ECI was tested only in a simulated home environment, it can be easily adapted to a real environment increasing the user independence at home.

Endnotes

[1] http://aideproject.umh.es/

[2] http://www.thinksmartbox.com

[3] http://www.tobii.com

Abbreviations

AAC: Augmentative and alternative communication; ADL: Activity of daily living; BCI: Brain computer interface; CRF: Conditional random field; ECI: Environment control interface; EEG: Electroencephalography; EOG: Electrooculography; HOV: Horizontal oculoversion; MI: Motor Imagery; SMR-ERD: Sensorimotor rhythm event-related desynchronization; SVM: Support vector machine; tlx: task load index

Authors' contributions

ABM, SM, SRS and NGA designed the study. ABM, SE, JAB, LDL and SD collect the data. SD developed the environment control interface. LDL designed the virtual home environment. ABM, SE and JAB interpreted and analyze the data. ABM, SE created the figures. ABM, SE, JAB, LDL and SD wrote the manuscript. SM, NGA and SRS deeply revised the manuscript. ABM, SE, JAB, LDL, SE, MN, SM, SRS and NGA edited the manuscript. All authors read and approved the final manuscript.

Ethics approval and consent to participate

This study was conducted according to the declaration of Helsinki and had ethical approval by the Office Research Ethics Northern Ireland (June 2016) – approval granted for AIDE project (15/NE/0384). All subjects gave written informed consent prior to data collection.

Consent for publication

Participants gave written informed consent to data treatment in this research study and permission to publish anonymous data and results.

Competing interests

Sergio Domingo is a software developer at BJ Adaptaciones, the developer of SHX software. Sergio Domingo declares no competing interests. The rest of the authors declare no competing interests.

Publisher's Note

Springer Nature remains neutral with regard to jurisdictional claims in published maps and institutional affiliations.

Author details

[1] Miguel Hernández University of Elche, Av. Universidad w/n, Ed. Innova, 03202 Elche, Spain. [2] BJ Adaptaciones, St Mare de Déu del Coll, 70, 08023 Barcelona, Spain. [3] The Cedar Foundation, 1 Upper Lisburn Road, BT10 0GW Belfast, UK. [4] University Hospital of Tuebingen, Applied Neurotechnology Lab, Calwerstr. 14, D-72076 Tübingen, Germany. [5] Clinical Neurotechnology Laboratory, Neuroscience Research Center (NWFZ), Charité University Medicine Berlin, Charitéplatz 1, 10117 Berlin, Germany.

References

1. World Health Organization. Neurological Disorders: Public Health Challenges. Geneva: World Health Organization; 2006. http://www.who.int/iris/handle/10665/43605.
2. Winstein CJ, Stein J, Arena R, Bates B, Cherney LR, Cramer SC, Deruyter F, Eng JJ, Fisher B, Harvey RL, et al. Guidelines for adult stroke rehabilitation and recovery: a guideline for healthcare professionals from the american heart association/american stroke association. Stroke. 2016;47(6):98–169.
3. Sellers EW, Vaughan TM, Wolpaw JR. A brain-computer interface for long-term independent home use. Amyotroph Lateral Scler. 2010;11(5):449–55.
4. Ball MM, Perkins MM, Whittington FJ, Hollingsworth C, King SV, Combs BL. Independence in assisted living. J Aging Stud. 2004;18(4):467–83.
5. Ball MM, Perkins MM, Whittington FJ, Connell BR, Hollingsworth C, King SV, Elrod CL, Combs BL. Managing decline in assisted living: The key to aging in place. J Gerontol B Psychol Sci Soc Sci. 2004;59(4):202–12.
6. Struijk LNA, Egsgaard LL, Lontis R, Gaihede M, Bentsen B. Wireless intraoral tongue control of an assistive robotic arm for individuals with tetraplegia. J Neuroengineering Rehabil. 2017;14(1):110.
7. Brandt Å, Samuelsson K, Töytäri O, Salminen A-L. Activity and participation, quality of life and user satisfaction outcomes of environmental control systems and smart home technology: a systematic review. Disabil Rehabil Assist Technol. 2011;6(3):189–206.
8. Agree EM, Freedman VA, Cornman JC, Wolf DA, Marcotte JE. Reconsidering substitution in long-term care: when does assistive technology take the place of personal care? J Gerontol B Psychol Soc Sci. 2005;60(5):272–80.
9. O'Neill B, Moran K, Gillespie A. Scaffolding rehabilitation behaviour using a voice-mediated assistive technology for cognition. Neuropsychol Rehabil. 2010;20(4):509–27.
10. Lupu RG, Ungureanu F, Siriteanu V. Eye tracking mouse for human computer interaction. In: E-Health and Bioengineering Conference (EHB), 2013. IEEE; 2013. p. 1–4. https://doi.org/10.1109/EHB.2013.6707244.
11. Adjouadi M, Sesin A, Ayala M, Cabrerizo M. Remote eye gaze tracking system as a computer interface for persons with severe motor disability. In: International Conference on Computers for Handicapped Persons. Berlin: Springer; 2004. p. 761–9. https://doi.org/10.1007/978-3-540-27817-7_113.
12. Biswas P, Langdon P. A new input system for disabled users involving eye gaze tracker and scanning interface. J Assist Technol. 2011;5(2):58–66.
13. Miralles F, Vargiu E, Rafael-Palou X, Sola M, Dauwalder S, Guger C, Hintermuller C, Espinosa A, Lowish H, Martin S, Armstrong E, Daly J. Brain?computer interfaces on track to home: Results of the evaluation at disabled end-users? homes and lessons learnt. Front ICT. 2015;2:25. https://doi.org/10.3389/fict.2015.00025.
14. Wolpaw JR, Birbaumer N, McFarland DJ, Pfurtscheller G, Vaughan TM. Brain–computer interfaces for communication and control. Clin Neurophysiol. 2002;113(6):767–91.
15. Cincotti F, Mattia D, Aloise F, Bufalari S, Schalk G, Oriolo G, Cherubini A, Marciani MG, Babiloni F. Non-invasive brain–computer interface system: towards its application as assistive technology. Brain Res Bull. 2008;75(6):796–803.
16. Witkowski M, Gómez C, Opisso E, Medina J, Cortese M, Cempini M, Carrozza MC, Cohen LG, Birbaumer N, Vitiello N. Hybrid eeg/eog-based brain/neural hand exoskeleton restores fully independent daily living activities after quadriplegia. Sci Robot. 2016;1(1):eaag3296. https://doi.org/10.1126/scirobotics.aag3296.
17. Soekadar SR, Witkowski M, Mellinger J, Ramos A, Birbaumer N, Cohen LG. Erd-based online brain-machine interfaces (bmi) in the context of neurorehabilitation: optimizing bmi learning and performance. IEEE Trans Neural Syst Rehabil Eng: Publ IEEE Eng Med Biol Soc. 2011;19(5):542–9.
18. Lafferty J, McCallum A, Pereira FC. Conditional random fields: Probabilistic models for segmenting and labeling sequence data. In: Proceedings of the Eighteenth International Conference on Machine Learning (ICML '01). San Francisco: Morgan Kaufmann Publishers Inc.; 2001. p. 282–289. http://portal.acm.org/citation.cfm?id=655813.
19. Schalk G, McFarland DJ, Hinterberger T, Birbaumer N, Wolpaw JR. Bci2000: a general-purpose brain-computer interface (bci) system. IEEE Trans Biomed Eng. 2004;51(6):1034–43.
20. Barios JA, Ezquerro S, Bertomeu-Motos A, Nann M, Badesa FJ, Fernandez E, Soekada SR, Garcia-Aracil N. Synchronization of slow cortical rhythms during motor imagery-based brain-machine interface control. Int J Neural Syst. 2018. in press.
21. Rabiner LR. A tutorial on hidden Markov models and selected applications in speech recognition. Proc IEEE. 1989;77(2):257–86.
22. Quinn TJ, Langhorne P, Stott DJ. Barthel index for stroke trials: development, properties, and application. Stroke. 2011;42(4):1146–51.
23. Hart SG, Staveland LE. Development of nasa-tlx (task load index): Results of empirical and theoretical research. In: Advances in Psychology, vol 52. North Holland: Elsevier; 1988. p. 139–83. https://doi.org/10.1016/S0166-4115(08)62386-9.

Abdel-Aziz, Y. I.; Karara, H. M. and Hauck, M. (2015), 'Direct Linear Transformation from Comparator Coordinates into Object Space Coordinates in Close-Range Photogrammetry', *Photogrammetric Engineering & Remote Sensing* **81**(2), pp. 103–107, DOI: `10.14358/PERS.81.2.103` (page 12).

Aggarwal, J. K. and Cai, Q. (1999), 'Human Motion Analysis: A Review', *Computer Vision and Image Understanding* **73**(3), pp. 428–440, DOI: `10.1006/cviu.1998.0744` (pages 12, 13).

Ahsan, R.; Ibrahimy, M. and Khalifa, O. (2009), 'EMG signal classification for human computer interaction: a review', *European Journal of Scientific Research* **33**(3), pp. 480–501, Retrieved from `http://www.academia.edu/download/2804697/318scxi62oxzwkf.pdf` (page 16).

Alon, G.; Levitt, A. F. and McCarthy, P. A. (2007), 'Functional Electrical Stimulation Enhancement of Upper Extremity Functional Recovery During Stroke Rehabilitation: A Pilot Study', *Neurorehabilitation and Neural Repair* **21**(3), pp. 207–215, DOI: `10.1177/1545968306297871` (page 2).

Amirabdollahian, F.; Loureiro, R.; Gradwell, E.; Collin, C.; Harwin, W. and Johnson, G. (2007), 'Multivariate analysis of the Fugl-Meyer outcome measures assessing the effectiveness of GENTLE/S robot-mediated stroke therapy', *Journal of NeuroEngineering and Rehabilitation* **4**(1), p. 4, DOI: `10.1186/1743-0003-4-4` (page 10).

Araque, A.; Parpura, V.; Sanzgiri, R. P. and Haydon, P. G. (1999), 'Tripartite synapses: glia, the unacknowledged partner', *Trends in Neurosciences* **22**(5), pp. 208–215, DOI: `10.1016/S0166-2236(98)01349-6` (page 1).

Association of Assistive Technology Act Programs (1998), *Assistive Technology Act of 1998*, Retrieved from `https://www.ataporg.org/` (page 15).

Bachmann, E. R.; Duman, I.; Usta, U. Y.; McGhee, R. B.; Yun, X. P. and Zyda, M. J. (1999), 'Orientation tracking for humans and robots using inertial sensors', in: *Proceedings of the 1999 IEEE International Symposium on Computational Intelligence in Robotics and Automation*, pp. 187–194, DOI: `10.1109/CIRA.1999.810047` (page 14).

Badesa, F.; Morales, R.; Garcia-Aracil, N.; Sabater, J.; Casals, A. and Zollo, L. (2014), 'Auto-adaptive robot-aided therapy using machine

learning techniques', *Computer Methods and Programs in Biomedicine* **116**(2), New methods of human-robot interaction in medical practice, pp. 123–130, DOI: `10.1016/j.cmpb.2013.09.011` (page 81).

Bagg, S. and Forrest, W. (1988), 'A biomechanical analysis of scapular rotation during arm abduction in the scapular plane', *American Journal of Physical Medicine & Rehabilitation* **67**(6), pp. 238–245, Retrieved from `https://www.ncbi.nlm.nih.gov/pubmed/3196449` (page 21).

Barea, R.; Boquete, L.; Rodriguez-Ascariz, J. M.; Ortega, S. and López, E. (2011), 'Sensory System for Implementing a Human–Computer Interface Based on Electrooculography', *Sensors* **11**(1), pp. 310–328, DOI: `10.3390/s110100310` (page 17).

Basteris, A.; Nijenhuis, S.; Stienen, A.; Buurke, J.; Prange, G. and Amirabdollahian, F. (2014), 'Training modalities in robot-mediated upper limb rehabilitation in stroke: a framework for classification based on a systematic review', *Journal of neuroengineering and rehabilitation* **11**(111), p. 15, DOI: `10.1186/1743-0003-11-111` (page 15).

Beebe, J. A. and Lang, C. E. (2009), 'Active Range of Motion Predicts Upper Extremity Function 3 Months After Stroke', *Stroke* **40**(5), pp. 1772–1779, DOI: `10.1161/STROKEAHA.108.536763` (page 4).

Berger, H. (1929), 'Über das elektrenkephalogramm des menschen', *European archives of psychiatry and clinical neuroscience* **87**(1), pp. 527–570, DOI: `10.1007/BF01797193` (page 17).

Bertomeu-Motos, **A.**; Morales, R.; Lledó, L. D.; Díez, J. A.; Catalan, J. M. and Garcia-Aracil, N. (2015a), 'Kinematic reconstruction of the human arm joints in robot-aided therapies with Hermes robot', in: *2015 37th Annual International Conference of the IEEE Engineering in Medicine and Biology Society (EMBC)*, pp. 1190–1193, DOI: `10.1109/EMBC.2015.7318579` (page 21).

Bertomeu-Motos, **A.**; Lledó, L. D.; Díez, J. A.; Catalan, J. M.; Ezquerro, S.; Badesa, F. J. and Garcia-Aracil, N. (2015b), 'Estimation of Human Arm Joints Using Two Wireless Sensors in Robotic Rehabilitation Tasks', *Sensors* **15**(12), pp. 30571–30583, DOI: `10.3390/s151229818` (pages v, 7, 43, 87).

Bertomeu-Motos, **A.**; Blanco, A.; Badesa, F. J.; Barios, J. A.; Zollo, L. and Garcia-Aracil, N. (2018), 'Human arm joints reconstruction algorithm in rehabilitation therapies assisted by end-effector robotic devices', *Journal of NeuroEngineering and Rehabilitation* **15**(1), p. 10, DOI: `10.1186/s12984-018-0348-0` (pages v, 7, 21, 87).

Bertomeu-Motos, **A.**; Ezquerro, S.; Barios, J. A.; Lledó, L. D.; Domingo, S.; Nann, M.; Martin, S.; Soekadar, S. R. and Garcia-Aracil, N. (2019), 'User activity recognition system to improve the performance of environmental control interfaces: a pilot study with patients', *Journal of NeuroEngineering and Rehabilitation* **16**(1), p. 10, DOI: 10.1186/s12984-018-0477-5 (pages v, 8, 65, 87).

Birbaumer, N.; Kubler, A.; Ghanayim, N.; Hinterberger, T.; Perelmouter, J.; Kaiser, J.; Iversen, I.; Kotchoubey, B.; Neumann, N. and Flor, H. (2000), 'The thought translation device (TTD) for completely paralyzed patients', *IEEE Transactions on Rehabilitation Engineering* **8**(2), pp. 190–193, DOI: 10.1109/86.847812 (page 17).

Blakemore, C. and Cooper, G. F. (1970), 'Development of the Brain depends on the Visual Environment', *Nature* **228**, pp. 477–478, DOI: 10.1038/228477a0 (page 17).

Bohannon, R. W. and Smith, M. B. (1987), 'Interrater reliability of a modified Ashworth scale of muscle spasticity', *Physical therapy* **67**(2), pp. 206–207, DOI: 10.1093/ptj/67.2.206 (pages 3, 37, 56).

Bohil, C. J.; Alicea, B. and Biocca, F. A. (2011), 'Virtual reality in neuroscience research and therapy', *Nature Reviews Neuroscience* **12**, Review Article, pp. 752–762, DOI: 10.1038/nrn3122 (page 2).

Bouvier, B.; Duprey, S.; Claudon, L.; Dumas, R. and Savescu, A. (2015), 'Upper Limb Kinematics Using Inertial and Magnetic Sensors: Comparison of Sensor-to-Segment Calibrations', *Sensors* **15**(8), pp. 18813–18833, DOI: 10.3390/s150818813 (page 54).

Bradley, N. and Poppen, W. (2003), 'Assistive technology, computers and Internet may decrease sense of isolation for homebound elderly and disabled persons', *Technology and disability* **15**(1), pp. 19–25, Retrieved from https://content.iospress.com/articles/technology-and-disability/tad00113 (pages 3, 4).

Bulling, A. and Gellersen, H. (2010), 'Toward Mobile Eye-Based Human-Computer Interaction', *IEEE Pervasive Computing* **9**(4), pp. 8–12, DOI: 10.1109/MPRV.2010.86 (page 17).

Bulling, A.; Ward, J. A.; Gellersen, H. and Troster, G. (2011), 'Eye Movement Analysis for Activity Recognition Using Electrooculography', *IEEE Transactions on Pattern Analysis and Machine Intelligence* **33**(4), pp. 741–753, DOI: 10.1109/TPAMI.2010.86 (page 17).

Bulling, A.; Roggen, D. and Tröster, G. (2009), 'Wearable EOG goggles: Seamless sensing and context-awareness in everyday environments', *Journal of Ambient Intelligence and Smart Environments* **1**(2), pp. 157–171, DOI: 10.3233/AIS-2009-0020 (page 17).

Burgar, C.; Lum, P.; Shor, P. and Van der Loos, H. (2000), 'Development of robots for rehabilitation therapy: The Palo Alto VA/Stanford experience', *Journal of rehabilitation research and development* **37**(6), pp. 663–674, Retrieved from `https://www.rehab.research.va.gov/jour/00/37/6/pdf/burgar.pdf` (page 10).

Burke, J. W.; McNeill, M.; Charles, D.; Morrow, P.; Crosbie, J. and McDonough, S. (2009), 'Serious Games for Upper Limb Rehabilitation Following Stroke', in: *Proceedings of the 2009 Conference in Games and Virtual Worlds for Serious Applications*, pp. 103–110, DOI: `10.1109/VS-GAMES.2009.17` (page 13).

Burke, J.; McNeill, M. D. J.; Charles, D.; Morrow, P.; Crosbie, J. and McDonough, S. (2009), 'Optimising engagement for stroke rehabilitation using serious games', *The Visual Computer* **25**, pp. 1085–1099, DOI: `10.1007/s00371-009-0387-4` (page 12).

Bussmann, J.; Tulen, J.; van Herel, E. and Stam, H. (1998), 'Quantification of physical activities by means of ambulatory accelerometry: a validation study', *Psychophysiology* **35**(5), pp. 488–496, Retrieved from `https://www.cambridge.org/core/product/CCBBFE34A50EC653328DC4A5BFADD13B` (page 14).

Cameirão, M. S.; Bermúdez i Badia, S.; Duarte, E.; Frisoli, A. and Verschure, P. F. M. J. (2012), 'The Combined Impact of Virtual Reality Neurorehabilitation and Its Interfaces on Upper Extremity Functional Recovery in Patients With Chronic Stroke', *Stroke* **43**(10), pp. 2720–2728, DOI: `10.1161/STROKEAHA.112.653196` (page 3).

Carse, B.; Meadows, B.; Bowers, R. and Rowe, P. (2013), 'Affordable clinical gait analysis: An assessment of the marker tracking accuracy of a new low-cost optical 3D motion analysis system', *Physiotherapy* **99**(4), pp. 347–351, DOI: `10.1016/j.physio.2013.03.001` (page 12).

Charlton, I. W.; Tate, P.; Smyth, P. and Roren, L. (2004), 'Repeatability of an optimised lower body model', *Gait & Posture* **20**(2), pp. 213–221, DOI: `10.1016/j.gaitpost.2003.09.004` (page 13).

Chaudhary, U.; Birbaumer, N. and Ramos-Murguialday, A. (2016), 'Brain-computer interfaces for communication and rehabilitation', *Nature Reviews Neurology* **12**, Review Article, pp. 513–525, DOI: `10.1038/nrneurol.2016.113` (page 2).

Chen, Y.-L.; Lai, J.-S.; Luh, J.-J. and Kuo, T.-S. (2002), 'SEMG-controlled telephone interface for people with disabilities', *Journal of Medical Engineering & Technology* **26**(4), pp. 173–176, DOI: `10.1080/03091900210127933` (page 16).

Colombo, G.; Joerg, M.; Schreier, R.; Dietz, V. et al. (2000), 'Treadmill training of paraplegic patients using a robotic orthosis', *Journal of rehabilitation research and development* **37**(6), pp. 693–700, Retrieved from `https://www.rehab.research.va.gov/jour/00/37/6/colombo.htm` (page 11).

Cooper, G.; Sheret, I.; McMillian, L.; Siliverdis, K.; Sha, N.; Hodgins, D.; Kenney, L. and Howard, D. (2009), 'Inertial sensor-based knee flexion/extension angle estimation', *Journal of Biomechanics* **42**(16), pp. 2678–2685, DOI: `10.1016/j.jbiomech.2009.08.004` (page 14).

Coote, S.; Murphy, B.; Harwin, W. and Stokes, E. (2008), 'The effect of the GENTLE/s robot-mediated therapy system on arm function after stroke', *Clinical Rehabilitation* **22**(5), pp. 395–405, DOI: `10.1177/0269215507085060` (page 10).

Corke, P. I. (2011), *Robotics, Vision & Control: Fundamental Algorithms in MATLAB*, Springer, ISBN: 978-3642201431 (page 32).

Cramer, S. C. (2008), 'Repairing the human brain after stroke: I. Mechanisms of spontaneous recovery', *Annals of neurology* **63**(3), pp. 272–287, DOI: `10.1002/ana.21393` (page 1).

Csató, L. and Opper, M. (2002), 'Sparse on-line Gaussian processes', *Neural computation* **14**(3), pp. 641–668, DOI: `10.1162/089976602317250933` (page 55).

Culmer, P. R.; Jackson, A. E.; Makower, S. G.; Cozens, J. A.; Levesley, M. C.; Mon-Williams, M. and Bhakta, B. (2011), 'A novel robotic system for quantifying arm kinematics and kinetics: Description and evaluation in therapist-assisted passive arm movements post-stroke', *Journal of Neuroscience Methods* **197**(2), pp. 259–269, DOI: `10.1016/j.jneumeth.2011.03.004` (page 10).

Demain, S.; Burridge, J.; Ellis-Hill, C.; Hughes, A.-M.; Yardley, L.; Tedesco-Triccas, L. and Swain, I. (2013), 'Assistive technologies after stroke: self-management or fending for yourself? A focus group study', *BMC health services research* **13**(334), pp. 1–12, DOI: `10.1186/1472-6963-13-334` (pages 15, 53).

Denavit, J. and Hartenberg, R. S. (1955), 'A kinematic notation for lower pair mechanisms based on matrices', *Journal of applied mechanics* **77**(2), pp. 215–221 (page 22).

Dimyan, M. A. and Cohen, L. G. (2011), 'Neuroplasticity in the context of motor rehabilitation after stroke', *Nature Reviews Neurology* **7**, Review Article, pp. 76–85, DOI: `10.1038/nrneurol.2010.200` (page 2).

Dobkin, B. H. (2005), 'Rehabilitation after Stroke', *New England Journal of Medicine* **352**(16), pp. 1677–1684, DOI: `10.1056/NEJMcp043511` (page 3).

Dodakian, L.; McKenzie, A. L.; Le, V.; See, J.; Pearson-Fuhrhop, K.; Burke Quinlan, E.; Zhou, R. J.; Augsberger, R.; Tran, X. A.; Friedman, N.; Reinkensmeyer, D. J. and Cramer, S. C. (2017), 'A Home-Based Telerehabilitation Program for Patients With Stroke', *Neurorehabilitation and Neural Repair* **31**(10-11), pp. 923–933, DOI: `10.1177/1545968317733818` (page 16).

Donchin, E.; Spencer, K. M. and Wijesinghe, R. (2000), 'The mental prosthesis: assessing the speed of a P300-based brain-computer interface', *IEEE Transactions on Rehabilitation Engineering* **8**(2), pp. 174–179, DOI: `10.1109/86.847808` (page 17).

Donnan, G. A.; Fisher, M.; Macleod, M. and Davis, S. M. (2008), 'Stroke', *The Lancet* **371**(9624), pp. 1612–1623, DOI: `10.1016/S0140-6736(08)60694-7` (page 1).

Duret, C.; Grosmaire, A.-G. and Krebs, H. I. (2019), 'Robot-Assisted Therapy in Upper Extremity Hemiparesis: Overview of an Evidence-Based Approach', *Frontiers in Neurology* **10**(412), p. 8, DOI: `10.3389/fneur.2019.00412` (page 3).

El-Gohary, M. and McNames, J. (2015), 'Human Joint Angle Estimation with Inertial Sensors and Validation with A Robot Arm', *IEEE Transactions on Biomedical Engineering* **62**(7), pp. 1759–1767, DOI: `10.1109/TBME.2015.2403368` (page 54).

European Comission (2010), *European Disability Strategy 2010-2020: Renewed Commitment to a Barrier-Free Europe*, Brussels: European Comission, Retrieved from `https://ec.europa.eu/eip/ageing/standards/general/general-documents/european-disability-strategy-2010-2020_en` (page 3).

Federación Española de Daño Cerebral (2016), *Las personas con Daño Cerebral Adquirido en España*, FEDACE: Federación Española de Daño Cerebral, Retrieved from `https://fedace.org/epidemiologia_dano_cerebral.html` (page 3).

Federolf, P. (2013), 'A Novel Approach to Solve the "Missing Marker Problem" in Marker-Based Motion Analysis That Exploits the Segment Coordination Patterns in Multi-Limb Motion Data', *PLOS ONE* **8**(10), pp. 1–13, DOI: `10.1371/journal.pone.0078689` (page 13).

Feigin, V. L.; Forouzanfar, M. H.; Krishnamurthi, R.; Mensah, G. A.; Connor, M.; Bennett, D. A.; Moran, A. E.; Sacco, R. L.; Anderson, L.; Truelsen, T.; O'Donnell, M.; Venketasubramanian, N.; Barker-Collo,

S.; Lawes, C. M. M.; Wang, W.; Shinohara, Y.; Witt, E.; Ezzati, M.; Naghavi, M. and Murray, C. (2014), 'Global and regional burden of stroke during 1990-2010: findings from the Global Burden of Disease Study 2010', *The Lancet* **383**(9913), pp. 245–255, DOI: `10.1016/S0140-6736(13)61953-4` (page 3).

Fong, D. and Chan, Y. (2010), 'The Use of Wearable Inertial Motion Sensors in Human Lower Limb Biomechanics Studies: A Systematic Review', *Sensors* **10**(12), pp. 11556–11565, DOI: `10.3390/s101211556` (page 14).

Fugl-Meyer, A. R.; Jääskö, L; Leyman, I.; Olsson, S. and Steglind, S. (1975), 'The post-stroke hemiplegic patient. 1. a method for evaluation of physical performance.', *Scandinavian journal of rehabilitation medicine* **7**(1), pp. 13–31, Retrieved from `https://www.ncbi.nlm.nih.gov/pubmed/1135616` (pages 3, 37).

Generalitat Valenciana (2017), *Estrategia Daño Cerebral Adquirido en la Comunitat Valenciana 2017-2020*, Generalitat Valenciana: Conselleria de Sanitat Universal i Salut Pública, Retrieved from `http://www.san.gva.es/web/dgas/estrategia-dca` (page 3).

Gibbs, F. A.; Gibbs, E. L. and Lennox, W. G. (1937), 'Effect on the electro-encephalogram of certain drugs which influence nervous activity', *Archives of Internal Medicine* **60**(1), pp. 154–166, DOI: `10.1001/archinte.1937.00180010159012` (page 17).

Gips, J.; DiMattia, P.; Curran, F. X. and Olivieri, P. (1996), 'EagleEyes: An eye control system for persons with disabilities', in: *Proceedings of the 11th international conference on technology and persons with disabilities*, pp. 1–15, Retrieved from `http://cs.bc.edu/~gips/EagleEyes1996.pdf` (page 17).

González-Ortega, D.; Díaz-Pernas, F. J.; Martínez-Zarzuela, M. and Antón-Rodríguez, M. (2014), 'A Kinect-based system for cognitive rehabilitation exercises monitoring', *Computer Methods and Programs in Biomedicine* **113**(2), pp. 620–631, DOI: `10.1016/j.cmpb.2013.10.014` (page 14).

Gryfe, P.; Kurtz, I.; Gutmann, M. and Laiken, G. (1996), 'Freedom through a single switch: coping and communicating with artificial ventilation', *Journal of the Neurological Sciences* **139**, Amyotrophic Lateral Sclerosis/Motor Neurone Disease, pp. 132–133, DOI: `10.1016/0022-510X(96)00086-X` (page 16).

Hansen, D. W. and Ji, Q. (2010), 'In the Eye of the Beholder: A Survey of Models for Eyes and Gaze', *IEEE Transactions on Pattern Analysis and*

Machine Intelligence **32**(3), pp. 478–500, DOI: `10.1109/TPAMI.2009.30` (page 17).

Hart, S. G. and Staveland, L. E. (1988), 'Development of NASA-TLX (Task Load Index): Results of Empirical and Theoretical Research', *Advances in Psychology* **52**, pp. 139–183, DOI: `https://doi.org/10.1016/S0166-4115(08)62386-9` (page 69).

He, J.; Koeneman, E. J.; Schultz, R.; Huang, H; Wanberg, J.; Herring, D.; Sugar, T.; Herman, R and Koeneman, J. (2005), 'Design of a robotic upper extremity repetitive therapy device', in: *Proceedings of the 9th IEEE International Conference on Rehabilitation Robotics*, pp. 95–98, DOI: `10.1109/ICORR.2005.1501060` (page 11).

Hingtgen, B.; McGuire, J. R.; Wang, M. and Harris, G. F. (2006), 'An upper extremity kinematic model for evaluation of hemiparetic stroke', *Journal of Biomechanics* **39**(4), pp. 681–688, DOI: `10.1016/j.jbiomech.2005.01.008` (page 4).

Hislop, H.; Avers, D. and Brown, M. (2013), *Daniels and Worthingham's muscle Testing: Techniques of manual examination and performance testing*, Elsevier Health Sciences, ISBN: 978-8131235133 (page 56).

Hogan, N.; Krebs, H. I.; Charnnarong, J.; Srikrishna, P. and Sharon, A. (1992), 'MIT-MANUS: a workstation for manual therapy and training. I', in: *Proceedings of the 1992 IEEE International Workshop on Robot and Human Communication*, pp. 161–165, DOI: `10.1109/ROMAN.1992.253895` (pages 3, 10, 15).

Housman, S. J.; Le, V.; Rahman, T.; Sanchez, R. J. and Reinkensmeyer, D. J. (2007), 'Arm-Training with T-WREX After Chronic Stroke: Preliminary Results of a Randomized Controlled Trial', in: *Proceedings of the IEEE 10th International Conference on Rehabilitation Robotics*, pp. 562–568, DOI: `10.1109/ICORR.2007.4428481` (page 11).

Inman, V.; Saunders, M. and Abbott, L. (1996), 'Observations of the Function of the Shoulder Joint', *Clinical Orthopaedics and Related Research* **330**, pp. 3–12, DOI: `10.1097/00003086-199609000-00002` (page 21).

Jackson, A.; Culmer, P.; Makower, S.; Levesley, M.; Richardson, R.; Cozens, A.; Williams, M. M. and Bhakta, B. (2007), 'Initial patient testing of iPAM - a robotic system for Stroke rehabilitation', in: *Proceedings of the 10th IEEE International Conference on Rehabilitation Robotics*, pp. 250–256, DOI: `10.1016/j.jneumeth.2011.03.004` (page 10).

Jaeger, H. (2001), 'The "echo state" approach to analysing and training recurrent neural networks-with an erratum note', *German National*

Research Center for Information Technology, Bremen, Germany, Technical Report **148**, p. 47, Retrieved from `http://minds.jacobs-university.de/uploads/papers/EchoStatesTechRep.pdf` (page 55).

Jakob, R. (1998), 'Readings in intelligent user interfaces', in: ed. by M. Myabury and W. Wahlster, Morgan Kaufmann Publishers, chap. The use of eye movements in human-computer interaction techniques: what you look at is what you get, pp. 65–83, ISBN: 1-55860-444-8 (page 17).

Jarrassé, N.; Proietti, T.; Crocher, V.; Robertson, J.; Sahbani, A.; Morel, G. and Roby-Brami, A. (2014), 'Robotic Exoskeletons: A Perspective for the Rehabilitation of Arm Coordination in Stroke Patients', *Frontiers in Human Neuroscience* **8**(947), pp. 1–13, DOI: `10.3389/fnhum.2014.00947` (page 11).

Johansson, G. (1975), 'Visual Motion Perception', *Scientific American* **232**(6), pp. 76–89, Retrieved from `http://www.jstor.org/stable/24949822` (page 12).

Johnson, M.; Loureiro, R. and Harwin, W. (2008), 'Collaborative tele-rehabilitation and robot-mediated therapy for stroke rehabilitation at home or clinic', *Intelligent Service Robotics* **1**(2), pp. 109–121, DOI: `10.1007/s11370-007-0010-3` (page 16).

Jones, T. A. (2017), 'Motor compensation and its effects on neural reorganization after stroke', *Nature Reviews Neuroscience* **18**, Review Article, pp. 267–280, DOI: `10.1038/nrn.2017.26` (page 42).

Kerr, A. L.; Cheng, S.-Y. and Jones, T. A. (2011), 'Experience-dependent neural plasticity in the adult damaged brain', *Journal of Communication Disorders* **44**(5), pp. 538–548, DOI: `10.1016/j.jcomdis.2011.04.011` (page 1).

Kiguchi, K.; Iwami, K.; Yasuda, M.; Watanabe, K. and Fukuda, T. (2003), 'An exoskeletal robot for human shoulder joint motion assist', *IEEE/ASME Transactions on Mechatronics* **8**(1), pp. 125–135, DOI: `10.1109/TMECH.2003.809168` (page 12).

Klamroth-Marganska, V.; Blanco, J.; Campen, K.; Curt, A.; Dietz, V.; Ettlin, T.; Felder, M.; Fellinghauer, B.; Guidali, M.; Kollmar, A.; Luft, A.; Nef, T.; Schuster-Amft, C.; Stahel, W. and Riener, R. (2014), 'Three-dimensional, task-specific robot therapy of the arm after stroke: a multicentre, parallel-group randomised trial', *The Lancet Neurology* **13**(2), pp. 159–166, DOI: `10.1016/S1474-4422(13)70305-3` (page 2).

Kleim, J. A. and Jones, T. A. (2008), 'Principles of Experience-Dependent Neural Plasticity: Implications for Rehabilitation After Brain

Damage', *Journal of Speech, Language, and Hearing Research* **51**(1), pp. 225–239, DOI: 10.1044/1092-4388(2008/018) (page 1).

Krebs, H. I.; Hogan, N.; Aisen, M. L. and Volpe, B. T. (1998), 'Robot-aided neurorehabilitation', *IEEE Transactions on Rehabilitation Engineering* **6**(1), pp. 75–87, DOI: 10.1109/86.662623 (pages 2, 9, 10).

Krebs, H.; Ferraro, M.; Buerger, S.; Newbery, M.; Makiyama, A.; Sandmann, M.; Lynch, D.; Volpe, B. and Hogan, N. (2004), 'Rehabilitation robotics: pilot trial of a spatial extension for MIT-Manus', *Journal of NeuroEngineering and Rehabilitation* **1**(5), pp. 1–15, DOI: 10.1186/1743-0003-1-5 (page 10).

Kreutz-Delgado, K.; Long, M. and Seraji, H. (1990), 'Kinematic analysis of 7 DoF anthropomorphic arms', in: *Proceedings of the 1990 IEEE International Conference on Robotics and Automation*, vol. 2, pp. 824–830, DOI: 10.1109/ROBOT.1990.126090 (pages 5, 21, 24, 26, 30).

Kwakkel, G.; Kollen, B. J.; van der Grond, J. and Prevo, A. J. H. (2003), 'Probability of Regaining Dexterity in the Flaccid Upper Limb', *Stroke* **34**(9), pp. 2181–2186, DOI: 10.1161/01.STR.0000087172.16305.CD (page 2).

Kwakkel, G.; Kollen, B. J. and Krebs, H. I. (2007), 'Effects of Robot-Assisted Therapy on Upper Limb Recovery After Stroke: A Systematic Review', *Neurorehabilitation and Neural Repair* **22**(2), pp. 111–121, DOI: 10.1177/1545968307305457 (pages 3, 10).

Kwakkel, G.; Kollen, B. and Twisk, J. (2019), 'Impact of Time on Improvement of Outcome After Stroke', *Stroke* **37**(9), pp. 2348–2353, DOI: 10.1161/01.str.0000238594.91938.1e (page 3).

Lafferty, J. D.; McCallum, A. and Pereira, F. C. N. (2001), 'Conditional Random Fields: Probabilistic Models for Segmenting and Labeling Sequence Data', in: *Proceedings of the 18th International Conference on Machine Learning*, pp. 282–289, ISBN: 1-55860-778-1, Retrieved from http://dl.acm.org/citation.cfm?id=645530.655813 (page 66).

Lenarčič, J. and Umek, A. (1994), 'Simple model of human arm reachable workspace', *IEEE Transactions on Systems, Man, and Cybernetics* **24**(8), pp. 1239–1246, DOI: 10.1109/21.299704 (page 21).

Lledó, L. D.; Díez, J. A.; **Bertomeu-Motos, A.**; Ezquerro, S.; Badesa, F. J.; Sabater-Navarro, J. M. and Garcia-Aracil, N. (2016), 'A Comparative Analysis of 2D and 3D Tasks for Virtual Reality Therapies Based on Robotic-Assisted Neurorehabilitation for Post-stroke Patients', *Frontiers in Aging Neuroscience* **8**, p. 205, DOI: 10.3389/fnagi.2016.00205 (pages 10, 38, 81).

Llinares, A.; Badesa, F. J.; Morales, R.; Garcia-Aracil, N.; Sabater, J. M. and Fernandez, E. (2013), 'Robotic assessment of the influence of age on upper-limb sensorimotor function', *Clinical Interventions in Aging* **8**, pp. 879–888, DOI: `10.2147/CIA.S45900` (page 10).

Lo, A. C.; Guarino, P. D.; Richards, L. G.; Haselkorn, J. K.; Wittenberg, G. F.; Federman, D. G.; Ringer, R. J.; Wagner, T. H.; Krebs, H. I.; Volpe, B. T.; Bever, C. T.; Bravata, D. M.; Duncan, P. W.; Corn, B. H.; Maffucci, A. D.; Nadeau, S. E.; Conroy, S. S.; Powell, J. M.; Huang, G. D. and Peduzzi, P. (2010), 'Robot-Assisted Therapy for Long-Term Upper-Limb Impairment after Stroke', *New England Journal of Medicine* **362**(19), pp. 1772–1783, DOI: `10.1056/NEJMoa0911341` (page 2).

Loureiro, R.; Amirabdollahian, F.; Topping, M.; Driessen, B. and Harwin, W. (2003), 'Upper limb robot mediated stroke therapy-Gentle's approach', *Autonomous Robots* **15**(1), pp. 35–51, DOI: `10.1023/A:1024436732030` (page 10).

Lum, P. S.; Burgar, C. G.; Shor, P. C.; Majmundar, M. and Loos, M. Van der (2002), 'Robot-assisted movement training compared with conventional therapy techniques for the rehabilitation of upper-limb motor function after stroke', *Archives of Physical Medicine and Rehabilitation* **83**(7), pp. 952–959, DOI: `10.1053/apmr.2001.33101` (pages 3, 10).

Lum, P. S.; Burgar, C.; Van der Loos, M.; Shor, P.; Majmundar, M. and Yap, R. (2006), 'MIME robotic device for upper-limb neurorehabilitation in subacute stroke subjects: A follow-up study', *Journal of rehabilitation research and development* **43**(5), pp. 631–642, DOI: `10.1682/JRRD.2005.02.0044` (page 10).

Maciejasz, P.; Eschweiler, J.; Gerlach-Hahn, K.; Jansen-Troy, A. and Leonhardt, S. (2014), 'A survey on robotic devices for upper limb rehabilitation', *Journal of Neuroengineering and Rehabilitation* **11**(3), pp. 1–29, DOI: `10.1186/1743-0003-11-3` (page 9).

Madgwick, S. O. H.; Harrison, A. J. L. and Vaidyanathan, R. (2011), 'Estimation of IMU and MARG orientation using a gradient descent algorithm', in: *Proceedings of the 2011 IEEE International Conference on Rehabilitation Robotics*, pp. 1–7, DOI: `10.1109/ICORR.2011.5975346` (pages 15, 47, 57).

Mar, J.; Álvarez-Sabín, J.; Oliva, J.; Becerra, V.; Casado, M. A.; Yébenes, M.; González-Rojas, N.; Arenillas, J. F.; Martínez-Zabaleta, M. T. and Rebollo, M. (2013), 'Los costes del ictus en España según su etiología. El protocolo del estudio CONOCES', *Neurología* **28**(6), pp. 332–339, DOI: `10.1016/j.nrl.2012.07.004` (page 3).

Marins, J. L.; Xiaoping Yun; Bachmann, E. R.; McGhee, R. B. and Zyda, M. J. (2001), 'An extended Kalman filter for quaternion-based orientation estimation using MARG sensors', in: *Proceedings of the 2001 IEEE International Conference on Intelligent Robots and Systems*, pp. 2003–2011, DOI: `10.1109/IROS.2001.976367` (page 15).

Matarić, M. J.; Eriksson, J.; Feil-Seifer, D. J. and Winstein, C. J. (2007), 'Socially assistive robotics for post-stroke rehabilitation', *Journal of NeuroEngineering and Rehabilitation* **4**(5), p. 9, DOI: `10.1186/1743-0003-4-5` (page 3).

Mayagoitia, R.; Nene, A. and Veltink, P. (2002), 'Accelerometer and rate gyroscope measurement of kinematics: an inexpensive alternative to optical motion analysis systems', *Journal of Biomechanics* **35**(4), pp. 537–542, DOI: `10.1016/S0021-9290(01)00231-7` (page 14).

Merletti, R. and Parker, P. A. (2004), *Electromyography: physiology, engineering, and non-invasive applications*, vol. 11, John Wiley & Sons, ISBN: 978-0471675808 (page 16).

Meyer, S.; Verheyden, G.; Brinkmann, N.; Dejaeger, E.; De Weerdt, W.; Feys, H.; Gantenbein, A.; Jenni, W.; Laenen, A.; Lincoln, N.; Putman, K.; Schuback, B.; Schupp, W.; Thijs, V. and De Wit, L. (2015), 'Functional and Motor Outcome 5 Years After Stroke Is Equivalent to Outcome at 2 Months', *Stroke* **46**(6), pp. 1613–1619, DOI: `10.1161/STROKEAHA.115.009421` (page 2).

Mihelj, M.; Podobnik, J. and Munih, M. (2018), 'Sensory Fusion of Magnetoinertial Data Based on Kinematic Model With Jacobian Weighted-Left-Pseudoinverse and Kalman-Adaptive Gains', *IEEE Transactions on Instrumentation and Measurement*, pp. 1–11, DOI: `10.1109/TIM.2018.2867891` (page 15).

Mihelj, M. (2006), 'Human arm kinematics for robot based rehabilitation', *Robotica* **24**(3), pp. 377–383, DOI: `10.1017/S0263574705002304` (page 18).

Miralles, F.; Vargiu, E.; Rafael-Palou, X.; Solà, M.; Dauwalder, S.; Guger, C.; Hintermüller, C.; Espinosa, A.; Lowish, H.; Martin, S.; Armstrong, E. and Daly, J. (2015), 'Brain-Computer Interfaces on Track to Home: Results of the Evaluation at Disabled End-Users' Homes and Lessons Learnt', *Frontiers in ICT* **2**(25), p. 9, DOI: `10.3389/fict.2015.00025` (page 18).

Moeslund, T. and Granum, E. (2001), 'A Survey of Computer Vision-Based Human Motion Capture', *Computer Vision and Image Understanding* **81**(3), pp. 231–268, DOI: `10.1006/cviu.2000.0897` (page 13).

Montagner, A.; Frisoli, A.; Borelli, L.; Procopio, C.; Bergamasco, M.; Carboncini, M. C. and Rossi, B. (2007), 'A pilot clinical study on robotic assisted rehabilitation in VR with an arm exoskeleton device', in: *Proceedings of the 2007 IEEE International Workshop on Virtual Rehabilitation*, pp. 57–64, DOI: `10.1109/ICVR.2007.4362131` (page 11).

Morales Vidal, R. (2014), 'Diseño y Control de Dispositivos Robóticos para la Administración Temprana de Terapias de Neuro-Rehabilitación', PhD dissertation, Universidad Miguel Hernández de Elche, Retrieved from `https://www.educacion.gob.es/teseo/mostrarRef.do?ref=1078008` (pages 18, 21, 77).

Moreno-Jiménez, E. P.; Flor-García, M.; Terreros-Roncal, J.; Rábano, A.; Cafini, F.; Pallas-Bazarra, N.; Ávila, J. and Llorens-Martín, M. (2019), 'Adult hippocampal neurogenesis is abundant in neurologically healthy subjects and drops sharply in patients with Alzheimer's disease', *Nature Medicine* **25**(4), pp. 554–560, DOI: `10.1038/s41591-019-0375-9` (page 1).

Murphy, M.; Willén, C. and Sunnerhagen, K. (2011), 'Kinematic Variables Quantifying Upper-Extremity Performance After Stroke During Reaching and Drinking From a Glass', *Neurorehabilitation and Neural Repair* **25**(1), pp. 71–80, DOI: `10.1177/1545968310370748` (page 12).

Murphy, T. H. and Corbett, D. (2009), 'Plasticity during stroke recovery: from synapse to behaviour', *Nature Reviews Neuroscience* **10**, pp. 861–872, DOI: `10.1038/nrn2735` (page 1).

NaturalPoint (2016), *Baseline Upper Body (25) markerset*, Accessed 30 Apr 2019, Retrieved from `https://v20.wiki.optitrack.com/index.php?title=Baseline_Upper_Body_(25)`, Accesed on 30/04/2019 (page 35).

Nef, T.; Mihelj, M.; Kiefer, G.; Perndl, C.; Muller, R. and Riener, R. (2007), 'ARMin - Exoskeleton for Arm Therapy in Stroke Patients', in: *Proceedings of the 2007 IEEE 10th International Conference on Rehabilitation Robotics*, pp. 68–74, DOI: `10.1109/ICORR.2007.4428408` (page 11).

Nichols-Larsen, D. S.; Clark, P. C.; Zeringue, A.; Greenspan, A. and Blanton, S. (2005), 'Factors Influencing Stroke Survivors' Quality of Life During Subacute Recovery', *Stroke* **36**(7), pp. 1480–1484, DOI: `10.1161/01.STR.0000170706.13595.4f` (page 15).

Nijenhuis, S.; Prange, G.; Amirabdollahian, F.; Sale, P.; Infarinato, F.; Nasr, N.; Mountain, G.; Hermens, H.; Stienen, A.; Buurke, J. and Rietman, J. (2015), 'Feasibility study into self-administered

training at home using an arm and hand device with motivational gaming environment in chronic stroke', *Journal of neuroengineering and rehabilitation* **12**(89), pp. 1–12, DOI: `10.1186/s12984-015-0080-y` (page 16).

Norton, K. and Olds, T. (1996), *Anthropometrica: a textbook of body measurement for sports and health courses*, UNSW press, ISBN: 978-0868402239 (page 23).

Novak, D.; Goršič, M.; Podobnik, J. and Munih, M. (2014), 'Toward Real-Time Automated Detection of Turns during Gait Using Wearable Inertial Measurement Units', *Sensors* **14**(10), pp. 18800–18822, DOI: `10.3390/s141018800` (page 14).

Papaleo, E.; Zollo, L.; Garcia-Aracil, N.; Badesa, F. J.; Morales, R.; Mazzoleni, S.; Sterzi, S. and Guglielmelli, E. (2015), 'Upper-limb kinematic reconstruction during stroke robot-aided therapy', *Medical & biological engineering & computing* **53**(9), pp. 815–828, DOI: `10.1007/s11517-015-1276-9` (pages 5, 6, 18, 21, 37, 39, 40, 42).

Pérez, R.; Costa, Ú.; Torrent, M.; Solana, J.; Opisso, E.; Cáceres, C.; Tormos, J.; Medina, J. and Gómez, E. (2010), 'Upper Limb Portable Motion Analysis System Based on Inertial Technology for Neurorehabilitation Purposes', *Sensors* **10**(12), pp. 10733–10751, DOI: `10.3390/s101210733` (page 14).

Poppe, R. (2007), 'Vision-based human motion analysis: An overview', *Computer Vision and Image Understanding* **108**(1), pp. 4–18, DOI: `10.1016/j.cviu.2006.10.016` (page 13).

Quinn, T. J.; Langhorne, P. and Stott, D. J. (2011), 'Barthel index for stroke trials: development, properties, and application', *Stroke* **42**(4), pp. 1146–1151, DOI: `10.1161/STROKEAHA.110.598540` (page 71).

Repnik, E.; Puh, U.; Goljar, N.; Munih, M. and Mihelj, M. (2018), 'Using Inertial Measurement Units and Electromyography to Quantify Movement during Action Research Arm Test Execution', *Sensors* **18**(9), pp. 1–23, DOI: `10.3390/s18092767` (page 12).

Riener, R.; Guidali, M.; Keller, U.; Duschau-Wicke, A.; Klamroth, V. and Nef, T. (2011), 'Transferring Armin to the clinics and industry', *Topics in Spinal Cord Injury Rehabilitation* **17**, pp. 54–59, DOI: `10.1310/sci1701-54` (page 11).

Sabatini, A. M. (2006), 'Quaternion-based extended Kalman filter for determining orientation by inertial and magnetic sensing', *IEEE Transactions on Biomedical Engineering* **53**(7), pp. 1346–1356, DOI: `10.1109/TBME.2006.875664` (page 15).

Saini, S.; Rambli, D. R. A.; Sulaiman, S.; Zakaria, M. N. and Mohd Shukri, S. R. (2012), 'A low-cost game framework for a home-based stroke rehabilitation system', in: *Proceedings of the 2012 International Conference on Computer Information Science*, vol. 1, pp. 55–60, DOI: `10.1109/ICCISci.2012.6297212` (page 14).

Sakoe, H. and Chiba, S. (1978), 'Dynamic programming algorithm optimization for spoken word recognition', *IEEE Transactions on Acoustics, Speech, and Signal Processing* **26**(1), pp. 43–49, DOI: `10.1109/TASSP.1978.1163055` (page 55).

Sanchez, R.; Reinkensmeyer, D.; Shah, P.; Liu, J.; Rao, S.; Smith, R.; Cramer, S.; Rahman, T. and Bobrow, J. (2004), 'Monitoring functional arm movement for home-based therapy after stroke', in: *Proceedings of the 26th Annual International Conference of the IEEE Engineering in Medicine and Biology Society*, vol. 2, pp. 4787–4790, DOI: `10.1109/IEMBS.2004.1404325` (page 11).

Santisteban, L.; Térémetz, M.; Bleton, J.-P.; Baron, J.-C.; Maier, M. A. and Lindberg, P. G. (2016), 'Upper Limb Outcome Measures Used in Stroke Rehabilitation Studies: A Systematic Literature Review', *PLOS ONE* **11**(5), pp. 1–16, DOI: `10.1371/journal.pone.0154792` (pages 3, 12).

Saunders, J. B.; Inman, V. T. and Eberhart, H. D. (1953), 'The major determinants in normal and pathological gait', *Journal of Bone and Joint Surgery* **35**(3), pp. 543–558, Retrieved from `https://www.ncbi.nlm.nih.gov/pubmed/13069544` (page 14).

Schaechter, J. D. (2004), 'Motor rehabilitation and brain plasticity after hemiparetic stroke', *Progress in Neurobiology* **73**(1), pp. 61–72, DOI: `10.1016/j.pneurobio.2004.04.001` (page 2).

Schalk, G.; McFarland, D. J.; Hinterberger, T.; Birbaumer, N. and Wolpaw, J. R. (2004), 'BCI2000: a general-purpose brain-computer interface (BCI) system', *IEEE Transactions on Biomedical Engineering* **51**(6), pp. 1034–1043, DOI: `10.1109/TBME.2004.827072` (page 84).

Seel, T.; Raisch, J. and Schauer, T. (2014), 'IMU-Based Joint Angle Measurement for Gait Analysis', *Sensors* **14**(4), pp. 6891–6909, DOI: `10.3390/s140406891` (page 14).

Sellers, E. W.; Vaughan, T. M. and Wolpaw, J. R. (2010), 'A brain-computer interface for long-term independent home use', *Amyotrophic Lateral Sclerosis* **11**(5), pp. 449–455, DOI: `10.3109/17482961003777470` (page 18).

Siciliano, B.; Sciavicco, L.; Villani, L. and Oriolo, G. (2010), *Robotics: modelling, planning and control*, Springer Science & Business Media, ISBN: 978-1846286414 (pages 25, 32).

Sivan, M.; Gallagher, J.; Makower, S.; Keeling, D.; Bhakta, B.; O'Connor, R. and Levesley, M. (2014), 'Home-based Computer Assisted Arm Rehabilitation (hCAAR) robotic device for upper limb exercise after stroke: results of a feasibility study in home setting', *Journal of neuroengineering and rehabilitation* **11**(1), p. 163, DOI: `10.1186/1743-0003-11-163` (page 16).

Soekadar, S. R.; Witkowski, M.; Gómez, C.; Opisso, E.; Medina, J.; Cortese, M.; Cempini, M.; Carrozza, M. C.; Cohen, L. G.; Birbaumer, N. and Vitiello, N. (2016), 'Hybrid EEG/EOG-based brain/neural hand exoskeleton restores fully independent daily living activities after quadriplegia', *Science Robotics* **1**(1), pp. 1–8, DOI: `10.1126/scirobotics.aag3296` (pages 17, 84).

Soh, H. and Demiris, Y. (2015), 'Spatio-Temporal Learning With the Online Finite and Infinite Echo-State Gaussian Processes', *IEEE Transactions on Neural Networks and Learning Systems* **26**(3), pp. 522–536, DOI: `10.1109/TNNLS.2014.2316291` (page 55).

Staubli, P.; Nef, T.; Klamroth-Marganska, V. and Riener, R. (2009), 'Effects of intensive arm training with the rehabilitation robot ARMin II in chronic stroke patients: four single-cases', *Journal of Neuroengineering and Rehabilitation* **6**(46), pp. 1–10, DOI: `10.1186/1743-0003-6-46` (page 11).

Taati, B.; Wang, R.; Huq, R.; Snoek, J. and Mihailidis, A. (2012), 'Vision-based posture assessment to detect and categorize compensation during robotic rehabilitation therapy', in: *Proceedings of the 4th IEEE International Conference on Biomedical Robotics and Biomechatronics*, pp. 1607–1613, DOI: `10.1109/BioRob.2012.6290668` (page 14).

Tai, K.; Blain, S. and Chau, T. (2008), 'A Review of Emerging Access Technologies for Individuals With Severe Motor Impairments', *Assistive Technology* **20**(4), PMID: 19160907, pp. 204–221, DOI: `10.1080/10400435.2008.10131947` (page 16).

Taub, E.; Uswatte, G. and Elbert, T. (2002), 'New treatments in neurorehabiliation founded on basic research', *Nature Reviews Neuroscience* **3**(3), pp. 228–236, DOI: `10.1038/nrn754` (page 1).

Truelsen, T.; Ekman, M. and Boysen, G. (2005), 'Cost of stroke in Europe', *European Journal of Neurology* **12**(1), pp. 78–84, DOI: `10.1111/j.1468-1331.2005.01199.x` (page 15).

Valero, E.; Sivanathan, A.; Bosché, F. and Abdel-Wahab, M. (2016), 'Musculoskeletal disorders in construction: A review and a novel system for activity tracking with body area network', *Applied Ergonomics* **54**, pp. 120–130, DOI: `10.1016/j.apergo.2015.11.020` (page 14).

Veltink, P. H.; Bussmann, H. J.; de Vries, W.; Martens, W. J. and Van Lummel, R. C. (1996), 'Detection of static and dynamic activities using uniaxial accelerometers', *IEEE Transactions on Rehabilitation Engineering* **4**(4), pp. 375–385, DOI: `10.1109/86.547939` (page 14).

Veneman, J. F.; Kruidhof, R.; Hekman, E. E. G.; Ekkelenkamp, R.; Van Asseldonk, E. H. F. and van der Kooij, H. (2007), 'Design and Evaluation of the LOPES Exoskeleton Robot for Interactive Gait Rehabilitation', *IEEE Transactions on Neural Systems and Rehabilitation Engineering* **15**(3), pp. 379–386, DOI: `10.1109/TNSRE.2007.903919` (page 11).

Vidal, J. J. (1977), 'Real-time detection of brain events in EEG', *Proceedings of the IEEE* **65**(5), pp. 633–641, DOI: `10.1109/PROC.1977.10542` (page 17).

Volpe, B. T.; Krebs, H. I.; Hogan, N.; Edelstein, L.; Diels, C. and Aisen, M. (2000), 'A novel approach to stroke rehabilitation', *Neurology* **54**(10), pp. 1938–1944, DOI: `10.1212/WNL.54.10.1938` (page 2).

Voss, D. E.; Ionta, M. K. and Myers, B. J. (1985), *Proprioceptive neuromuscular facilitation: patterns and techniques*, Harper & Row, ISBN: 978-0061425950 (page 33).

Webster, D. and Celik, O. (2014), 'Systematic review of Kinect applications in elderly care and stroke rehabilitation', *Journal of neuroengineering and rehabilitation* **11**(108), pp. 1–24, DOI: `10.1186/1743-0003-11-108` (page 14).

Windolf, M.; Götzen, N. and Morlock, M. (2008), 'Systematic accuracy and precision analysis of video motion capturing systems – exemplified on the Vicon-460 system', *Journal of Biomechanics* **41**(12), pp. 2776–2780, DOI: `10.1016/j.jbiomech.2008.06.024` (page 13).

Wittmann, F.; Held, J.; Lambercy, O.; Starkey, M.; Curt, A.; Höver, R.; Gassert, R.; Luft, A. and Gonzenbach, R. (2016), 'Self-directed arm therapy at home after stroke with a sensor-based virtual reality training system', *Journal of neuroengineering and rehabilitation* **13**(75), pp. 1–10, DOI: `10.1186/s12984-016-0182-1` (page 16).

Wolpaw, J. R.; McFarland, D. J. and Vaughan, T. M. (2000), 'Brain-computer interface research at the Wadsworth Center', *IEEE Transactions*

on Rehabilitation Engineering **8**(2), pp. 222–226, DOI: `10.1109/86.847823` (page 17).

Wolpaw, J. R.; Birbaumer, N.; J McFarland, D.; Pfurtscheller, G. and Vaughan, T. M. (2002), 'Brain-computer interfaces for communication and control', *Clinical Neurophysiology* **113**(6), pp. 767–791, DOI: `10.1016/S1388-2457(02)00057-3` (page 17).

World Health Organisation (2018a), *Global Health Estimates 2016: Deaths by Cause, Age, Sex and Country 2000-2016*, Genova: World Health Organisation, Retrieved from `http://www.who.int/healthinfo/global_burden_disease/estimates/en/` (page 3).

World Health Organisation (2018b), *Global Health Estimates Summary Tables: Projection of Deaths by Cause, Age and Sex, by Region*, Retrieved from `http://www.who.int/healthinfo/global_burden_disease/projections/en/` (page 3).

Wu, Q. and Boulanger, P. (2011), 'Real-Time Estimation of Missing Markers for Reconstruction of Human Motion', in: *Proceedings of the 13th Symposium on Virtual Reality*, pp. 161–168, DOI: `10.1109/SVR.2011.35` (page 13).

Yan, T.; Cempini, M.; Oddo, C. and Vitiello, N. (2015), 'Review of assistive strategies in powered lower-limb orthoses and exoskeletons', *Robotics and Autonomous Systems* **64**, pp. 120–136, DOI: `10.1016/j.robot.2014.09.032` (page 11).

Zhou, H. and Hu, H. (2008), 'Human motion tracking for rehabilitation – A survey', *Biomedical Signal Processing and Control* **3**(1), pp. 1–18, DOI: `10.1016/j.bspc.2007.09.001` (page 12).

Zhou, H.; Hu, H.; Harris, N. and Hammerton, J. (2006), 'Applications of wearable inertial sensors in estimation of upper limb movements', *Biomedical Signal Processing and Control* **1**(1), pp. 22 –32, DOI: `10.1016/j.bspc.2006.03.001` (pages 13, 14).

Zhou, H.; Stone, T.; Hu, H. and Harris, N. (2008), 'Use of multiple wearable inertial sensors in upper limb motion tracking', *Medical Engineering & Physics* **30**(1), pp. 123–133, DOI: `10.1016/j.medengphy.2006.11.010` (page 14).

de Vries, W. H. K.; Veeger, H. E. J.; Cutti, A. G.; Baten, C. and van der Helm, F. C. T. (2010), 'Functionally interpretable local coordinate systems for the upper extremity using inertial & magnetic measurement systems', *Journal of Biomechanics* **43**(10), pp. 1983–1988, DOI: `10.1016/j.jbiomech.2010.03.007` (page 54).

Šlajpah, S.; Kamnik, R. and Munih, M. (2017), 'Compensation for Magnetic Disturbances in Motion Estimation to Provide Feedback

to Wearable Robotic Systems', *IEEE Transactions on Neural Systems and Rehabilitation Engineering* **25**(12), pp. 2398–2406, DOI: 10.1109/TNSRE.2017.2760356 (page 15).